DISSERTATION

RECONCILING TRMM PRECIPITATION ESTIMATES RELATED TO EL NIÑO

SOUTHERN OSCILLATION VARIABILITY

Submitted by

David S. Henderson

Department of Atmospheric Science

In partial fulfillment of the requirements

For the Degree of Doctor of Philosophy

Colorado State University

Fort Collins, Colorado

Spring 2017

Doctoral Committee:

Advisor: Christian D. Kummerow

Susan C. van den Heever
Steven Rutledge
Branislav Notaros

ABSTRACT

RECONCILING TRMM PRECIPITATION ESTIMATES RELATED TO EL NIÑO

SOUTHERN OSCILLATION VARIABILITY

Over the tropical oceans, large discrepancies in TRMM passive and active microwave rainfall retrievals become apparent during El Niño-Southern Oscillation (ENSO) events, where TMI retrievals exhibit a systematic shift in precipitation seemingly correlated with ENSO phase, while the PR does not. To investigate the causality of this relationship, this dissertation focuses, both spatially and temporally, on the evolution of precipitation organization between El Niño and La Niña conditions and their impacts on TRMM TMI and PR retrieved precipitation through the use of ground validation (GV) and satellite-based sources. The precipitation validation is performed as a function of convective organization through implementation of defined precipitation regimes, which have physical characteristics consistent across meteorological regimes.

Before a full evaluation of TRMM retrieved rain rates is completed, an assessment of TRMM ground validation (GV) oceanic rain rate estimates is necessary. The robustness of radar-based GV rainfall estimates from the Kwajalein S-band KPOL radar are examined through comparisons with the Kwajalein rain gauge network. The TRMM-GV 2A53 rainfall product is found to heavily underestimate convective rain types, where prominent biases occur as precipitation becomes more organized. To further examine these rainfall biases, GV and polarimetrically-tuned rain rates are compared, where GV biases in both the 2A53 product and convective and stratiform Z-R relationships are minimized when the rain rate relationships are developed specifically as a function of precipitation regime. The results demonstrate that

exploration into precipitation regimes should be considered when deriving and evaluating rain relationships to establish the source and range of uncertainties existing within different precipitating systems.

TRMM radar (PR) and radiometer (TMI) rain rates are then evaluated though multiple case studies of collocated TRMM and KPOL rain rates at the 1°x1° and TMI footprint scale. The results of this study indicate that TRMM TMI and PR rainfall biases are best explained when derived as a function of organization and convective fraction. Large underestimates in both TMI and PR rain rates are associated with predominately convective rainfall across all regimes, where TMI rainfall underestimates both PR and GV rain rates. While PR rain rate estimates typically underestimate GV rainfall, TMI rain rates are heavily overestimated in rainfall regimes containing predominantly stratiform precipitation. Over the Kwajalein region, differences in TMI and PR rain rates seem to be driven by the occurrence of organized precipitation, where TMI-PR differences during El Niño conditions largely derive from MCS-like precipitating systems containing large stratiform precipitating regions. Application of the resultant biases helps mitigate the TMI-PR differences occurring between the ENSO phases and explain uncertainties introduced by the TMI Bayesian retrieval.

Expanding the analysis tropics-wide, TRMM discrepancies directly relate to a shift from isolated deep convection during La Niña events toward organized precipitation during El Niño events with the largest variability occurring in the Pacific basins. During El Niño conditions, an increase in stratiform raining fraction leads to an increase in TMI rain rates that is less prevalent in PR rain rate retrievals. Reanalysis and AIRS data indicate that higher occurrences in organized systems are aided by increased mid- and upper-tropospheric moisture accompanied by more frequent deep convection. During La Niña events tropical rainfall is dominated by isolated deep convective regimes associated with drier mid-tropospheric conditions and strong mid- and upper

level zonal wind shear. Application of the known TMI and PR biases yields increased consistency in PR rainfall with the radiometer-based TMI and GPCP rainfall estimates. The resultant satellite-based rainfall estimates are in general agreement when describing the response of tropical precipitation to ENSO induced variability in tropical SSTs.

ACKNOWLEDGEMENTS

DEDICATION

To my family and friends who have supported me throughout these many years.

"Go into the world and do well. But more importantly, go into the world and do good."

-Minor Myers Jr.

TABLE OF CONTENTS

CHAPTER 1

INTRODUCTION

1.1 Background and motivation

Continued exploration of precipitation variability and change has an immense environmental significance due to the active role of precipitation in global water and energy cycles. As a main component of the global energy cycle, latent heat released during precipitation processes helps drive the global atmospheric circulation; therefore, any anomaly in global precipitation directly influences the behavior of the Earth's weather and climate systems. A primary source of global precipitation is directly linked to the tropics - accounting for nearly two-thirds of the Earth's accumulated rainfall. Tao et al (2006) describes the large extent of precipitation across the tropics as the primary fuel for an atmospheric engine where latent heat released drives our atmospheric circulation through various teleconnection patterns emanating from the tropics throughout the mid- and upper-latitudes (Riehl and Malkus, 1958).

Because of the direct impact of precipitation on our Earth, it is necessary to continually observe and improve our understanding of land- and ocean-based precipitation. Land-based estimates of rainfall are generally derived from rain gauge networks (e.g. Wang et al. 2008), but ground-based radars can also be used to increase spatial coverage of rain rate estimates (e.g. Kirstetter et al., 2015; You et al. 2014). There are still many regions, however, where ground-based observations of precipitation are sparse – particularly over the oceans. In these regions, we depend on the use of satellite-based rainfall estimation, which are necessary to accurately portray the role of precipitation in water and energy budgets (Brown and Kummerow, 2014).

Quantitative measurements of precipitation through the use of satellites have progressed over the past few decades beginning with retrievals of rainfall from visible and infrared sensors aboard geostationary satellites to rain rates estimates retrieved through using measured upwelling microwave radiation (e.g. Barrett, 1970; Kidder and Vonder Haar, 1995; Hollinger et al., 1990; Wilheit, 1986). The launch of the Tropical Rainfall Measuring Mission (TRMM) satellite in 1997 introduced the first active precipitation radar (TRMM PR) and radiometer (TRMM TMI) tandem used to retrieve global precipitation estimates over the tropics and subtropics. The TRMM mission has been instrumental in helping to constrain global rainfall uncertainties and our understanding of precipitation variability in the tropics. Further, the inclusion of a spaceborne radar provided retrieval of the vertical distribution of hydrometeors, three-dimensional spatial distribution of radar reflectivities, and rain-type (convective/stratiform) classification. While the TRMM mission has provided remarkable improvements in the spatial structures of atmospheric hydrometeors, the TMI and PR rain rate retrievals rely on different physical assumptions when retrieving rain rates - resulting in situational dependent biases found between the products. These are quite pronounced during El Niño and La Niña events.

During a typical El Niño event, tropical ocean waters exhibit equatorial warm anomalies originating from the west coast of South America extending out toward the Central and West Pacific Ocean basins. The phenomenon was discovered nearby the coastal waters of Peru when warming of the adjoining waters affected the local fishing communities around Christmas – aptly leading to the naming of El Nino "The Boy" (Trenberth, 1997); Interestingly, this is not the only atmospheric phenomenon discovered due to anomalous fish harvesting – see historic records in the Pacific Decal Oscillation (PDO) (Chavez et al. 2003). El Niño events occur approximately every 2 to 7 years and are commonly followed by a period of anonymously cooler oceanic

temperatures, thusly named La Niña events. A second dominant mode in warm ENSO events, coined the El Nino Modoki has also been discovered, where the anomalous warm waters are consolidated in the central tropical Pacific, which in turn can entail its own set of associated teleconnection patterns (Ashok et al, 2007; Su et al. 2012).

With the advent of progressively advanced modeling and observing techniques over the past few decades we have been able to further pinpoint the origins and global impacts of ENSO events. The genesis of ENSO events have been described through the "recharge-discharge oscillator" hypothesis (Jin et al, 1997ab), who relate an increase in the depth of the thermocline to westerly wind anomalies, resulting in an increased volume of warm water in the Eastern Pacific. This warm anomaly is "discharged" through poleward transport and thus induces the cold phase of ENSO through the shallowing of the thermocline depth. During warm ENSO phases, rainfall is intensified along the equatorial pacific coincident with the warmer SST and surface convergence anomalies associated with El Niño events (Kim and Yu, 2012; Ratnam et al., 2011), however, ENSO driven perturbations affect rainfall estimates differently for passive and active microwave retrieval algorithms generating regional disagreements in rainfall intensity between the TMI and PR rainfall retrievals (Figure 1.1). These TRMM rain rate differences have been related to time-dependent regional fluctuations in cloud microphysics as well as variations in large-scale environmental properties (e.g. Berg et al., 2002, 2006; Masunaga and Kummerow, 2005; Munchak et al 2012), but still remain an issue in the current TRMM record.

Time-dependent regional differences in TMI and PR rain rates become particularly significant when trying to comprehend precipitation sensitivity to global temperatures. During warm ENSO phases, the TRMM microwave radiometer, along with most reanalyses and climate models, displays increased precipitation averaged across the tropical oceans related to
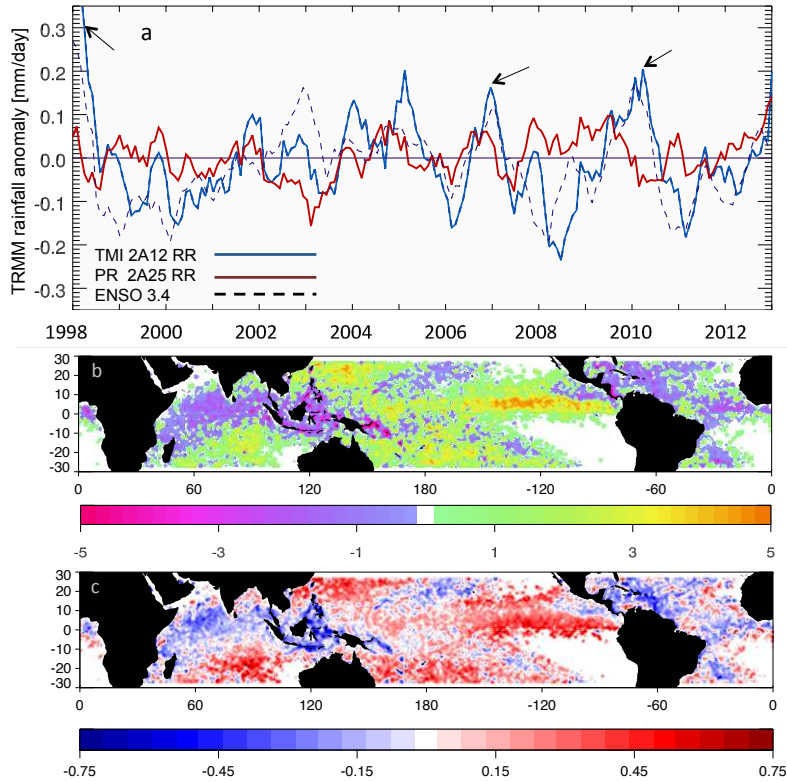
Figure 1.1 (a) Time series of tropical mean rainfall anomalies (30°N–30°S) from the TRMM PR 2A25 (red) and TMI 2A12 (blue) over the tropical oceans. Three isolated El Niño events (1998, 2007, and 2010) are highlighted with arrows. (b) Mean DJF TMI-PR oceanic rainfall differences [mm/day] for El Niño events over the TRMM mission and (c) the respective fractional difference between TMI and PR defined as (TMI-PR)/PR.

increased atmospheric convergence in the lower levels. The TRMM radar product, however, does not. Due to these dissimilarities, satellite-based observational estimates of rain rate sensitivity over the tropical oceans range from 2%/°C to 15%/°C (Liu et al., 2012; Wang et al. 2008; Gu et al. 2007), where current radiometer-based estimates of 20%/°C have been found (Robert Adler, personal communication). Further, the shorter observational record hinders a full assessment of ENSO variability in models due to large variability possible in ENSO cycles (e.g. Wittenberg, 2009); therefore, if large disparities exist between observational retrievals of precipitation in the tropics, validating model rainfall estimates becomes increasingly difficult.

4

Reconciling precipitation estimates at regional scales and global scales is necessary to establish a reliable precipitation time series, which will be essential for future model comparisons as well as aid to retrieval development for the recently launched Global Precipitation Mission (GPM) satellite (Hou et al., 2014). This dissertation focuses on evaluating the current TRMM precipitation climatology by investigating the origins for regional biases between the TMI and PR rainfall. The work combines ground validation analysis with oceanic satellite rain rate retrievals to independently assess TMI and PR precipitation biases for various precipitating systems as a function of their convective organization. The goal is to determine if the regional and tropics-wide differences in TMI and PR rainfall estimates can be explained through fluctuations between defined precipitation states, and how TRMM-GV related biases can be used to determine the expected inter-annual variability in observed rain rate intensity. The combined GV and satellite approach is outlined in the next section.

1.2 Dissertation Outline

In order to address the issues discussed above, we must not only the evaluate the individual TMI and PR rain rate retrievals, but also assess the accuracy of the rain rate retrievals implemented in satellite validation. To accomplish this, we break the research into three main sections: the analysis of ground validation techniques, ground validation evaluations of TMI and PR rainfall retrievals, and tropics-wide evaluation of precipitation bias sources to help constrain observational estimates of rain rate anomalies retrieved by TRMM. Much of the work takes advantage of new tools that had been developed throughout the TRMM mission; one in specific is a precipitation classification technique described by Elsaesser et al., (2010), who derive distinct precipitation regimes, which exhibit consistent physical characteristics across

meteorological regimes and thus offer the potential to improve estimates of rain rate retrieval uncertainties across the tropical oceans.

This dissertation is organized and presented as follows: A basic overview of introductory material has been presented in Chapter 1, however, more detailed explanations of background material will be presented in the following chapters. The bulk of the dissertation presented in Chapters 2-4 can be read as three individual manuscripts with their own respective introductions and conclusions. Chapter 2 focuses on individual rain rate retrieval methodologies commonly implemented in ground validation research and their ability to retrieve rainfall across individual precipitation regimes. The analysis describes the optimal retrieval methodologies when validating satellite-based rainfall, and also provides insight into uncertainties that may exist within previous validation efforts. The presented work in Chapter 2 was published in the *Journal of Applied Meteorology and Climatology* in Henderson et al. (2017a). Chapter 3 provides a comprehensive intercomparison of instantaneous rain rates retrieved by the TRMM TMI and PR to ground validation sources. The analysis compares TRMM rainfall to oceanic ground validation rain rates derived at the Kwajalein Atoll and ground-based rain rates during the DYNAMO field campaign. The chapter is centered on understanding the origins of rain rate discrepancies between the TRMM retrievals for precipitation types and ENSO phases and has been accepted to the *Journal of Atmospheric and Oceanic Technology*. Chapter 4 discusses the application of the results developed in Chapter 3 to examine the relationship between regional variations in precipitating systems and environmental characteristics to TMI-PR discrepancies across the tropical oceans. The chapter uses the precipitation regimes identify the physical sources leading to regional TMI and PR rainfall discrepancies and to help reconcile the relation between oceanic tropical precipitation and sea surface temperature observed within inter-annual time scales. The key findings of the dissertation are highlighted along with concluding remarks and suggestions for future work in Chapter 5.

CHAPTER 2

SENSITIVITY OF RAIN RATE ESTIMATES RELATED TO CONVECTIVE

ORGANIZATION: OBSERVATIONS FROM THE KWAJALEIN, RMI, RADAR

2.1 Introduction

Much of our knowledge of oceanic rainfall is obtained from microwave precipitation retrievals using space-borne satellite measurements. To aid in this endeavor the Tropical Rainfall Measuring Mission (TRMM, Kummerow et al., 1998) monitored precipitation systems in the tropics and subtropics with active and passive microwave sensors from November 1997 until it was recently decommissioned in 2015. The mission revolutionized precipitation measurements by including the first spaceborne precipitation radar (PR) in conjunction with the TRMM Microwave Imager (TMI). The success of the TRMM mission led to the follow-on Global Precipitation Measurement (GPM, Hou et al., 2014) Mission, which builds upon TRMM by adding an active dual-frequency precipitation radar (DPR) and passive GPM Microwave Imager (GMI) providing an extension to TRMM's long-standing climate record of precipitation measurement while extending spatial coverage to 65° N/S.

Ground validation of the TRMM and GPM missions has been continuously developed to provide benchmarks for algorithm developers that can be used to tune various assumptions required to retrieve rainfall rates (Kummerow et al., 2000; Bidwell et al., 2004; Wolff et al., 2005). Throughout the TRMM mission there have been numerous efforts to validate surface rain retrievals from TRMM TMI and PR using ground-based measurements (e.g.Wolff and Fisher 2008, 2009; Wang et al, 2013). The launch of the GPM mission embarked a new era of GV measurements focused on land, with improved ground-based instrumentation and field

campaigns (Peterson et al., 2013b; Barros et al., 2014; Wolff et al., 2015, and others). While these new campaigns will be essential to improve land-based estimates it is crucial to continue to improve rain rate validation over the oceans to include quantitative assessment of the techniques and algorithms used in GPM retrievals.

To improve oceanic validation, the KPOL radar was installed on the Kwajalein Atoll and is one of the few dual-polarized S-band radars located in an open-ocean tropical regime making it an invaluable GV site for comparison of rainfall with the TRMM and GPM precipitation radars (e.g., Houze et al. 2004; Chandrasekar et al., 2008). Recently, great effort has been made toward improving the quality of the GV measurements from the KPOL radar (Marks et al. 2009). The Kwajalein GV site is ideal for observing tropical oceanic convection due to its proximity to the intertropical convergence zone (ITCZ). Seasonal variations in the location of the ITCZ provide observations of wide variety of convective systems – particularly during the wet seasons occurring from September – December (Schumacher and Houze 2003, 2004, Houze et al., 2004). While the location is beneficial for observing a wide variety of precipitating systems, some limitations still need to be considered when evaluating satellite retrievals.

The TRMM-era KPOL operational radar-derived rain rate is obtained using radar reflectivity-rain rate (Z-R) relationship derived from the window probability matching method (WPMM, Rosenfeld et al., 1994). The Kwajalein Atoll contains six rain gauge sites that can be implemented in the derivation of radar-rain relationships. This sparse rain gauge network limits the derivation of WPMM relationships to an annual basis (Wolff et al, 2005; Wolff and Fisher, 2008). Because the WPMM Z–R relationships at Kwajalein can only be reconstructed each year, it is possible that seasonal changes in Z–R relationships are not captured by the annual WPMM Z-R, and individual events can still deviate from an annually derived mean rain rate relationship.

TRMM studies have demonstrated how shifts in meteorological regime result in variations in cloud morphology (Schumacher et al., 2004, Masunaga et al., 2006), and if ground-based retrievals are unable to capture this convective variability, pinpointing biases between GV and satellite estimates becomes more difficult to assess.

The high temporal resolution of ground validation observations provides sufficient sampling to study precipitation evolution and create a climatological representation of precipitation in the rainfall retrievals. TRMM and GPM retrievals are limited regionally to 15-20 satellite overpasses per month with only occasional overpasses containing significant rainfall (Schumacher and Houze, 2000). To be consistent with the climatological rainfall relationships, previous work quantified local biases in microwave precipitation retrievals at annual and multiannual time scales, however, the origins of the biases remain speculative and biases are highly variable when calculated month-to-month or shorter time scales (Wolff and Fisher, 2008; Wang et al. 2009). To aid this endeavor a validation procedure involving regime-based comparisons could help pinpoint sources of error at overpass timescales; connecting validation statistics to systems with similar physical properties, which can vary with monthly-seasonal shifts in meteorological regime (Berg et al., 2002, 2006). To do this we must first take steps to evaluate the performance of GV retrieval methodologies in a manner that can be linked to GV-satellite comparisons.

Due to infrequent sampling, observing regional convective variability from satellite measurements can be difficult as they provide an instantaneous snapshot of precipitation characteristics. To aid temporal limitations, cloud and precipitating systems are commonly grouped into similar convective states (e.g. Rossow et al., 2005; Nesbitt et al., 2000; Liu et al, 2007; Elsaesser et al., 2010, Houze et al., 2007; Duncan et al., 2014). Implementation of such classifications has assisted evaluation of TRMM precipitation characteristics beyond convective

and stratiform partitioning alone (e.g. Elsaesser and Kummerow, 2013; Masunaga 2012; Yokoyama et al. 2015, Barnes et al., 2015, Rassmusen et al., 2013). Recently, Elsaesser et al (2010) illustrated that clusters of convective precipitation from various organizational states were found self-similar and repeating over all tropical ocean basins. The work motivates the incorporation of precipitation regimes into the precipitation evaluation process as they provide validation statistics segregated by the precipitation regime in which they are developing. If precipitation regimes are used to assess the sensitivity of the GV products to convective variability, it provides a definitive pathway to apply results to satellite overpass comparisons.

This study aims to assess the impact of convective variability for common precipitation retrievals used in ground validation studies: WPMM – used in the operational TRMM GV products (Wolff et al., 2005), convective and stratiform partitioning, and polarimetrically-tuned Z-R approach. Specific convective and stratiform rainfall relationships can increase information content, but may not be able to fully capture physical properties between different rain events (Bringi et al, 2004). Finally, it is advantageous to use the Kwajalein KPOL polarimetric data to infer precipitation microphysics to assist retrieval assessment (Chandrasekar et al., 2008). Applying a polarimetrically-tuned Z-R relationship is beneficial as it is continually adjusted for each pixel as drop size distributions (DSD) evolve in time. By implementing the methodology described by Elsaesser et al (2010) we test if convective types influence validation statistics between radar-derived rainfall and ground gauge measurements and identify how predominant precipitation regimes influence rain rate relationships.

The procedures and data used within this analysis are provided in the following sections. Section 2.2 describes the standard TRMM products used in deriving the WPMM relationships, as well as describing the polarized-tuned rain retrieval and radar-based precipitation classification

methodology. Section 2.3 presents the results of the retrieval evaluations and concluding remarks and discussion can be found in Section 2.4.

2.2 Data sources and analysis

2.2.1 GV products

The Kwajalein GV site provides continuous radar information from the KPOL radar in conjunction with a network of ground rain gauges (Figure 2.1). The radar measurements arise from the dual-polarized S-band KPOL radar located on the southern edge of the Kwajalein Atoll. The Version 7 TRMM 2A53, 2A54, and 2A55 products for Kwajalein are utilized for this study over two wet season periods of September-November 2009 and September-November 2011 – periods where the radar is considered well calibrated within ±0.5 dB (Silberstein et al., 2008; Marks et al. 2009). Each product has a gridded horizontal resolution of 2 km × 2 km that extends 150 km from the KPOL radar site. The 2A53, 2A54, and 2A55 product provide instantaneous rain rates, classification of convective or stratiform precipitation type using the methods of Steiner et al. (1995), and 3D reflectivity fields, respectively. The 2A55 reflectivity product provides three-dimensional gridded data with a horizontal resolution of 2 km and vertical resolution of 1.5 km.

Surface rainfall measurements are collected through a series of rain gauges distributed around the atoll. The rain gauges are automated tipping bucket style and record at 0.254 mm intervals. The TRMM 2A56 rain gauge product is produced by interpolating the gauge surface rain rate measured tips into 1-minute intervals using a cubic spline–based algorithm (Wang et al., 2008). The Kwajalein gauge network consists of seven rain gauge locations on the Atoll, only six located outside the radar "cone of silence", and each location contains at least two gauges to
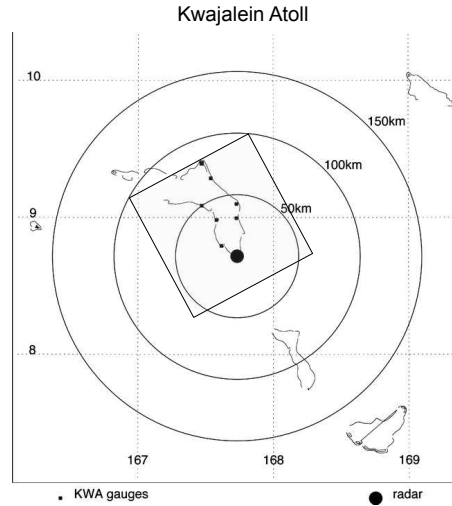
Figure 2.1 Bird's eye view of the Kwjalein Atoll with marked locations of rain gauges and radar site (adapted from Wolff et al., 2005). Radar data used for classification are contained within the overlaid 1°x1° area encompassing the atoll.

assist with quality control. For this work, if more than one gauge contains a valid rainfall estimate the gauge with the higher rain rate is used to reduce error that may occur if a gauge stops recording resulting in a reduced number of tips (D. Marks, personal comm.). Three levels of quality control procedures are implemented on a monthly basis by assessing the 1-minute interpolated rain rates (Wang et al., 2008), insuring valid radar observations (Marks et al. 2011), and through comparison with collocated radar-reflectivity data (Amitai, 2000). Monthly rain gauges observations for each gauge location that do not meet the quality control standards are not included in the analysis.

The Z–R relationships implemented in the 2A53 product are derived using the WPMM using the 1.5-km constant-altitude plan position indicator (CAPPI) level reflectivities and 7-minute rain gauge averages. The WPMM statistically matches quality-controlled reflectivities extracted from radar volume scans to gauge-estimated rain rates such that the probability distribution of the radar rain rates above the gauge is equal to that of the gauge rain rates at an annual level. The

derived 2A53 instantaneous rain-rate maps are available approximately every 10-min, corresponding to the volume scan interval of the KPOL radar. Comparison of radar and rain gauge data are only implemented if quality controlled data from both sources are valid. Data gaps associated with missing radar data are therefore not used in this study, however more than 90% of radar data were available during these time periods.

2.2.2 Radar derived products

a) Polarimetric data and rain rate estimates

Dual-polarimetric data allows the direct estimation of drop sizes used to improve rain rate retrieval accuracy (e.g. Gorgucci et al., 2000, 2001, Bringi et al., 2004, 2012). In this work we make use of the dual-polarized Kwajalein S-pol radar to provide increased information on drop microphysics and to retrieve rain rates tuned to polarimetric parameters. The Kwajalein S-Pol radar completes a volume scan, created from 18-PPI scans, approximately every 10 minutes. We utilize horizontal reflectivity Z_h (for notational simplicity we let $Z=Z_h$), differential reflectivity Z_{dr}, and the differential propagation phase K_{dp} to aid in the precipitation retrieval, and to infer information on precipitation characteristics. Detailed descriptions of the radar and improved data quality control procedures for the polarimetric data can be found in Marks et al. (2009, 2011).

This work makes use of the polarimetrically-tuned Z-R relation derived by Bringi et al. (2004). The retrieval continuously varies in space and time as storm microphysics evolves without the need to pre-classifying rain type. This procedure is based on retrieving the DSD parameters of a normalized Gamma model using polarimetric observations of Z_h, Z_{dr}, and K_{dp}. They begin with the assumption of a first-guess Z-R relationship of the form:

$$Z=aR^{1.5} \quad (2.1),$$

and adjust the coefficient, a, in Eq. 2.1 as the DSD evolves in space and time for each radar pixel. Rain rates are derived using the lowest radar plan position indicator (PPI) elevation scan and interpolated to 0.5 km. The technique has resulted in noticeably improved correlations with rain gauges while not requiring gauge data for calibration (Marks et al., 2009).

b) Classification of precipitating systems

This study, as well as throughout the rest of this dissertation, will separate precipitation into self-similar convective states following the architecture described by Elsaesser et al. (2010). Their work defined three distinct convective systems (akin to Johnson et al., 1999) through a k-means clustering methodology. The clusters were separated using TRMM PR derived echo top heights (ETH) in convective rainfall, mean rain rate of convective only precipitation, and the ratio of mean convective precipitation to the total contained in 1°x1° boxes within the TRMM PR swath. The methodology yields three tropical oceanic convective clusters further explored and interpreted in Elsaesser and Kummerow (2013) as: 1) Shallow, typically warm rain, congestus clouds with echo tops commonly below 5 km; 2) Deep unorganized convection; and 3) Deep organized convection containing substantial amounts of deep stratiform rainfall. The algorithm provides instantaneous classification of precipitation systems, which were found to be consistent in vertical structure, rainfall, and diabatic heating across meteorological regimes. This is significant, as the results from the precipitation regimes should remain consistent even for regions influenced by different synoptic conditions – providing results that can be exportable throughout the tropics.

Kwajalein KPOL GV data contain the necessary information to apply the clustering classification from a ground radar perspective. The application of the classification introduces a

novel way to identify oceanic raining systems in order to evaluate ground-based retrievals segregated by distinct precipitation regimes. Following the method described in Elsaesser et al. (2010), radar echo top heights for convective grid boxes and surface rainfall within a 1°x1° region surrounding the radar and gauge locations (shown in Figure 2.1) are input into the k-means clustering algorithm. To obtain a closer match to TRMM classification procedure, the horizontal reflectivity is averaged to a 4 km x 4 km and the vertical resolution was reprocessed from 1.5 km to 750m. Surface rain rates and precipitation identification are taken from the TRMM 2A53 and 2A54 products, respectively. All KPOL radar scans with valid QC for the two wet seasons described above are input into the k-means clustering algorithm, yielding nearly 17,000 radar volume scans containing raining cases.

2.3 Results

In the forthcoming sections we discuss the performance of the WPMM, polarimetrically tuned Z-R relationships, and convective and stratiform partitioned rainfall estimates and how the application of precipitation regimes can aid their evaluation. We first evaluate the rain estimates based on pairs of concurrent radar–gauge observations following the methods used in Wang and Wolff (2010) who compare TRMM 2A53 products with gauges at multiple time scales in Melbourne, FL. For this work, gauges are integrated to 10-minute intervals matched to the radar scan times for the precipitation regimes described above. The statistics are computed using the mean gauge rain rate from all locations and collocated radar products where both radar and gauge report non-zero rainfall. It should be noted that the rain gauges used in the comparison are not independent of 2A53 as the rain gauge data assist in creating the yearly WPMM Z-R. Dependent validation, however, is useful to assess inconsistencies in the rain rate relationship and the gauges provide a consistent reference when evaluating the rain retrievals.

Table 2.1 Rainfall characteristics from rain gauge and radar data associated with each precipitation regime for the 2009 and 2011 wet seasons. Mean rain rate and convective and stratiform information are derived using the TRMM 2A53 and 2A54 GV products. Values from Elsaesser et al., (2010) for rain rate and convective fraction are listed in parentheses.

2009	Number of cases identified	Percent of Total cases Identified	Total Gauge Accumulation	Mean Rain Rate – 2A53 [mm/hr]	Fraction of convective rainfall	Valid WPMM Windows	WPMM Windows with Rain
Shallow Convection	2832	37%	178 mm	1.7 (2.1)	1.5% (2.7%)	570	124
Deep Isolated Convection	3680	48%	1480 mm	9.6 (14.2)	5.2% (7.1%)	3083	1047
Organized Convection	1143	15%	1843 mm	44.8 (53.9)	15.1% (9.9%)	2503	1114
2011	Number of cases Identified	Percent of Total cases Identified	Total Gauge Accumulation	Mean Rain Rate- 2A53 [mm/hr]	Fraction of convective rainfall	Valid WPMM Windows	WPMM Windows with Rain
Shallow Convection	3596	39%	205 mm	1.4 (2.1)	1.4% (2.7%)	770	187
Deep Isolated Convection	4430	48%	1715 mm	12.5 (14.2)	6.6% (7.1%)	3934	1446
Organized Convection	1195	13%	1290 mm	42.6 (53.9)	17.4% (9.9%)	1840	745

Kwajalein rain gauge observations from the September-November months of the 2009 and 2011 wet seasons are used to evaluate the radar-derived rainfall products. Characteristics of the precipitation regimes and their associated gauge measurements used to derive Z-R relationships are shown in Table 2.1. The rain gauge accumulation is defined as the cumulative rainfall from all valid rain gauges over each wet season period. The wet seasons provide a subset of precipitating systems compared to what is observed annually, where intense convective systems occur more frequently. Shallow and deep convection are the most prominent precipitation types over the two seasons, however, due to the sparse nature of shallow convection, fewer cases are captured by the rain gauges. Organized systems account for the majority of accumulated rainfall measured by the gauges with higher accumulation in the 2009 wet season associated with increased frequency in precipitation during an El Niño event. Mean rain rates and convective
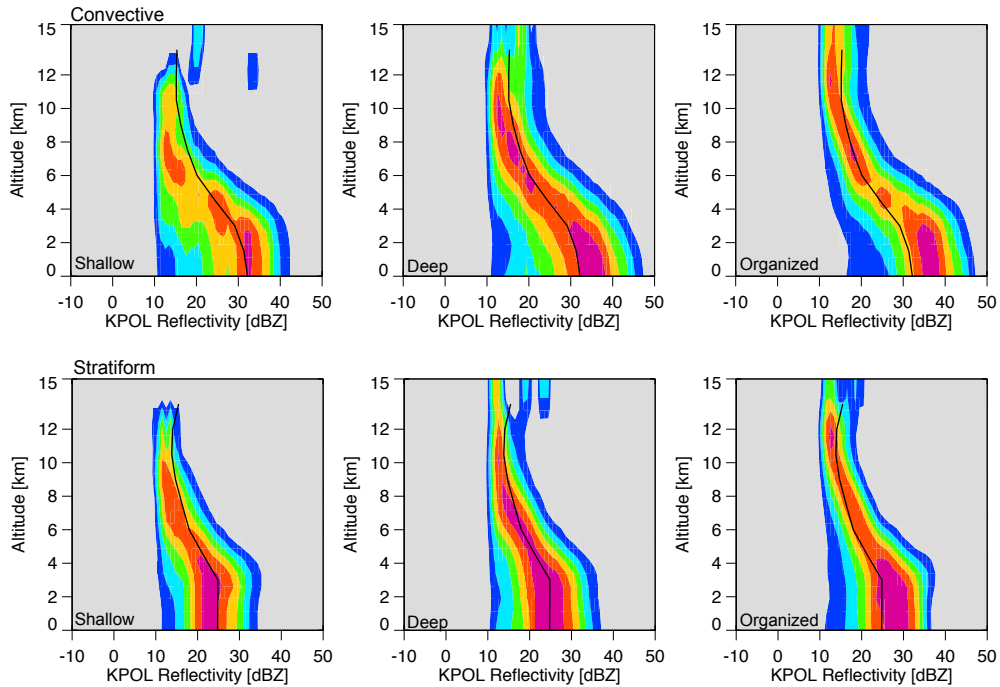
Figure 2.2 Contoured frequency by altitude diagrams (CFADs) of mean reflectivity profiles from the KPOL radar occurring for each precipitation regime split by (top) convective rainfall and (bottom) stratiform rainfall. The CFADs are created over the two wet seasons by binning by altitude every 750 m and reflectivities are binned in 1 dB increments (truncated at 10 dBZ). The mean reflectivity profile is included for each panel (solid line).

fractions, main drivers in the k-means cluster classification, are consistent with Elsaesser et al (2010) mean characteristics over the tropical oceans, however the convective fractions are slightly higher for organized rainfall regimes. The higher fraction likely corresponds to a higher frequency of embedded convective rain identified from the Kwajalein radar algorithms in stratiform areas (Schumacher et al., 2003).

The distribution of reflectivity profiles for each of the three precipitation regimes, separated into (top panels) convective and (bottom panels) stratiform rainfall type, is illustrated in Figure 2.2 using contoured frequency by altitude diagrams (CFADs). The overall mean reflectivity profile for each rain type is included to provide a visual reference when comparing the precipitation regimes. The CFADs of convective precipitation show a monotonic increase in the maximum

17
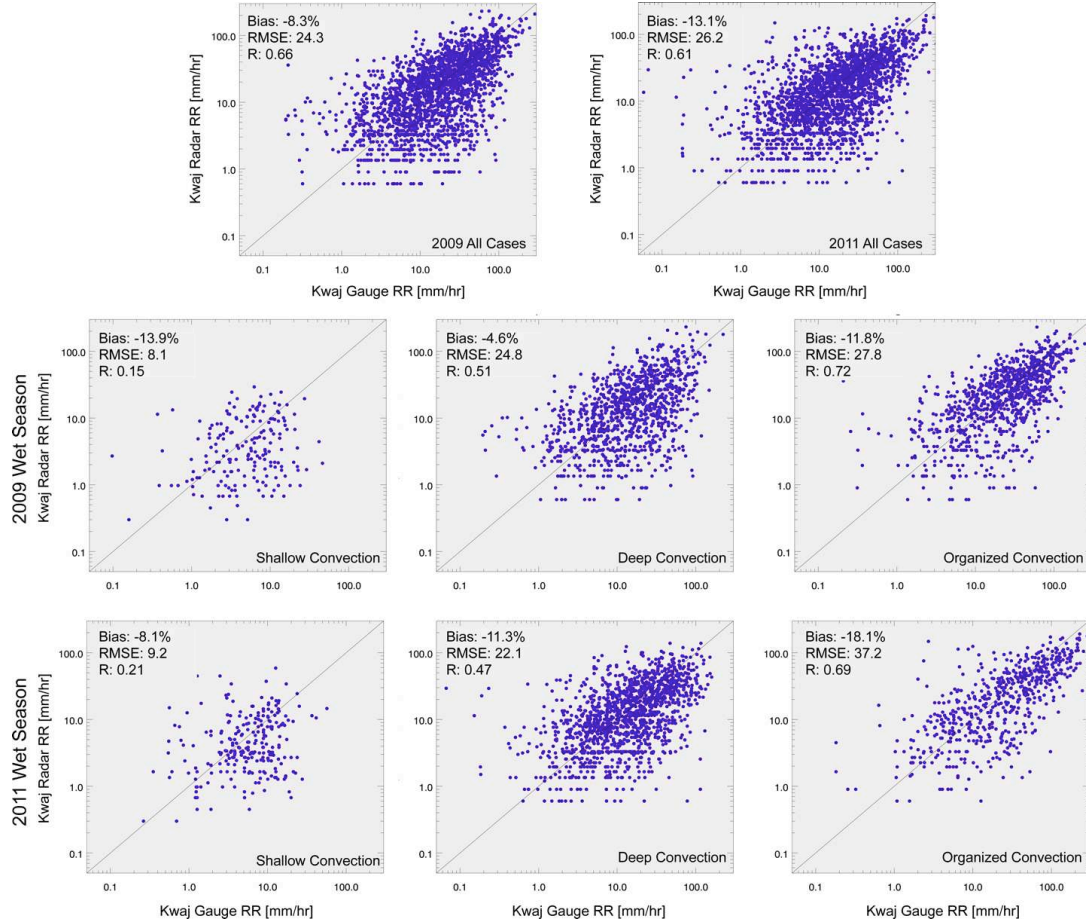
Figure 2.3 Scatterplots of KWAJ radar (2A53 product) and 10-minute integrated gauge rain rates for the 2009 and 2011 wet seasons for the shallow, deep isolated, and organized convective regimes. Comparisons are shown for (top) all regimes together and split by each precipitation regimes for (middle) 2009 and (bottom) 2011. Radar derived rain rates for the 2A53 product is found along the ordinate axis and rain gauges estimates along the abscissa. The percent bias, RMSE [mm/hr], and correlation coefficient are also shown for each panel. The precipitation regime observed for each comparison is labeled in the bottom right corner of each panel.

occurrence of near surface reflectivity as well as an increase in the maximum height attained as a function of organization. Further, similar to the Elsaesser et al. (2010) results, shallow and deep precipitation regimes contain higher frequency of shallow light raining convection near 17 dBZ below 5km in altitude. The stratiform CFADs also exhibit the monotonic increase in near surface reflectivity. While deep and organized precipitation regimes contain similar maximum heights and occurrences, the organized regimes exhibit evidence of a stronger bright band signature. It is

interesting to note that stratiform rainfall occurring in the shallow precipitation regime also contains a bright band signature, albeit occurring at much lower radar reflectivities.

2.3.1 Integrating precipitation regimes into WPMM Z-R relationships

Comparisons of rain gauge rain rates and radar-derived rain rates, segregated by the precipitation regimes, from the 2A53 product are displayed in Figure 2.3. Included in each panel is percent bias, root mean square error, and correlation between the rain gauge rain estimate and the concurrent radar retrieved rain rate. For this work the percent bias is defined as,

$$Percent\ Bias = \frac{\sum_{i=1}^{N}[R_i - G_i]}{\sum_{i=1}^{N}[G_i]}\ X\ 100\ ,\qquad (2.2)$$

where, R_i and G_i are the radar and integrated gauge derived rain rates, respectively. Large amount of scatter exists for all precipitating systems, which is expected when comparing rainfall measurements at the instantaneous time scale. In general, the relationship between radar and gauge rain rates between 2009 and 2011 are fairly consistent. While annual comparisons of radar and gauges are largely unbiased the radar derived rain rates are negatively biased overall for the wet seasons analyzed here. This is particularly noticeable during the 2011 wet season bias due to a higher frequency of heavy rainfall underestimated associated with organized convection. Bias between gauge and radar estimates are worst for organized convective events during the 2009 and 2011 wet seasons and are negatively biased by 11.8% and 18.1%, respectively. Shallow convection biases are typically largely negative, however the rain rates are lower compared to the deep convective and organized precipitation regimes. Deep convection and organized convection contain nearly equal cases above and below the one-to-one line, but positively biased rain rate comparisons occur at much lower rain rates. Negative biases for deep and organized
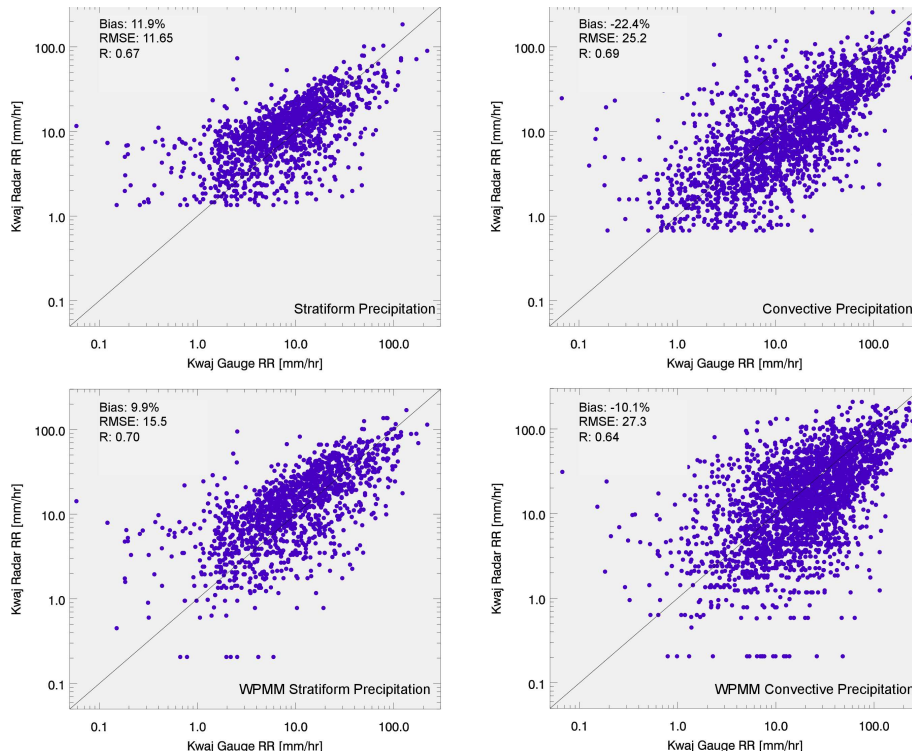
Figure 2.4 Scatterplots of radar derived rain rates and 10-minute integrated gauge rain rates for the 2009 and 2011 wet seasons split into convective and stratiform precipitation type as derived from the TRMM GV 2A54 product. Comparisons are shown for (top) a convectional power law Z-R relationship derived from the KWAJEX field campaign and (bottom) for the TRMM GV 2A53 rainfall product derived using the WPMM. Radar derived rain rates are found along the ordinate axis and rain gauges estimates along the abscissa. The percent bias, RMSE [mm/hr], and correlation coefficient are also shown for each panel. The precipitation type observed for each comparison is labeled in the bottom right corner of each panel.

precipitation regimes are driven by underestimation at higher rain rates. Above 10 mm hr^{-1} (~76% of cases) nearly 80 percent of radar estimates are underestimated with biases of -28% for deep convection and -35% for organized convection. This is significant as the majority of rainfall accumulation is accounted for by these two regimes.

Rao et al. (2001) relate the overestimation of lighter rainfall and underestimation by more intense rainfall derived from a single Z-R relationship directly to stratiform and convective rainfall. To examine this, all precipitation regimes in 2009 and 2011 are separated into convective or stratiform components using the TRMM 2A54 classification (Figure 2.4). We first examine biases using a conventional Z-R relationship of $Z = 175R^{1.5}$ derived from the Kwajalein

Atoll Field Experiment (KWAJEX, Fiorino 2002). Clear separation in biases in stratiform (+12.9%) and convective rainfall (-22.4%) is observed. These biases are larger in magnitude compared to the WPMM, which was designed to better capture climatological rain rates; however similar separation in biases still exist as well for convective (-10.1%) and stratiform (+9.9%) rainfall demonstrating that WPMM relationships do not contain the information required to fully capture the DSD variability between the different precipitating types. While convection is negatively biased overall, large scatter exists largely from isolated deep convective comparisons. When comparing convective rain rates < 30 mm hr^{-1} for deep isolated precipitation regimes the radar derived rainfall overestimate gauges by 6.2%. This lighter rainfall is typical during the dry season months and may provide explanation for the unbiased result on the annual level.

The overall negative biases observed for both wet seasons seem to be weighted by the underestimation of convective precipitation in organized convective systems. The differences in rainfall products are regulated in terms of frequency of occurrence by the convective events. The biases are a direct result of the increased occurrence of intense rainfall during the wet season time period that cannot be captured by the WPMM relationship and is a pattern that should be consistently observed for a given wet season period at the Kwajalein site. This effect of sampling at a sub-year time scale could be even further amplified when comparing GV and satellite measurements are compared on a sampling scale closer to satellites. When reducing the temporal scale to 12-48 hours (not shown) we found the bias estimates to be variable dependent on the occurrence of the individual precipitating regimes. This temporal aspect is not the only concern as the sparse rain gauge distribution can complicate error statistics as well (e.g Habib and Krajewski, 2002). To better understand the impact the precipitation regimes impart on rain rate

estimates, a spatially and temporally matched comparison is ideal. The dual-polarization availability from the KPOL radar provides spatially and temporally matched data – offering further insight into how much the WPMM estimates may miss in the shorter-term due to convective variability.

2.3.2 KPOL polarimetric estimates

Retrieving rain rates using the dual-polarized KPOL data is advantageous as the retrievals are fully independent of the rain gauges and do not require convective and stratiform separation. For this reason the TRMM-GPM GV office has recommended increased use of dual-polarimetric rainfall retrievals in precipitation validation (Peterson et al., 2013a). For this reason, it is essential to also assess polarimetrically tuned rain rate estimates with ground gauges to understand where uncertainties may occur and how they may relate to the WPMM results. Further, dual-polarimetric measurements from the KPOL radar can be used to understand microphysical differences in precipitation regimes as well as reveal precipitation variability that may be missed by the annually derived WPMM for each precipitation regime. The polarimetrically tuned rain rates are compared with the ground gauges, in a similar manner as the above section, for each precipitation regime and wet season (Figure 2.5). The dual-polarimetrically tuned rain rates are manipulated by DSD parameters on a gate-by-gate instantaneous manner providing improved validation statistics with the ground gauge measurements compared to the annual WPMM derived rain rates. Bias, RMSE, and correlations (0.89 in organized convection) with gauges are improved for each case during both wet seasons; however, significant outliers do exist in the comparisons. With the exception of organized convection in 2011, biases from the polarimetrically tuned rain rates are below 10% demonstrating overall improvement.
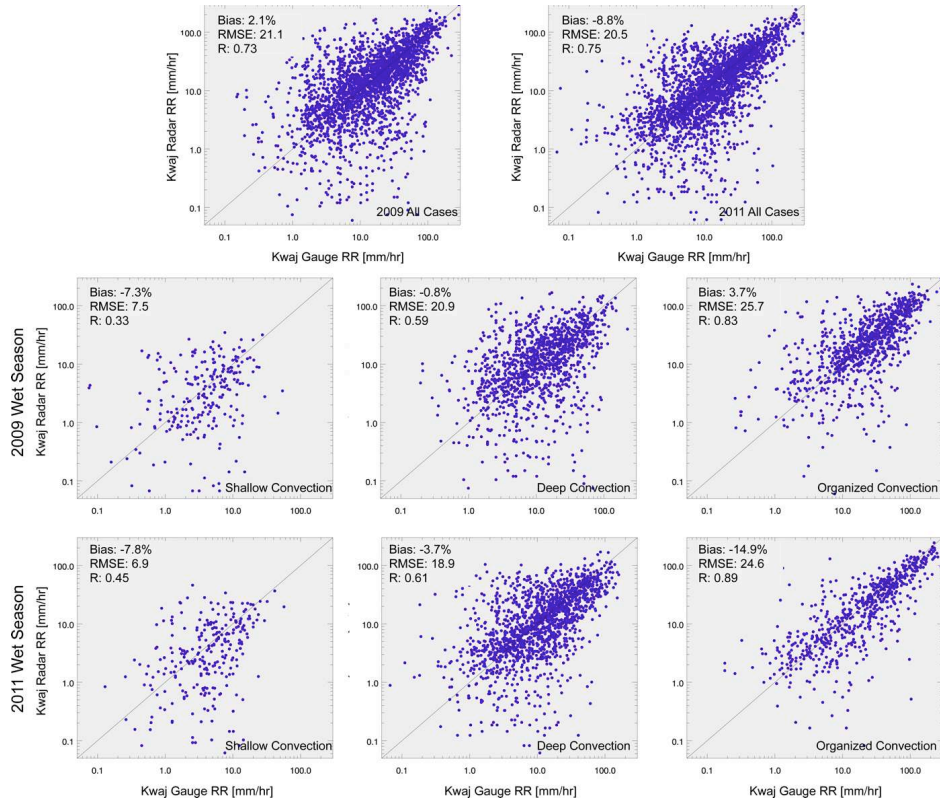
Figure 2.5 Same as Figure 2.2 except for polarimetrically tuned rain rate estimates occurring over both wet seasons.

The reduced RMSE, particularly in 2011, validates that DSD variation is likely driving the large amount of scatter found in the WPMM comparisons. For example, in higher rates the rain rate retrieval incorporates K_{dp} to help differentiate DSDs and seems to be an important factor in improving comparisons with the gauges. Negative biases for the organized regimes are caused by a few extreme rainfall events, but still show improvement compared to the annual WPMM estimates. Removal of these events yields bias estimates similar to the 2009 wet period, however it is difficult to differentiate if the large negative bias are noise related to outliers. Slight underestimation of rain rates exist in deep isolated precipitation regimes with biases reduced to -0.8% in 2009 and -3.7% in 2011. Overall, the retrieval demonstrates the ability to capture rainfall variability from the regimes and is beneficial as the methods are independent of rain gauges and precipitation type partitioning. The retrieval described by Bringi et al. (2004) is one

of many ways of deriving rainfall from dual-polarimetric data, however the improved error statistics found in these comparisons provide a strong foundation in how the DSD information content is useful when evaluating the retrieved rainfall.

The polarimetrically tuned rain rate retrieval provides rain estimates for each grid box throughout the 1°x1° classification region. The increased spatial sampling is beneficial to examine regime-based precipitation variability that may be missed by the WPMM relationships through the use of the matched radar reflectivity-rain rate pairs. To observe precipitation variability that may be missed by WPMM, rain rate-reflectivity relationships are examined for all wet season data using 2D histograms colored by frequency of occurrence for each regime (Figure 2.6). To aid in this visualization, convective and stratiform power law relationships (described in Thompson et al., 2015) and the TRMM 2A53 annual WPMM Z-R relationships are also plotted to help illustrate the scale of variability occurring when evaluating each regime. In general, the large amount of variability throughout each radar reflectivity bin indicates the range of rain rates the annual WPMM relationships are unable to capture during the wet seasons. The radar-rain pairs in Figure 2.6 provide additional evidence that the annual Z-R WPMM relationships generally overestimate stratiform precipitation (bottom panels) and underestimate convective rainfall (top panels), most notable in the deep isolated and organized regimes. In stratiform rainfall, radar-rain pairs are generally located to the left of the annual WPMM relationship and whereas convective rainfall radar-rain pairs are generally located to the right of the annual WPMM relationship, particularly at higher rain rates. Unique characteristics emerge for the predominant areas of occurrence within each regime. In stratiform rainfall there is a clear shift in occurrence and variance in the radar rain pairs for each precipitation regime. Radar-rain pairs within the
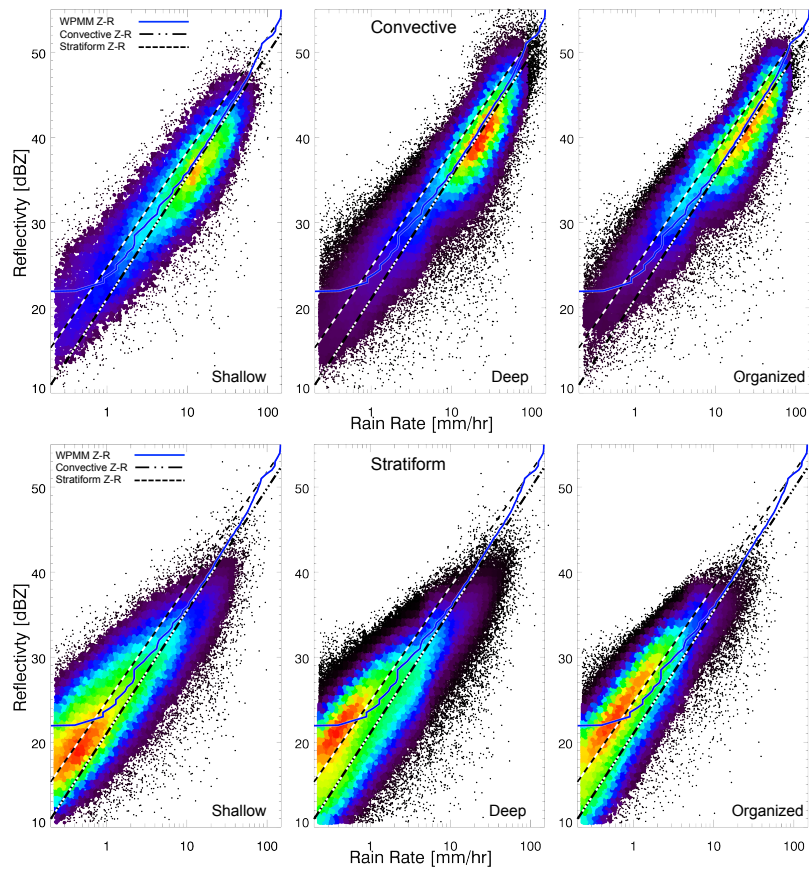
Figure 2.6 Density plots, combined from both wet seasons, of concurrent rain-radar observations from the KPOL radar. Rain estimates (abscissa) are derived using the methods of Bringi et al (2004) and are taken from the lowest PPI scan of the radar and matched with the (ordinate) 1.5 km radar reflectivity measurements. Each precipitation regime is split into (top) convective only rainfall and (bottom) stratiform only rainfall. Data plotted are taken from valid radar matches within the 1°x1° area shown in Figure 1.1 The 2009 annual WPMM (solid) and convective (stratiform) Z-R relationships [broken line: upper (lower)] are displayed for reference. Colors indicate frequency and are normalized to illustrate percent of maximum occurrence.

organized regimes contain increased occurrence of heavier raining stratiform precipitation where points lie to the left of the WPMM relationship line for $Z < 35$ dBZ. For convective rainfall, the majority of radar-rain pairs in deep isolated regimes lie to the right of the WPMM relationship line for $Z \sim 40$ dBZ indicating higher rain rates for a similar reflectivity. Similarly, radar-rain pairs within the organized regimes lie to the right of the WPMM relationship, however, the highly occurring points extends toward 50 dBZ where the radar-rain pairs begin to converge toward the WPMM relationship.
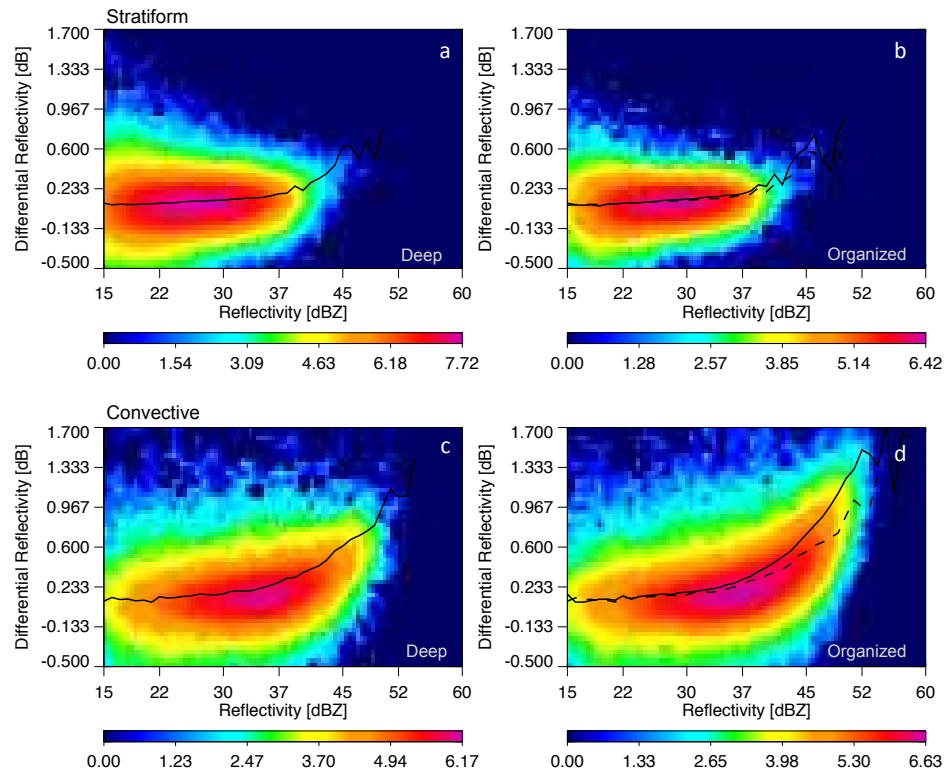
Figure 2.7 Density plot displaying the frequency of occurrence plots of Z_{dr} for a given Z, where Z is binned in 0.5 dBZ increments. The panels include data from the 2009 wet season for (a) stratiform rainfall occurring in isolated deep precipitation regimes, (b) stratiform rainfall occurring in organized precipitation regimes, (c) convective rainfall occurring in isolated deep precipitation regimes, and (d) convective rainfall occurring in organized precipitation regimes (d). Mean Z_{dr} is included for each bin (solid line). Mean Z_{dr} for deep isolate precipitation regimes are included in the right panels to aid visual comparison (dashed line). Color scale is shown in log(number).

The polarimetric variables can also be used to further explore differences in convective and stratiform precipitation characteristics related to these regimes. We utilize reflectivity Z (dBZ) and Z_{dr} (dB) from the lowest interpolated level to infer differences in the median drop size between the precipitating systems in the 2009 wet season [in a similar manner as Bringi et al., (2012)]. Figure 2.7 shows the frequency of occurrence of Z_{dr} for a given Z for raining pixels occurring in deep isolated and organized regimes. The solid line indicates mean Z_{dr} for reflectivity bins of 0.5-dBZ widths and the mean Z_{dr} for deep isolated regimes are repeated in the

organized regime panels to aid visual comparison (dashed line in Panels b,d). For convective rainfall, light rainfall ($Z < 20$ dBZ) has a high occurrence near 0 dB in Z_{dr} indicating that these cases are likely drizzle or light rainfall associated with shallow convection with smaller spherical drops. For both stratiform and convective rain, there are small differences in Z_{dr} between the regimes from 20 dBZ $< Z <$ 30 dBZ. This suggests that differences found in the rainfall relationship in this reflectivity not be largely attributable by mean drop diameter, but instead the number concentration (Steiner et al, 2004b; visualized in Fig. 19 Thompson et al. 2015). Differences in convective rainfall occurring in deep isolated regimes and in organized regimes seem to be attributable to an increase in median drop size, as indicated by higher Z_{dr}, for $Z > 35$ dBZ. This is illustrated by the divergence of mean Z_{dr} values in panel d, where beginning at 35 dBZ, mean Z_{dr} values for the organized regime (solid line) continually diverge from the Z_{dr} values associated with rainfall occurring in deep isolated regimes (dashed). This disparity in median drop size indicated by the regimes may be useful in the validation of satellite-based rainfall as DSD variability has been demonstrated as a source of uncertainty in rain rate retrievals (Munchak et al., 2012).

2.3.3 Regime-based relationships

Over the oceans, biases found between satellite derived rainfall products have been directly related to discrepancies in the characteristics in raining systems and variability in the synoptic meteorological conditions (Berg et al. 2002, Berg et al. 2006). To relate precipitating systems across regions, validation efforts commonly group precipitating systems by their physical characteristics, such as size or rainfall intensity, or by segregating rain rate comparisons into convective and stratiform components; however, WPMM methodologies and convective and

stratiform partitioning may need to be redefined regionally across the tropics. Therefore, understanding rain rate relationship sensitivity to the individual precipitation regimes is an important factor.

Regime-based rain rate relationships are derived specifically for the WPMM and convective/stratiform Z-R relationships to assess how sampling of the individual regimes influences rain rate relationships. The above section demonstrated that polarimetric data prove to be a useful tool for understanding the variability missed by the WPMM relationships. In the following sections, rain rate relationships will now be compared to the spatially and temporally matched polarimetrically tuned rain rate estimates. Because the self-similar regimes are represented in terms of their distribution of clouds and precipitation within a 1°x1° region, the polarimetrically tuned rain rates allow an independent assessment using all raining pixels in the 1°x1° region – providing a comparison that is representative of the precipitation characteristics associated within each precipitation regime. Statistics between the rainfall estimates will be presented as before, with the polarimetrically tuned results used as reference.

a) Regime-Derived WPMM relationships

The results thus far have demonstrated the issue of applying an annual WPMM Z-R to instantaneous data. For a given radar derived rain rate, a multitude of solutions exist from the gauges as well as the polarimetrically tuned estimates (as shown in Figure 2.3 and 2.5). The results show that regime occurrence may help to regulate overall biases, but they do not fully demonstrate the direct impact each regime has on the WPMM rain rate relationships. This can be further examined through derivation of rain relationships for individual precipitation regimes; demonstrating the error that may occur in GV comparisons if only a single precipitation regime is sampled. By re-deriving the WPMM relationships for each precipitation regime we can get a

28
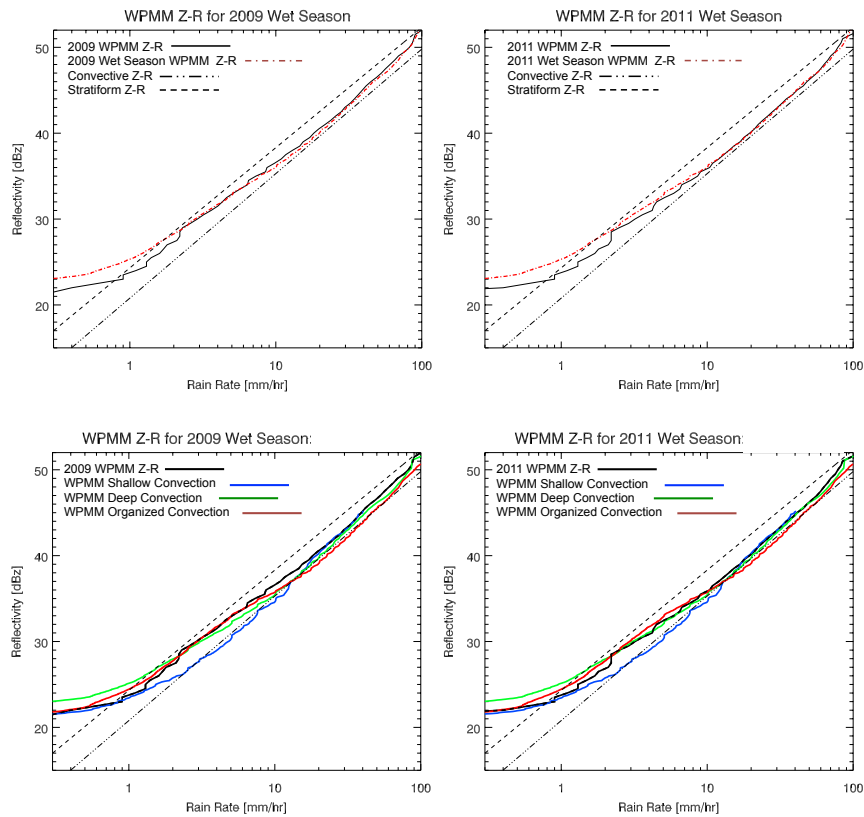
Figure 2.8 Z-R relationships derived using the WPMM for (top) all data in the 2009 and 2011 wet seasons (red dashed) and their respective annual WPMM relationship (solid). The wet season relationships are then derived for (bottom) the individual precipitation regimes. In the bottom two plots line colors are representative the annual WPMM relationship (black) and the regime types: Shallow precipitation regime (blue), deep isolated precipitation regime (green), and organized precipitation regime (red).

sense of the error that may occur in the GV product at the instantaneous level.

Z-R relationships are created for each convective state using the WPMM using combined data from the 2009 and 2011 wet seasons (Figure 2.8). The majority of annual rainfall occurs during the Kwajalein wet season (Houze et al., 2004), therefore, each precipitation regime meets the rain gauge accumulation (Table 2.1) requirements set by Rosenfeld et al. (1994) to produce stable Z-R relationships. Data points from all three precipitation regimes are first included in the WPMM
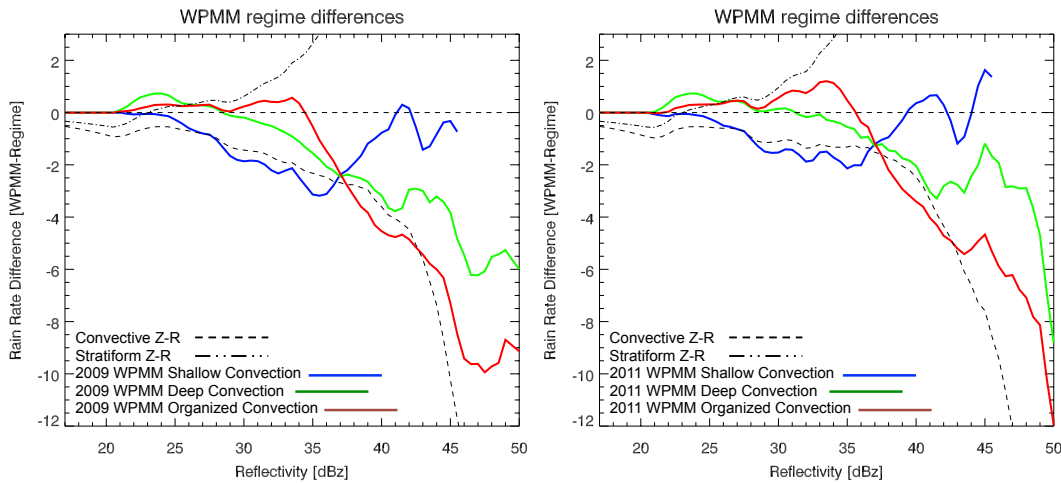
Figure 2.9 Deviations (Regime WPMM-Annual WPMM) between the regime-based WPMM Z-R relationships and the annually derived WPMM Z-R Relationships for all data in the 2009 and 2011 wet seasons displayed in the bottom panels of Figure 7. Line Colors are representative of the regime types: Shallow convection (blue), deep isolated convection (green), and organized convection (red). Deviations with convective (stratiform) Z-R relations are shown for reference [broken line: lower (upper)].

derivation and produce a WPMM Z-R relationship qualitatively similar to the annual WPMM results; however, application of the WPMM to the individual precipitation regimes yields three more distinctive Z-R relationships, where deep isolated and organized regimes are similar in structure, but become separated at higher rain rates > 10 mm/hr. The regime-derived Z-Rs qualitatively resemble the data occurring most frequent in radar-rain rates pairs displayed in Figure 2.5 and the spread in the regime-based relationships illustrates possible uncertainty within the WPMM retrieval that could be observed if in the absence of precipitation regime based validation.

Rain rate deviations between the wet season regime-based WPMM and the annual WPMM relationships illustrate the extent of rain rate differences for a specified reflectivity in the Z-R relationships (Figure 2.9). Similar to the rain gauge results, the annual WPMM relationships overestimate light rain, particularly when identified as stratiform, and underestimates from

intense convective rain, and nearly always underestimates rain from shallow convection. The largest differences occur with higher rain rates from organized precipitation regimes where rain rate retrievals differ up to 10 mm hr^{-1} at Z > 40 dBZ - near the edge of radar-rain rate occurrence in the polarimetrically tuned and convective-stratiform partitioned estimates (described in the next section). Deep isolated rainfall becomes negatively biased by 2-4 mm hr^{-1} from 35 dBZ < Z < 40 dBZ, where radar-rain rate pairs are more common for the precipitation regime. This pattern of larger rain rate disparities at higher rain rates, as convective intensity increases, is echoed in the rain gauge biases described in Section 2.3.1. Minor differences in the rain rate deviations exist between the two wet seasons related to the precipitating system characteristics observed annually by the radar and rain gauges. For example, the 2009 annual WPMM improves the representation of light stratiform rainfall compared to the 2011 wet season, as this type of rainfall occurs more frequently near the West Pacific during El Niño events (Masunaga et al, 2005; Schumacher et al. 2003, 2004). The accuracy of these deviations can be assessed through an independent comparison with the polarimetrically tuned rain rate estimates and if accurate the bias for all convective states should reduce toward zero.

Rain rates for the 2A53 product and the regime-based WPMM are compared to the polarimetrically tuned rainfall estimates (Table 2.2). Comparison using the 2009 and 2011 wet season WPMM Z-R relationships reveals marked improvement with polarimetrically tuned estimates for all cases. The lower biases compared to the 2A53 comparisons instill confidence in the magnitudes of the regime-based deviations; however, the RMSE among the regimes remain nearly identical as the annual WPMM results. The deviations found between the regime-based WPMM and annual WPMM relationships confirm that the Z-R relationship is limited in its

Table 2.2 Validation error statistics for regime based Z-R relationships over the 2009 and 2011 wet seasons. Values are first compared for the 2A53 annual WPMM relationships [top section (2A53 minus polarimatrically tuned estimates)] and then using regime derived WPMM relationships [bottom section (Regime-based minus polarimatrically tuned estimates)].

	2A53 - Pol	All Cases	Shallow Regime	Deep Isolated Regime	Organized Regime
2009	Bias [%]	-12.6	-23.6	-16.3	-11.8
	RMSE [mm hr^{-1}]	9.7	10.1	8.5	10.8
2011	Bias [%]	-7.4	-16.4	-12.0	-6.7
	RMSE [mm hr^{-1}]	9.1	9.3	8.7	9.3
	Regime - Pol	All Cases	Shallow Regime	Deep Isolated Regime	Organized Regime
2009	Bias [%]	-3.2	-5.9	-4.7	-1.3
	RMSE [mm hr^{-1}]	9.2	8.3	8.2	11.7
2011	Bias [%]	+1.2	3.2	-3.7	+0.4
	RMSE [mm hr^{-1}]	8.8	8.4	9.6	8.8

ability to represent convective variability. The reduction in bias in both wet seasons found when using the precipitation regimes demonstrates that the errors between the rainfall product are likely consistent over time. It is also important to note, that while not shown, the reduction in error is largely found in convective rainfall while stratiform rainfall remains positively biased by a few percent. While TRMM-GPM GV office produces a convective and stratiform partitioning (based on Steiner et al., 1995), the operational 2A53 product has no classification or rain-type clustering included. However, the large amount of scatter found in the convective rainfall comparison (Figure 2.4) suggests that even climatologically derived convective and stratiform relationships will struggle to fully capture precipitation variability. This enforces the findings of Elsaesser et al. (2010) who found precipitation characteristics to be dissimilar between precipitation regimes for convective cores of equal vertical depth and rain rate. It is reasonable to extend the study of the precipitation regimes to further investigate their impact on radar-rain rate relationships that improve representation of DSD variability associated with convective and stratiform rain types.

b) Convective and Stratiform Z-R Relationships

Power-law relations are commonly developed to relate radar reflectivity to rain rate for characteristic modes of DSD variability in convective and stratiform regions – such as implemented in the TRMM-GPM radar retrievals (Iguchi et al., 2000, 2010). For this reason, it can be useful to study satellite biases as a function of their convective and stratiform components (e.g. Liu and Zipster 2014, Seo et al 2007, Rasmussen and Houze, 2013), however, we do not understand if these relationships are able to fully capture oceanic precipitation variability associated within defined regimes. To better understand this, convective and stratiform relationships are derived specifically for the 2009 wet season and for the deep isolated and organized regimes and then compared to the polarimetrically tuned estimates. Understanding the sensitivity of the convective and stratiform Z-R relationships provides another measure of the information present in the regimes that can be used in validation to help isolate error estimates.

Convective and stratiform Z-R relationships are derived using matched pairs of radar and rain gauge data averaged over three minute intervals centered on the radar scan time. Data from the 2009 wet season are used to derive the relationships for deep convective and organized precipitation regimes and the TRMM GV 2A54 convective and stratiform classification product partitions rain rates. Due to possible spatio-temporal differences that occur between gauge-radar comparisons, rain rate and reflectivity information are only utilized if the nearest neighboring pixels share the same precipitation type. This helps to minimize "leakage" that may occur in defining rain rates from one precipitation type to the other when calculating the Z-R relationships. To start, we use orthogonal linear regression to derive the power-law relationships to help minimize errors in the R and Z directions perpendicular to the best-fit line (Campos and

Zawadzki, 2000). The relationships are applied to the KPOL reflectivities and compared to the matched polarimetrically tuned estimates, providing an independent comparison of the rain rates.

Overall, convective and stratiform relationships for all raining systems agree well with estimates from the DYNAMO field experiment (Thompson et al. 2015), which is not surprising as the two studies are climatologically similar. Clear separation exists between the convective and stratiform relationships (Figure 2.10). These relationships can vary when gauges are integrated over different time scales (Steiner et al., 2004a), however the overall result for each case remains similar. Error statistics comparing polarimetrically tuned rain rates and the derived convective and stratiform Z-R relationships are shown in Tables 2.3 and 2.4. The derived relationships perform well over all precipitating systems with the biases between the gauges and radar-derived convective and stratiform power-law relationships of a few percent. The derived Z-R relationships seem to capture the majority of rain rate-reflectivity pairs partitioned by the TRMM GV 2A54 product providing proper separation of DSD variability that the operational WPMM could not. The RMSE still remains similar to the WPMM methods pointing to variability in rainfall still unaccounted for. This becomes more evident when the Z-R relationships are further defined by each precipitation regime.

Figure 2.10 Z-R relationships for (top) convective and (bottom) stratiform events derived using orthogonal linear regression best-fit line from the 2009 wet season. Colors indicate frequency and are normalized to illustrate percent of maximum occurrence.

35

Table 2.3 The Z-R relationship equations and their parameters derived for the convective and stratiform rainfall at the Kwajalein Atoll. Parameters are shown for all systems and specifically for deep isolated precipitation regimes and organized precipitation regimes.

	Parameter	Convection Only	Stratiform Only	Convection-Deep Isolated	Convection-Organized	Stratiform-Deep Isolated	Stratiform-Organized
Derived Z-R ($Z = a\mathrm{R}^b$)	a	125	265	150	99	239	282
	b	1.44	1.42	1.35	1.52	1.4	1.45

Table 2.4. Validation error statistics for Z-R relationships derived specifically for convective and stratiform rainfall. Values are first presented using all convective and stratiform data (top section) and then using regime specific relationships (bottom section).

All Data	All Convection	All Stratiform	Convection-Deep Isolated	Convection-Organized	Stratiform-Deep Isolated	Stratiform-Organized
Bias [%]	-1.2	-0.84	+4.2	-8.7	-3.6	+3.9
RMSE [mm hr^{-1}]	11.2	4.7	10.0	12.4	3.9	4.8
Regime	All Convection	All Stratiform	Convection-Deep Isolated	Convection-Organized	Stratiform-Deep Isolated	Stratiform-Organized
Bias [%]	-0.8	-0.74	+0.6	-1.6	-2.1	+1.1
RMSE [mm hr^{-1}]	11.1	4.7	10.9	11.3	4.1	5.0

Using the methodology above, convective and stratiform relationships are partitioned by the regimes (Figure 2.11). Differences are most notable with convective cases where data points from the deep isolated convection more-or-less straddle the convective power law, however while there is overlap, the largest frequency bins in organized convective rainfall are found to be somewhat separated. Compared to the polarimetrically tuned estimates, the single convective Z-R relationship is biased high for deep convective systems and biased low for organized convection for 2009 by +4.2% and -8.7%, respectively. The most frequently occurring points captured by the gauges in organized convection lie to the right (below) the Z-R relation derived for all convective cases and deep isolated convective points lay on or slightly to the left (above) the Z-R relation. The differences in the stratiform cases are not as high in magnitude with organized systems negatively biased and the deep convective systems positively biased. The segregated cases indicate that regime specific information may help to better represent the offset data points from
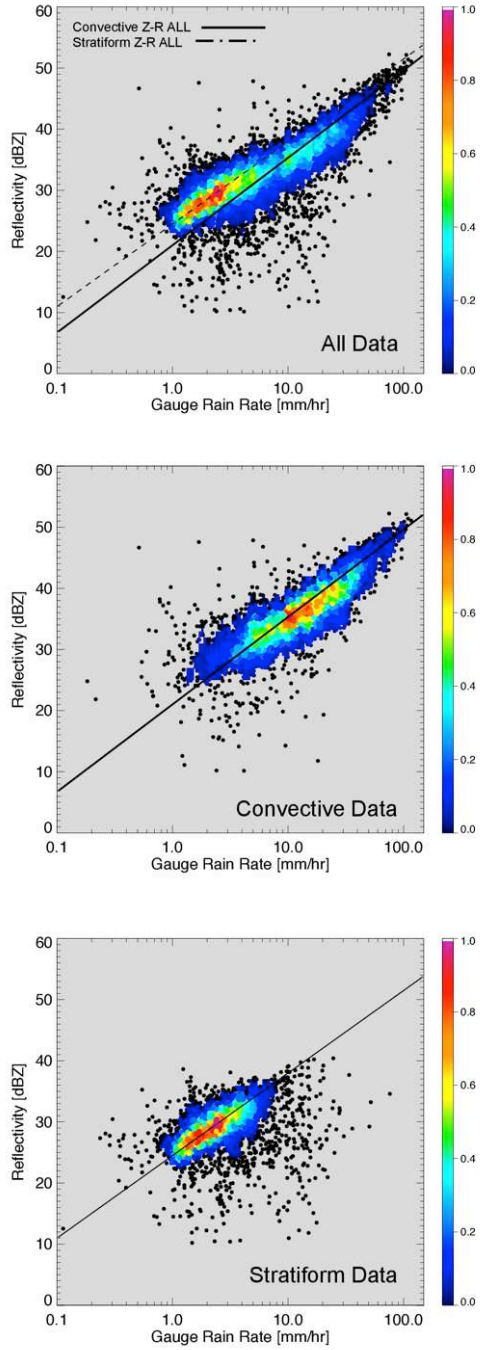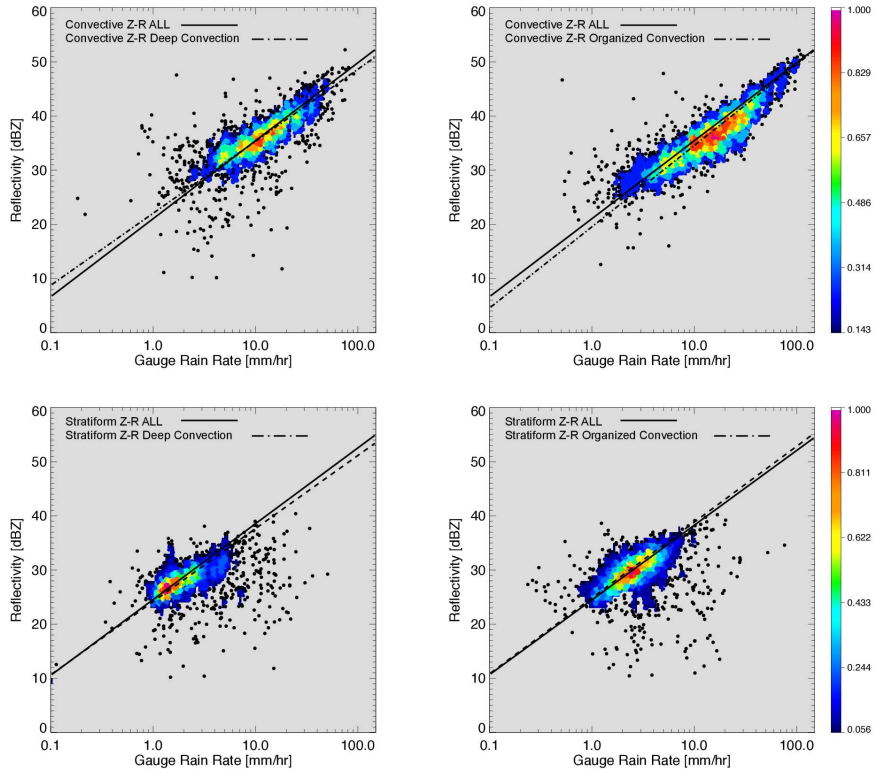
Figure 2.11. Z-R relationships for (top) convective and (bottom) stratiform events derived using orthogonal linear regression best-fit line from the 2009 wet season. The relationships are now segregated into (left) the isolated deep and (right) organized precipitation regimes. For each panel the regime-based convective or stratiform Z-R relationships (dashed) are displayed along with the overall convective or stratiform Z-R relationship (solid) from Figure 9 included as reference. Colors indicate frequency and are normalized to illustrate percent of maximum occurrence.

the single convective and stratiform Z-R relationships. To test this, the convective and stratiform relationships are re-derived specifically for the deep isolated convective and organized regimes. The regime-based convective and stratiform Z-R relationships are shown with dashed lines in Figure 2.11. The regime relationships provide better fits for both precipitation regimes as demonstrated by the reduced bias in Table 2.4. The new relationships reduce the bias for all cases with the relationship specific to organized convection reducing the strong negative bias to 1.6%.

The resulting reduction in error is significant as it demonstrates that uncertainty in the WPMM methodology cannot be removed by the introduction of convective and stratiform relationships; even with convective and stratiform partitioning the precipitation regime dependence remains an important element to consider. Using convective and stratiform relationships for GV may be an overall improvement compared to operational application of TRMM-GV WPMM, however, season-to-season GV evaluations may not be robust, as precipitation regime occurrence will vary spatially over time. When evaluating satellite and GV products, the physically relatable precipitation regimes provide improved information content on rain estimation sensitivity that would go unnoticed if precipitating systems were not segregated. The differences found between the regimes are not simply from random storm-to-storm variability, but instead to direct differences in the precipitation microphysics between the two regimes (as described in Section 3.2). Changes in precipitation microphysics have been theoretically shown to alter Z-R relationships (Steiner et al., 2004b) and have been found in individual case studies previously at the Kwajalein Atoll (Bringi et al., 2012).

2.4 Conclusions and discussion

Ground validation is an essential component of the TRMM-GPM missions to aid in the evaluation of rain rate retrievals derived from spaceborne satellite observations. This study presents a novel approach to evaluate oceanic radar-rain rate estimates through the introduction of self-similar precipitation regimes. The regimes, identified using a clustering analysis first described by Elsaesser et al. (2010) and Elsaesser and Kummerow (2013), segregate the rain rates comparisons to evaluate the regime-based variability in rainfall estimates derived from WPMM, and polarimetrically tuned rainfall, and convective and stratiform partitioned Z-R. This

methodology is advantageous as it can quantitatively distinguish the contribution of error in GV and satellite-based rain rate retrievals related to the defined precipitation regimes, which are consistent over the tropical oceans.

To understand how precipitation regimes can impact GV efforts, the regimes are first implemented to test if GV products can capture convective variability during the wet season months of September-November for 2009 and 2011. The TRMM 2A53 product and polarimetrically tuned estimates are compared with spatiotemporally matched quality-controlled gauge rain rates located on Kwajalein atoll segregated by each regime. The 2A53 rain rates relative to the ground gauges underestimate all wet season precipitating systems by 9.3% in 2009 and 13.1% in 2011; these underestimates are largely related to the organized convective systems where biases at higher rain rates reach 35%. The annual WPMM relationships used in the 2A53 product typically overestimate stratiform rainfall and underestimate shallow convective rainfall. The polarimetrically-tuned rainfall estimates revealed improved biases compared to the 2A53 product as well as increased correlations with gauges and a reduction in scatter as evidenced in reduced RMSE values. Further, polarimetrically tuned radar-rain rate pairs demonstrate a multitude of solutions that cannot be captured by the 2A53 WPMM estimates, which are seemingly consistent between the two wet seasons. In particular, deep isolated convection is commonly underestimated for $Z > 30\text{--}40$ dBZ and similar for organized convection with underestimations extending toward more extreme rain rates where $Z > 40$ dBZ.

The regimes are then used to identify how predominant regimes may influence WPMM and convective/stratiform rain rate relationships. WPMM Z-R relationships are first derived specifically for each individual regime. WPMM Z-R relationships derived for rainfall occurring in shallow precipitation regimes highly resemble that of a convective Z-R power law

39
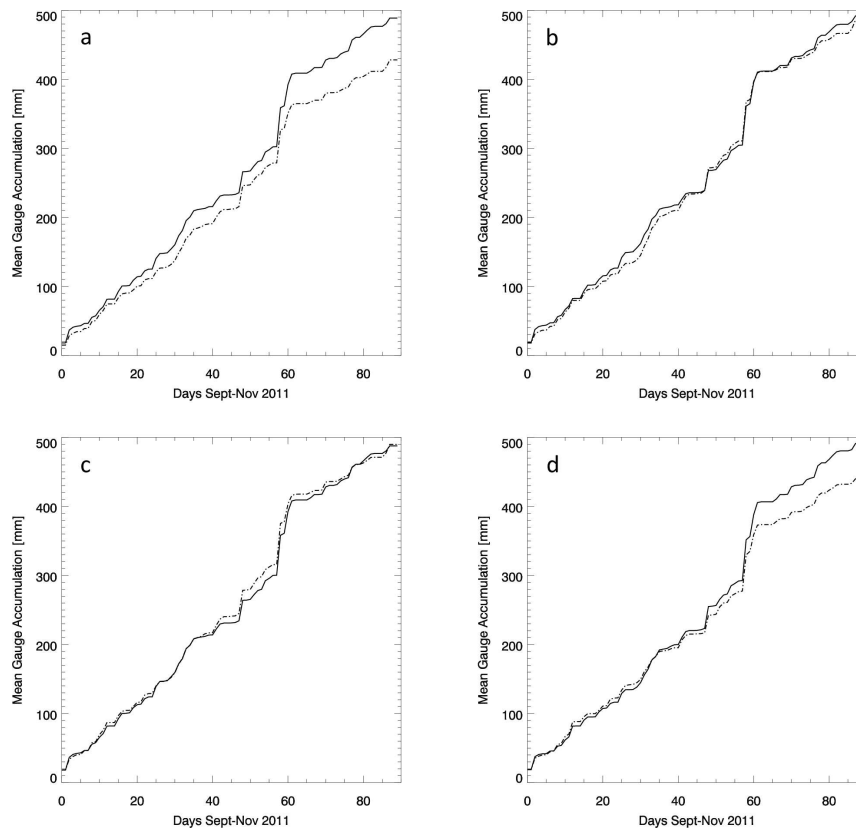
Figure 2.12. Cumulative rainfall averaged from gauges (solid) and radar-derived estimates (dashed) occurring over the 2011 wet season; the 2011 season experienced less gaps in radar data compared to 2009. Included are comparisons for the (a) 2011 annual WPMM data (TRMM 2A53 product), (b) convective/stratiform Z-R derived rainfall, (c) regime-based WPMM derived rainfall, and (d), polarimetrically tuned rain estimates.

relationship, while deep isolated convection and organized convection relationships shift from a stratiform-like relationship at lighter rain rates then toward a convective relationship as the rain rate increases. Differences between the regime-based relationships and the 2A53 Z-R relationships differ by a few mm hr^{-1} (approaching 10% difference), however the deviations show a near monotonic increase as rain intensity increases. The improved information content found from regime-oriented validation is also demonstrated by implementing comparisons with convective and stratiform Z-R relationships. Individual convective and stratiform relationships do not eliminate regime-based biases from deep isolated convective (+4%) and organized

40

precipitation regimes (-9%). These regime-based biases are greatly reduced when convective and stratiform Z-R relationships are derived specifically for the deep isolated convective and organized precipitation regimes where biases are reduced to less than 3%.

While the qualitative and quantitative assessment of the rain retrievals is necessary to improve our validation capabilities, it is beneficial to identify how the errors affect the retrievals on the observed seasonal timescale. To visualize this, comparison of rainfall accumulation between radar derived estimates and gauges for all raining systems during the 2011 wet season are shown in Figure 2.12. The 2A53 product consistently underestimates rainfall as the negative bias associated with convective rainfall continually drives the radar accumulations farther from the gauges. The regime-based WPMM and derived convective-stratiform Z-R derived accumulations compare quite well with the gauge accumulation, which is consistent with the low biases described in Tables 2 and 3. It should be noted, however, that the convective/stratiform Z-R relationships used to derive the accumulation in Figure 2.12b exhibited increases in bias when split into deep and organized precipitation regimes. For this reason, we test if accumulation is affected if rain is only accumulated for an individual precipitation regime. The convective and stratiform-based accumulations seem to be balanced by deep convective systems (organized systems), which are found to overestimate (underestimate) over the 2011 wet season, consistent with the bias patterns found in Table 2.4; therefore, the accumulations could be temporally dependent as changes in the occurrence of the precipitation regimes could skew the overall accumulation. The negative biases in the polarimetrically tuned estimates are caused by individual heavy rainfall events throughout the wet season. The rain accumulations match very well with the gauges except for a few organized convective events. Overall, the polarimetric retrieval performs well for each regime, however errors may exist in more extreme rainfall.

The divergence in rainfall accumulations in the 2A53 estimates encourages discussion pertaining to previous validation studies at the Kwajalein site. For example, Wolff and Fisher (2008) stated that both TRMM PR and TRMM TMI underestimate rainfall compared to the 2A53 by 13.7% and 7.9%, respectively. The underestimation was consistent for multiple years related to issues with the retrievals at higher rain rates. The results of this study suggest that these bias estimates may be underestimated more than originally described depending on the precipitation regimes observed over that period. Future studies evaluating TRMM rain rates would benefit through the use of dual-polarimetric estimates, as they are able to capture the DSD variability, however this capability is not always available. In this case, specific convective and stratiform relationships provide improved estimates if proper partitioning is possible (Bringi et al, 2003, 2009; Thompson et al., 2015) or specific regime-based estimates if enough data is available. Moreover, the results of this study motivate further use of precipitation regimes in future TRMM-GPM GV endeavors – particularly to further differentiate satellite bias estimates with GV-radar estimates. Due to the self-similar nature within the precipitation regimes it is likely that similar error patterns could be recorded at other GV sites.

CHAPTER 3

A REGIME-BASED EVALUATION OF TRMM OCEANIC PRECIPITATION BIASES

3.1 Introduction

Oceanic precipitation in the tropics accounts for nearly two-thirds of the Earth's total precipitation and is a driving force for variability of Earth's weather, climate, water cycle, and energy budget. The most profound interannual variability in tropical oceanic precipitation occurs with the El Niño-Southern Oscillation (ENSO) where anomalies in equatorial Pacific sea surface temperatures (SST) influence variations in the structure of atmospheric wind, temperature, and moisture. These variations bring about changes in the cloud distribution and regional precipitation throughout the tropical oceans (Alexander et al. 2002; Held and Soden, 2006; Su and Jiang, 2012). In the current state we depend on satellite observations to study these anomalies in oceanic precipitation due to the scarcity of reliable observations at the surface. The Tropical Rainfall Measuring Mission (TRMM, Kummerow et al. 1998) satellite provided consistent quantification of the evolving rainfall field for 16 years – dating from 1998 through 2014. The TRMM mission revolutionized precipitation remote sensing by complementing the TRMM Microwave Imager (TMI) with the TRMM Precipitation Radar (PR) - the first spaceborne precipitation radar.

Variations in regional precipitation characteristics have been observed using TRMM TMI and PR data during various ENSO events (e.g. Schumacher et al., 2000, 2003; Masunaga et al., 2006 Berg et al., 2002). These perturbations in precipitation are not in agreement between TMI and PR, where the differences in tropics-wide TRMM rain rate anomalies associated with ENSO

43
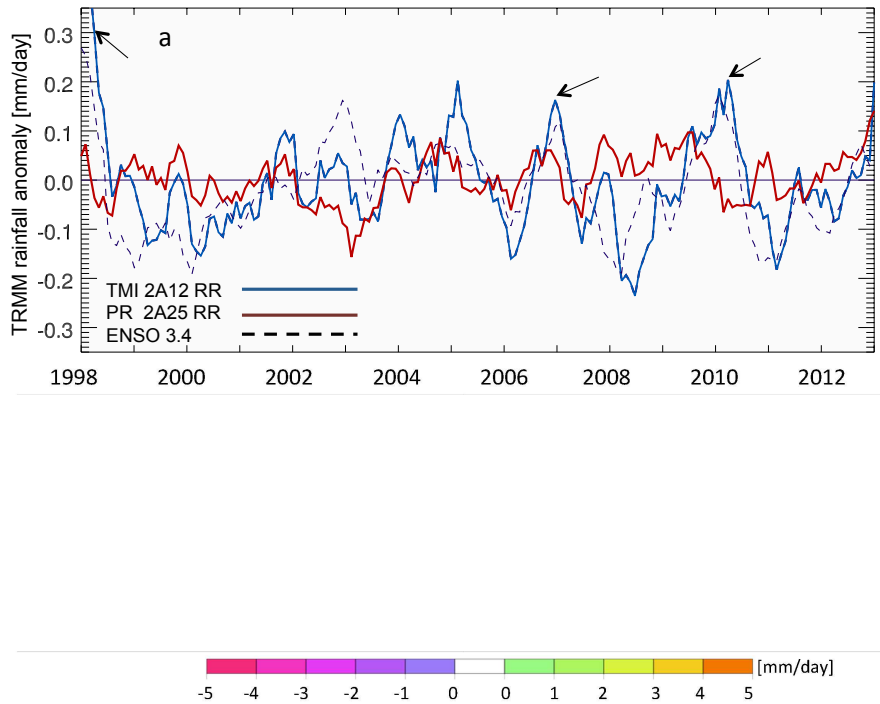
Figure 3.1. (a) Time series of tropical mean rainfall anomalies (As in Figure 1.1) from the TRMM PR 2A25 (red) and TMI 2A12 (blue) over the tropical oceans. Three isolated El Niño events (1998, 2007, and 2010) are highlighted with arrows. (b) TMI-PR differences for a 3-month mean for December 2008, January 2009, February 2009. (c) TMI-PR differences for a 3-month mean for December 2009, January 2010, February 2010.

variability are found to be driven by precipitation occurring over the tropical oceans (e.g. Adler et al., 2008; Wang et al., 2008). Figure 3.1a displays TMI and PR oceanic precipitation anomalies occurring throughout the TRMM mission. Time-dependent discrepancies between the TMI and PR rain rate anomalies are visible between the varying phases of ENSO, where TMI rain rates exhibit variability correlated with the ENSO 3.4 index, and PR does not. As an example, differences between TMI and PR are observed during isolated El Niño events in 1998, 2007, and 2010; these events contributed to a notable increase in oceanic precipitation anomalies from passive microwave rain estimates, whereas the active PR rainfall remains nearly constant.

The opposite occurs during La Niña time periods, where TMI rain rates are generally underestimated compared to PR.

The discrepancies occurring between the TRMM precipitation products are driven by systematic shifts in regional biases (Figure 3.1b and 3.1c). During the 2008-2009 La Niña event (Figure 3.1b) large underestimates in TMI rainfall compared to PR are readily observed. During the peak of the 2009-2010 El Niño changes in the mean precipitation state drive differences toward an overestimation of TMI rain rates within a large region located in the Central and Western Pacific (Figure 3.1c). Because the TMI and PR retrievals rely on different physics when retrieving rain rates, situational dependent biases found between the products have been related to differences in regional cloud microphysics as well as variations in large-scale environmental properties (Berg et al., 2002, 2006, Masunaga and Kummerow, 2005). In order to understand retrieval accuracy, however, it is beneficial to collocate TRMM estimates with an independent validation source to estimate satellite retrieval error (Wolff and Fisher 2008, 2009; Kirstetter et al., 2012).

Previous studies have characterized associated differences between the TMI and PR precipitation retrievals related to larger-scale environmental features or precipitation microphysics (e.g. Berg et al. 2002, 2006; Nesbitt et al., 2004; Shige et al., 2006, 2008; Adler et al. 2012; Seo et al., 2007, 2015). In order to grasp the magnitude of difference between the satellite products, while also understanding which products produce an accurate retrieval, an independent source of rainfall estimates such as described in the TRMM-GPM Ground Validation (GV) program (Wolff et. al., 2005) becomes necessary.

The GV network located on the Kwajalein Atoll provides the opportunity to advance our knowledge of oceanic precipitation uncertainty (e.g. Schumacher et al. 2003; Wolff and Fisher

2008, 2009; Bringi et al., 2012, Munchak et al., 2011). While the above referenced studies have aided validation of random and systematic errors occurring in TRMM instantaneous rain rate estimates, there is still lack of a thorough assessment of the PR and TMI retrievals in relation to situational dependent biases that occur with ENSO induced variability. Wolff and Fisher (2008) demonstrated that annual biases between TRMM rain rates and GV will vary from year-to-year. Based upon the regional differences in Figure 3.1, it can be hypothesized that the mean cloud state is substantially different between the ENSO phases. If TRMM biases relate to changes precipitation properties, it might be beneficial to focus validation on distinct precipitating systems that represent TRMM rain rate biases consistently throughout space and time.

To ensure representation of the diverse nature of convection within the tropics, recent work has begun to segregate precipitation events by large-scale features (e.g. Rasmussen et al., 2014; Liu et al., 2015; Seo et al., 2015; Petkovic and Kummerow, 2016; Henderson et al., 2017). Further, Wang and Adler (2008) discussed how increased information on the large-scale environment might be necessary to reconcile TMI and PR discrepancies related to ENSO. Elsaesser et al (2010) describe such a methodology to classify the level of organization within a precipitating system through the use of a k-means clustering classification. The k-means clustering classifies precipitation regimes based on a cloud properties within 1°x1° boxes along the PR swath. These precipitating systems exhibit self-similar characteristics across the global oceans and thus were recommended for use in validation exercises due to their applicability across synoptic regions. By prompting such validation procedures, the contribution of defined convective systems to precipitation biases can be derived. Then by observing the changes in the occurrence of each precipitation regime we can assess the impact of each precipitation regime on TRMM rainfall discrepancies over time.

To thoroughly comprehend the sources of regional biases between TMI and PR observed over the tropical oceans we extend GV efforts to compare instantaneous TMI and PR rain rates as a function of their large-scale convective organization. This work looks to advance assessments of bias by providing bias estimates associated with individual convective systems using observations from the Kwajalein GV site and Dynamics of the MJO (DYNAMO) field campaign The Kwajalein GV site and the DYNAMO campaign are ideal oceanic locations for examining TRMM biases due to their proximity to frequent and diverse convective systems. The DYNAMO field campaign has provided new insights into the multiscale processes during MJO initiation over the Indian Ocean This includes ground radar-based datasets to observe the varying the convective population and precipitating systems (e.g., Zuluaga and Houze 2013; Powell and Houze 2013), which can be used to check the consistency of results derived at the Kwajalein Atoll. The ground-based observations are then used to investigate precipitation retrievals to help understand how these validation results can propagate into retrieval development.

3.2 Data Sources and methodology

3.2.1 TRMM-GPM ground validation products

The Kwajalein GV site provides continuous radar information from the dual-polarized S-band KPOL radar. Data from the KPOL site is used to validate TRMM observations from the time period of 2008-2013. The time period of 2008-2013 is chosen as it is documented to contain stable calibrated reflectivity data within ±0.5 dB (Silberstein et al., 2008; Marks et al. 2009). As an alternative to the KPOL-derived TRMM GV 2A53 rain rate product, which implements the window probability matching method (WPMM; Rosenfeld et al. 1994) to estimate surface rainfall at GV sites, this work utilizes rain rate measurements calculated by applying the

methodology of Bringi et al. (2004) to the dual-polarized variables from the KPOL radar. The method utilizes the horizontal reflectivity Z_h, differential reflectivity Z_{dr}, and the differential propagation K_{dp} phase to dynamically adjust the coefficient "a" in the Z-R relationship $Z=aR^{1.5}$ on a pixel-by-pixel basis, which results in noticeably improved correlations with rain gauges without the need for rain gauge calibration (Marks et al., 2009; Henderson et al., 2017). Rain type separation for the KPOL radar rain rates are provided in the Version 7 TRMM-GV 2A54 product and the ground validation products are gridded in a Cartesian coordinate dataset with horizontal resolution of 2 km.

3.2.2 TRMM satellite products

a) TRMM TMI 2A12 product and the GPROF rainfall algorithm

TMI is a nine-channel passive microwave radiometer that observes brightness temperatures (T_b) at five frequencies (10.65, 19.35, 21.3, 37.0, and 85.5 GHz). The Goddard Profiling Algorithm (GPROF), introduced in Kummerow et al. (1996), utilizes a Bayesian framework to instantaneously retrieve hydrometer profiles by relating observed T_bs to entries in an a priori database and has been implemented operationally for multiple spaceborne radiometers including the rain rates retrieved in the TRMM TMI 2A12 rainfall product. The database contains sufficient entries to realistically represent climatological tropical cloud profiles, where each entry consists of matched PR rain rates averaged across each 21-GHz footprint (~19km x 31km) and TMI T_bs at their native resolution. The application of Bayes' theorem allows the derivation of the most probable rain rate using the observed set of TMI brightness temperatures,

$$\Pr(R|T_b) = \Pr(R) \, x \, \Pr(T_b|R) \qquad (3.1)$$

where Pr(R) is the probability of observing a rain profile R, in this case over the tropical oceans, and Pr(TbIR) is the probability of one of TMI channels observing a T_b given a particular rain profile R within the a priori database. The surface rain rate, convective fraction of rainfall, and other atmospheric state parameters are derived by calculating their expected value from weighted a priori database entries. The current iteration of GPROF replaced a cloud resolving model-based database with an observationally generated database created using TRMM PR observations that are separated by surface temperature and total precipitable water (Kummerow et al., 2011) and has recently expanded the Bayesian inversion for both land and ocean surface types (Kummerow et al. 2015). This work uses oceanic data from the Version 7 TRMM data release, which utilizes GPROF 2010-V2.

b) TRMM Precipitation Radar 2A25 product

The use of active precipitation radars, such as the TRMM PR, allows observations of precipitation properties in three-dimensional space. In this work, data from the TRMM precipitation radar Version 7 2A25 product provides surface rain rate estimates and rain type partitioning. The three-dimensional observations available from the radar product provide pixel-by-pixel vertical profiles of rain rates as well as rain type classification using a combination of vertical and horizontal reflectivity gradients (Awaka et al. 1998; Steiner et al. 1995). The 13.8 GHz (Ku band) operational frequency can be attenuated in heavier rainfall, therefore, before rain rates are be derived, PR reflectivities are corrected using hybrid methodology described by Iguchi et al. (2000; 2009), which is a combination of the surface reference technique (Meneghini et al. 2000) and the Hitschfeld and Bordan (1954) method. Using the rain type classification

describe above, attenuation corrected reflectivities are applied to individual Z-R relationships to derive the vertical profile of rain rates within each PR pixel.

3.2.3 NCAR dual-polarimetric S-PolKa radar

The DYNAMO field campaign was launched to further understand the cloud and environmental processes that are necessary to initiate a Madden Julian Oscillation (MJO) event. The field experiment captured multiple MJO events throughout the campaign and was able to observe a wide variety of convective precipitating systems (e.g Yoneyama et al., 2013; Johnson and Ciesielski, 2013; Xu et al., 2015). The National Center for Atmospheric Research (NCAR) dual-polarimetric S-PolKa (0.8 cm K_a-band) radar located on the Addu Atoll (0.63° S and 73.10°E) during the DYNAMO field campaign continuously collected data spanning 28 September 2011 to 15 January 2012, a time where deep convective activity was common due to frequent MJO events. The data are gridded with a horizontal resolution of 2 km and vertical resolution of 0.5 km. Rain type partitioning is applied using the methods of Steiner et al. (1995) and rain rates are computed by a best fit polarimetric algorithm described in Chandrasekar, et al (1990, 1993). The hybrid approach utilizes combinations four Z-R relations: 1) Z_H-only; 2) Z_H and Z_{DR}; 3) Z_{DR} and K_{DP}, or 4) K_{DP}-only, depending on measured magnitudes of the polarimetric variables. Full details of the S-pol radar during the DYNAMO campaign can be found at https://www.eol.ucar.edu/projects/dynamo/spol/.

3.2.4 Conducting the TRMM comparisons

The Kwajalein GV site and the DYNAMO campaign are ideal oceanic locations for examining TRMM biases due to their proximity to frequent and diverse convective systems. To identify individual precipitating systems we categorize their level of organization following the

methodology described in Elsaesser et al (2010). Known for their self-similar properties, the precipitation regimes described in Elsaesser et al. (2010) have been used to relate numerous precipitation and atmospheric properties (e.g. Elsaesser and Kummerow, 2013; Duncan et al., 2014; Hannah et al., 2015; Petkovic and Kummerow, 2016; Henderson et al., 2016; Liu et al., 2016). All classified regimes throughout this manuscript were defined following the procedures of Elsaesser et al. (2010) and Elsaesser and Kummerow (2013) by implementing TRMM PR data to establish three distinct precipitation regimes defined as follows: 1) Shallow, typically warm rain, congestus clouds with echo tops commonly below 5 km; 2) Deep unorganized convection; and 3) Deep organized convection containing substantial amounts of deep stratiform rainfall. The classification takes advantage of the TRMM PR's ability to measure vertical profiles of hydrometeors, identifying the level of system organization by precipitation depth (echo top heights), rainfall intensity, and convective and stratiform contributions to the overall rainfall located within 1° x 1° grid boxes along the TRMM PR swath. The advantage of the Elsaesser et al (2010) classification lies in the fact that the defined convective systems are found to be self-similar in nature across the tropical oceans, thus the validation statistics should be extendable to other oceanic regions observed by the TRMM satellite.

Table 3.1. Summary of all convection regimes identified for the TRMM overpasses for Kwajalein (2008-2013) and over the DYNAMO field campaign. The DYNAMO data was taken from the S-PolKa radar dating from September 2011-January 2012. Included are the total cases observed for each regime, their fraction of occurrence for observed cases.

	All Cases Identified	Shallow Regime	Deep Isolated Regime	Organized Regime
Kwajalein KPOL	438 (--)	123 (29%)	169 (38%)	146 (32%)
DYNAMO SPOL	(176) (--)	86 (49%)	54 (31%)	36 (20%)

To compare satellite-based and ground-based rainfall retrievals at the Kwajalein site, multiple case studies from 2008-2013 are analyzed, while data from the DYNAMO campaign are obtained from the S-PolKa radar for all valid data collected from September 2011- January-2012. For each TRMM orbit overpassing the Kwajalein or DYNAMO sites, rainfall occurring in a 1° x 1° region within the PR swath, and contained within the ground radar volume sweep, are classified using TRMM PR information according to the classification process described above. Ground radar data and TRMM TMI data are matched using nearest neighbor to each 1° x 1° region within the PR swath and mean rain rates over each 1° x 1° region is compared. The ground-based rain rate estimates offer an independent quality controlled dataset to be used for validation and will be considered the in situ truth when comparing rain rates and rain type. Near surface rain rates derived from the dual-polarized KPOL data are computed using the lowest radar plan position indicator (PPI) elevation scan and interpolated to 0.5 km. Precipitation from the S-PolKa radar reflectivity data are estimated using the lowest non-zero value of Z between the surface to 2 km above ground level. The ground-based data present the best opportunity for validating the TRMM overpasses due to comparisons in a fully immersed oceanic environment and the ability of dual-polarized retrievals to represent precipitation variability occurring between precipitation regimes (Henderson et al., 2017).

Table 3.1 provides a summary of the number of cases identified for each regime in the Kwajalein and DYNAMO regions along with their respective percentage of the total. To optimize rainfall occurrence found within the Kwajalein GV-satellite overpasses and minimize error due to differences in temporal sampling, cases are chosen where overpasses occur within 5 minutes between the ground and satellite overpasses, contain 5% or higher rain volume, and the nadir PR pixel occurs within 50 km of the ground-based radar. While the amount of rainfall

within the radar scan varies for each overpass, on average each overpasses yields four classified precipitation regimes. All overpasses are included for the DYNAMO campaign where overpasses occur within 5 minutes between the ground and satellite overpasses within 100 km of the radar location.

3.3 Comparison of rainfall retrieved between TRMM and ground observations

3.3.1 Kwajalein Atoll (Western Pacific Ocean)

To begin the validation process, we first check consistency with Wolff and Fisher (2008) who compared TRMM rain rates to the TRMM GV 2A53 product finding both TMI and PR underestimate the GV retrievals by 7.9% and 13.7%, respectively. Bias is defined as the difference in rain rate expressed as a percentage ($\frac{TRMM-GV}{GV}$). Using the Kwajalein case studies, biases between TRMM and the GV dual-polarized estimates yield underestimates of 12.8% and 17.4% for TMI and PR, respectively. This result is expected as the WPMM-based rain rates used in TRMM 2A53 have been found to underestimate rain rates over the Kwajalein site (Henderson et al., 2017). If the 2A53 product is used instead, we find a similar underestimation of 10.2% and 15.6% for TMI and PR, respectively. The bias estimates confirm the overall tendency for both TRMM retrievals to underestimate compared to validation rain rates at Kwajalein, however, when observing each case study individually the sources of the bias can be more readily distinguished (Figure 3.2). Figure 3.2 presents the compilation of mean rain rates calculated from TMI and PR compared to the dual-polarized tuned GV estimates for all precipitation regimes cases analyzed.
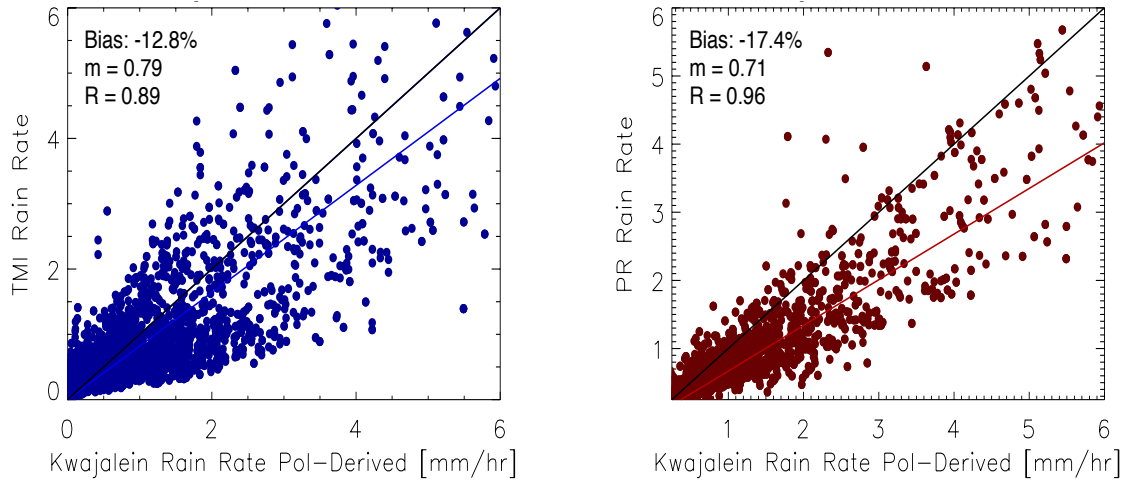
Figure 3.2. Scatterplots of the TMI (left) and PR (right) vs Kwajalein GV rain rate estimates for each 1° × 1° box identified by the TRMM overpasses. Included in each panel is the bias, slope of the best line fit, and correlation with the GV estimates.

Included in Figure 3.2 are the correlation between the satellite product and GV, percent bias, and slope of the best line fit. The TRMM 2A25 rain rates exhibit consistent underestimation compared to the GV estimates (Figure 3.2b), whereas TRMM TMI 2A12 rain rates are highly variable with regions of both positively and negatively biased rain rates when compared to the Kwajalein GV rain rates (Figure 3.2a). It can be hypothesized that the different regions of positive and negative bias are related to precipitation characteristics associated with different precipitation systems; this can be tested by applying the precipitation regime classification of Elsaesser et al. (2010) to the rain rate comparisons.

Figure 3.3 presents comparisons of mean instantaneous rain rates averaged over each 1° x 1° region from TRMM TMI and PR precipitation retrievals with GV separated by the precipitation regimes identified using Elsaesser et al. (2010). Based upon the regime separation, the TRMM PR rain rates exhibit systematically increasing bias categorized by system organization, where shallow precipitation is underestimated by 10.1%, deep isolated convection is underestimated by
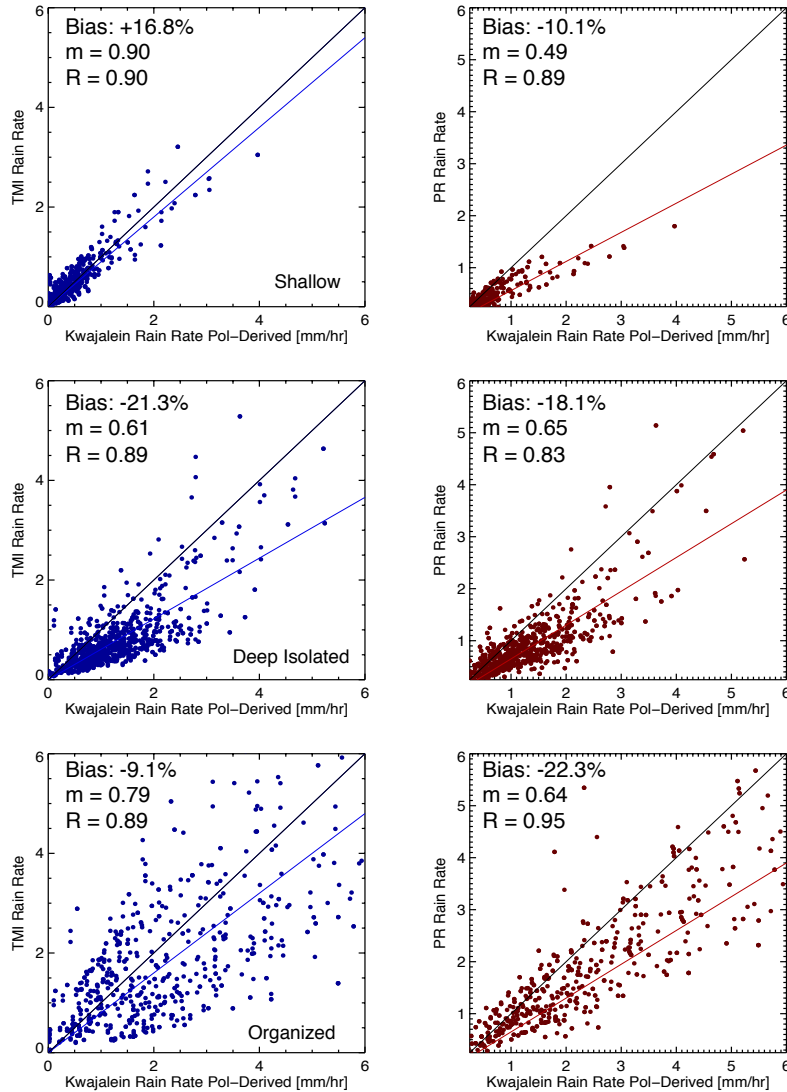
Figure 3.3. Same as Figure 3.2 except for split into the convective regimes of shallow convective regime (top), deep isolated convective regime (middle), and organized convective regime (bottom).

18.1%, and organization convective systems are underestimated by 22.3%. This pattern mimics what is found in previous work (e.g. Wolff and Fisher 2008; 2009; Rasmussen et al., 2013), where PR bias is generally related to precipitation intensity. For TMI, Shallow convective systems for TMI and GV agree fairly well with TMI slightly overestimating the precipitation by 6.8%, while like the PR biases, deep unorganized convective systems underestimate by 21.3%. The bimodal bias pattern found with TMI rain rate estimates is exemplified in the organized

precipitation regime, where the overall bias is an underestimation of 9.1%. The PR rain rate comparisons help support the idea that biases are able to be distinguished through the precipitation regimes; however, TMI still exhibits positive and negative regions of bias associated with the organized convective systems. Recent work by Seo et al. (2015) discovered that positive biases between TMI and PR might be attributed to regions of stratiform rainfall contained within the within the TMI footprint/field of view (FOV).

Table 3.2. Bias statistics for between the TRMM PR and TMI rain rates compared to the dual-polarized rain rates estimates at the Kwajalein GV site as a function of convective regime. Values are first compared for convective cases (convection fraction > 0.50) and then for stratiform cases (convection fraction < 0.50).

Convective	All	Shallow	Deep Isolated	Organized
PR Bias [%]	-22.4	-12.8	-23.4	-26.1
TMI Bias [%]	-32.2	+5.5	-37.8	-30.3
TMI-PR [%]	-23.2	+10.9	-24.8	-14.1
Stratiform	All	Shallow	Deep Isolated	Organized
PR Bias [%]	-6.1	-11.4	-8.4	-2.6
TMI Bias [%]	+27.9	+25.5	+8.1	+33.4
TMI-PR [%]	+36.7	+38.8	+23.5	+37.5

Biases related to convective fraction within each precipitation regime reveal a clearer separation for both TMI and PR rain rate estimates (Figure 3.4). Using the matched Kwajalein rain rates within the 1° x 1° regime classified using the PR data, we define the convective fraction as the fraction of total rainfall contributed by convective rainfall within each precipitation regime. A convective case is described where the convection fraction > 0.50 and a stratiform case where the convective fraction is < 0.50. In Figure 3.4 forefront patterns emerge in TMI and PR biases. First, there is clear separation of biases between stratiform and convective cases in TMI, whereas PR typically underestimates all cases. TMI rain rates are overestimated compared to GV when the convective fraction is below 0.50 by 27.9%, whereas the PR retrieval
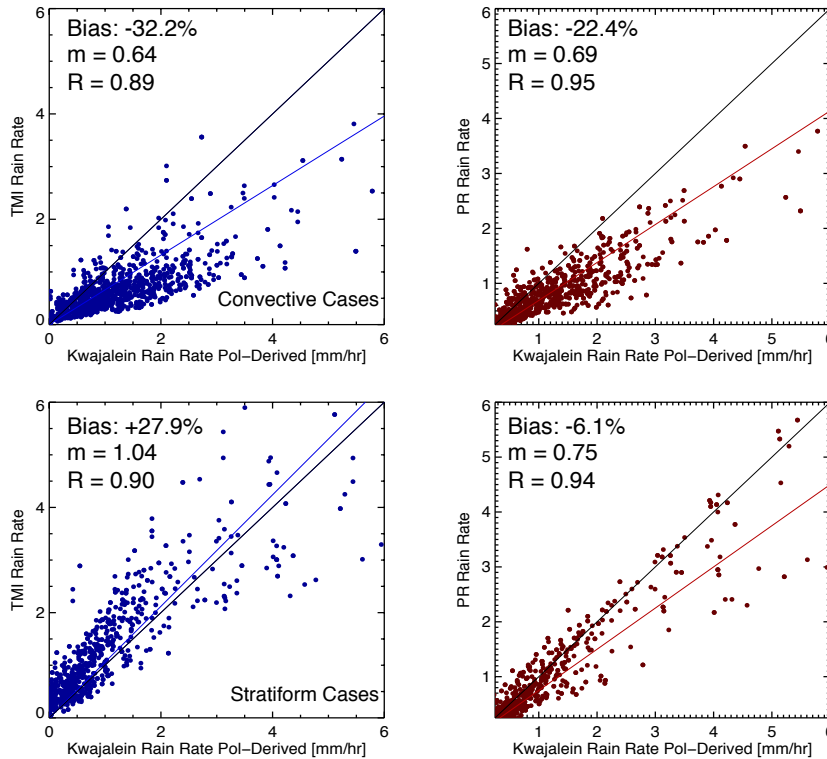
Figure 3.4. Same as Figure 3.2 except as a function of convective fraction. A convective case is described where the convection fraction > 0.50 (top) and a stratiform case where the convective fraction is < 0.50 (bottom). See Table 3.2 for validation statistics related to each convective regime.

exhibits improved comparisons with the GV analysis underestimating by 6.1%. The positively biased portion of TMI comparisons are linked to organized systems containing predominately stratiform rainfall (Table 3.2). As explained in Elsaesser et al. (2010), these organized convective systems are generally attributed with large deep anvils regions and a higher fraction of stratiform precipitation. When comparing TRMM and GV rain rate estimates for convective rainfall cases, the largest differences between TRMM and GV occur with TMI rain rates where convective cases are underestimated by 37.8% in deep isolated regimes and stratiform cases are overestimated by 37.5% in organized regimes.

To further the rain rate comparisons, the differences between TMI and the PR rain rates are also included in Table 3.2. For the predominantly stratiform cases, the largest discrepancies

between TMI and PR occur within organized convective systems where TMI overestimates PR by +37.5%. For convective rainfall cases, differences for each regime yield: +10.9% for shallow convection, -24.8% for deep isolated convection, and -14.1% for organize convective systems. TMI and PR rain rate estimates both underestimate GV validation in convective cases; however, the TMI rain rates exhibit significant underestimation compared to the PR retrieval in deep isolated and organized regimes as well. The variability between PR and TMI differences is largely driven by the TMI rain rates across the different regimes, which becomes evident in the deep isolated and organized regimes. In predominantly stratiform cases, while opposite in sign, the TMI and PR biases are similar in magnitude yielding a difference of +23.5%. This difference escalates to +37.5% in organized regimes driven by an increase in bias of 25% in TMI rain rates.

3.3.2 DYNAMO (Central Indian Ocean)

Data available from the DYNAMO field experiment provides a unique dataset to further examine the Kwajalein GV bias results. Across the Indian Ocean, the MJO is the dominant form of convective variability on intra-seasonal scales, where cycles in deep convection occur approximately every 30–90 days. Even though a different synoptic environment influences the convection, similar regime-based bias patterns should still exist within the Indian Ocean; the regime-based precipitation characteristics described in Elsaesser et al (2010) were found to be consistent across ocean basins. In this section we repeat our analysis utilizing the DYNAMO data to provide a consistency check on the regime-based biases that were observed over the Kwajalein GV region.
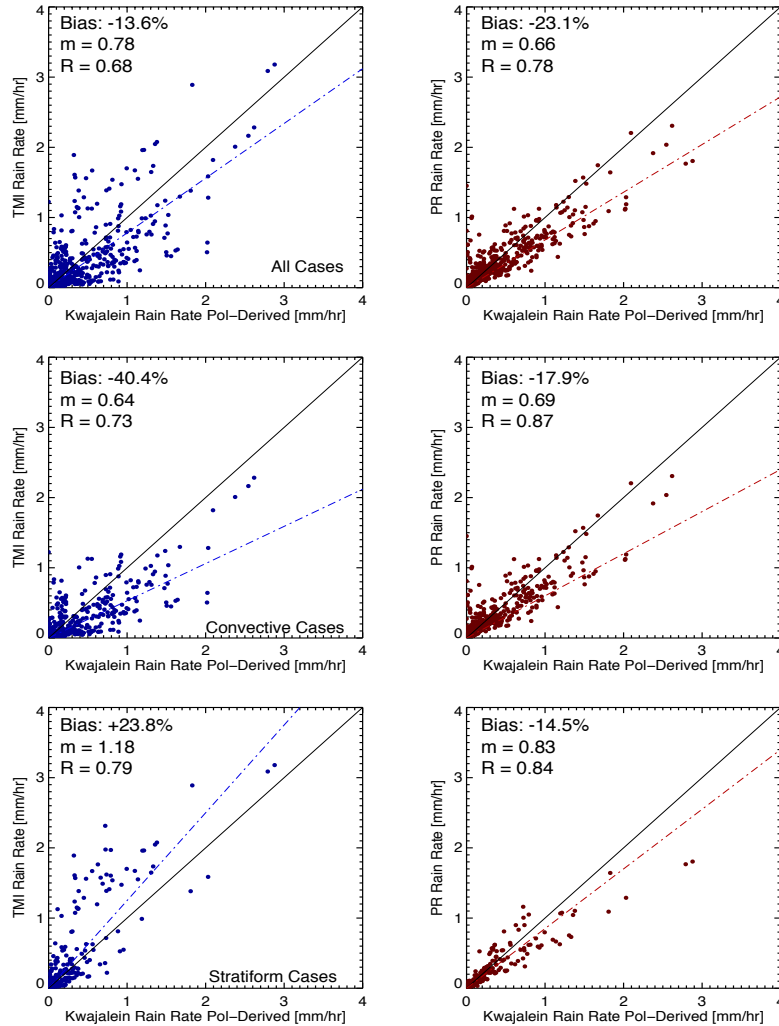
Figure 3.5. Same as Figure 4 except derived from the DYNAMO field campaign. The results for all cases are also included with (top) all cases, (middle) convective cases, and (bottom) stratiform cases. See Table 3.3 for validation statistics related to each convective regime.

We extend the analysis to the Central Indian Ocean to compare the TRMM PR and TMI retrievals to dual-polarimetric tuned radar estimates from the S-PolKa radar. The S-PolKa radar completed measurements continuously from September 2011-January 2012.

The S-PolKa radar completed measurements continuously from September 2011-January 2012. Validation statistics are completed in the same manner as the Kwajalein analysis, where regimes are identified by TRMM PR and the mean rain rates compared over 1°x1° regions. Validation statistics for all overpasses of the S-PolKa radar are presented in Table 3.3. Figure

3.5 presents the comparison of mean rain rates for TMI and PR overpasses compared to S-PolKa measurements derived during the DYNAMO campaign. Here the rain rates are presented with all raining cases as well as split into convective and stratiform cases using the definitions described above. Overall, both TMI and PR rain rates display a similar pattern to the results found within the Kwajalein region.

Table 3.3 Bias statistics for between the TRMM PR and TMI rain rates rain rates computed from the S-PolKa radar during the DYNAMO field campaign as a function of convective regime. Values are compared for all cases, convective cases (convection fraction > 0.50), and for stratiform cases (convection fraction < 0.50).

All Cases	All	Shallow	Deep Isolated	Organized
PR Bias [%]	-23.1	-12.1	-17.8	-18.0
TMI Bias [%]	-13.6	+6.2	-29.9	-2.3
Convective	All	Shallow	Deep Isolated	Organized
PR Bias [%]	-17.9	-0.5	-17.7	-27.8
TMI Bias [%]	-40.4	+13.0	-36.9	-32.2
Stratiform	All	Shallow	Deep Isolated	Organized
PR Bias [%]	-14.5	-15.8	-18.6	-18.0
TMI Bias [%]	+23.8	+21.1	+13.5	+41.5

When all systems are included in the bias calculation, we find a bias of -13.6% and -23.1% for TMI and PR rain rates, respectively (shown in Figure 3.5). The bias patterns agree quite well with what was found using the KPOL radar rain estimates above. A similar pattern of scatter is found in TMI rain rates above and below the one-to-one line in Figure 3.5a, therefore, the TRMM biases are still likely linked to convective and stratiform rainfall within each regime. Precipitating systems containing mostly convective rainfall are found to underestimate compared to the ground validation with biases ranging from -0.5% to -27.8% for PR, and TMI heavily underestimates by -36.9% and -32.2% in deep isolated and organized regimes, respectively; This confirms that the TMI rain rate systematically underestimate GV and PR in these regimes (Table 3.3). Predominantly stratiform cases are generally underestimated for PR across the regimes,

whereas TMI overestimates stratiform cases with biases ranging from +13.5 to +41.5. The corresponding bias patterns in precipitation type and each precipitation regime is consistent over the DYNAMO field campaign region with results found using KPOL. The consistency in the bias patterns provides confidence that the regime-based bias results could be consistent in other oceanic environments.

3.3.3 Convective and stratiform biases at the TMI footprint level

Information content in deriving TMI and PR biases is increased when calculated as a function of their convective environments and split by their convective fractions. The clear bias patterns make a strong case for the use of regime-based analysis; however, they do not provide definitive proof that the TRMM biases are not related to variability in convective or stratiform rain type alone. The amount of convective and stratiform rainfall varies between each precipitation regime (Elsaesser et al. 2010; Henderson et al. 2017), where Elsaesser et al (2010) find that the contribution of stratiform rainfall increases from 30%, 40%, and 50% for shallow, deep isolated, and organized regimes, respectively. Therefore, it remains plausible that biases associated with each precipitation regime are directed by systematic shifts in stratiform or convective rainfall, where biases could be invariant between the precipitation regimes. To examine this further, TMI and PR biases are derived at the pixel level within each precipitation regime at the Kwajalein GV site on TMI FOV scale. Validation on this scale is useful to ensure comparisons remain focused on each precipitation type and using the TMI footprint scale aids in reducing random errors due to spatial and temporal discrepancies, which typically arise due to differing observing times between the satellite and ground radar (Houze et al., 2004).
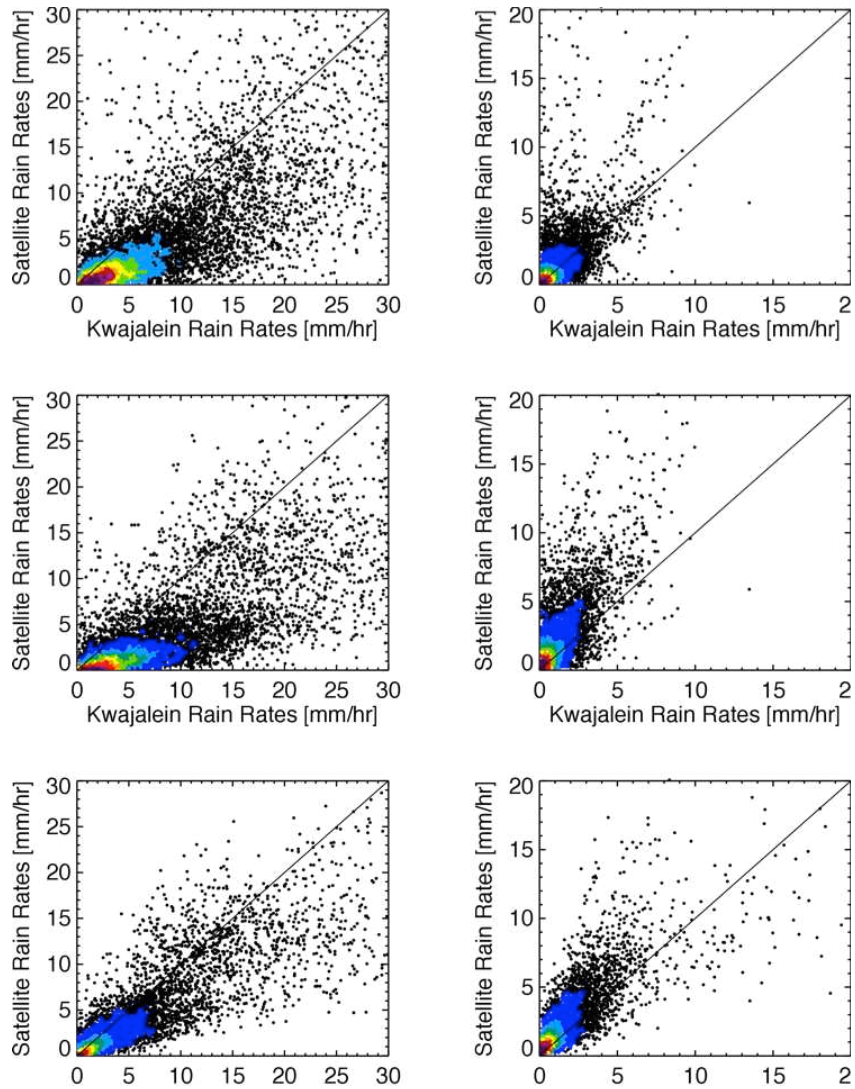
Figure 3.6. Density plots of the comparisons made at the TMI footprint scale for convective and stratiform rainfall. Shown are comparisons with Kwajalein for (a) PR convective, (c) TMI convective, (b) PR stratiform, and (d) TMI stratiform. Differences between TMI and PR are shown in (e) for convective rain rates and (f) for stratiform rain rates. For panels a-e the abscissa axis is defined as the Kwajalein rain rate and the ordinate axis is defined as either the PR or TMI rain rate and in panels e-f the abscissa axis is defined as the PR rain rate and the ordinate axis is defined the TMI rain rate.

Rain rates are compared following the footprint matching approach outlined in Wolff and Fisher (2008) who average PR and Kwajalein rain rates within a 7 km radius around each TMI observed rain rate. Matched KPOL rain rates with the 7km radius are used to define convective and stratiform rainfall cases, defined where the convective or stratiform rainfall fraction exceeds 90% in the TMI FOV. The resulting comparisons are displayed in Figure 3.6 and the associated

biases for each sensor in Table 3.4. The biases found within the footprint scale are generally

higher, but expected as large scale averaging can smooth out bias estimates (Wolff and Fisher,

2008), however further bias separation is found as a function of its large-scale precipitation

Table 3.4. Bias statistics for convective and stratiform rainfall at the TMI footprint scale between the TRMM PR and TMI rain rates. Rain rates are compared to the dual-polarized rain rates estimates at the Kwajalein GV site as a function of convective regime.

Convective TMI FOV	All	Shallow	Deep Isolated	Organized
PR Bias [%]	-34.8	-15.9	-52.2	-28.6
TMI Bias [%]	-50.9	-30.9	-66.8	-47.9
TMI-PR [%]	-24.7	-20.3	-30.5	-27.9
Stratiform TMI FOV	All	Shallow	Deep Isolated	Organized
PR Bias [%]	+17.2	-22.4	+24.0	+7.4
TMI Bias [%]	+77.8	+13.2	+49.4	+92.3
TMI-PR [%]	+39.7	+46.1	+20.5	+63.7

regime. For convective rain rates, TMI and PR still underestimate in nearly all cases overall.

Here, the largest underestimation occurs in deep isolated precipitation regimes, where PR and

TMI underestimate by -52.2% and -66.8%, respectively. In stratiform rainfall, the continued

pattern of TMI overestimating compared to both Kwajalein and PR is consistent through all

regimes. TMI significantly overestimates Kwajalein rain rates by 92.3% within organized

precipitation regimes, whereas PR slightly overestimates by 7.4%. Both TMI and PR

overestimate (49.4% and 24.0%, respectively) in deep isolated convection.

Convective and stratiform biases are further examined by observing the mean rain rates for

each sensor binned in 0.5 mm/hr increments (Figure 3.7). The PR retrieval compares best with

Kwajalein rain rates for both convective and stratiform rainfall (Figure 3.7a). As rainfall

intensity increases, both PR and TMI heavily underestimate in convective rainfall, where TMI

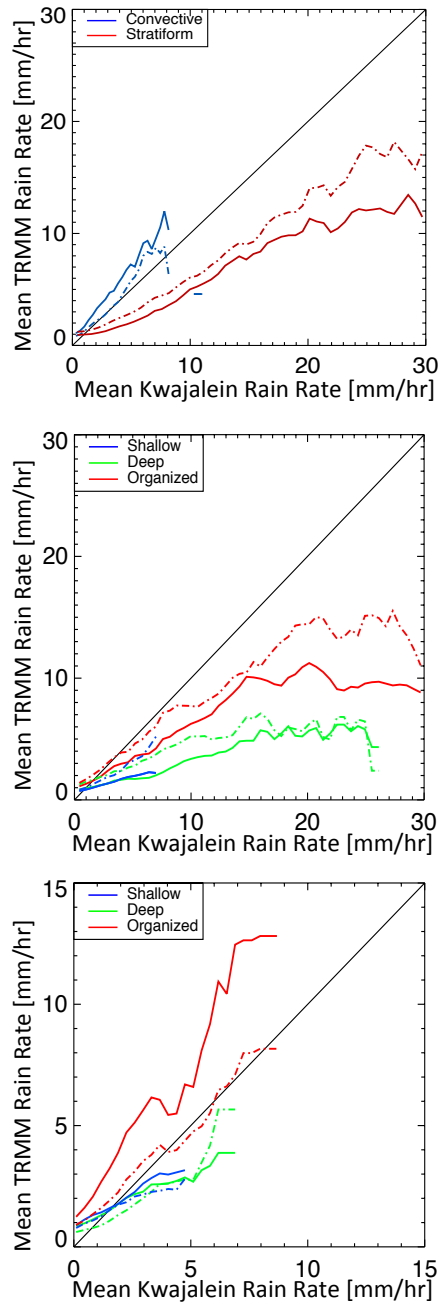Figure 3.7. Comparisons of the PR (dashed) and TMI (solid) mean rain rates with the dual-polarized estimates from the KPOL radar. Comparisons are made at the TMI footprint scale for convective and stratiform rainfall. Rain rate profiles as shown for (top) all collocated convective and stratiform cases, (middle) convective only segregated by regime, and (bottom) stratiform only segregated by regime

64

consistently underestimates PR. Within stratiform rainfall the PR retrieval matches well with Kwajalein for rain rates < 5 mm/hr, whereas TMI consistently overestimates Kwajalein in stratiform rainfall with a near monotonic increase in bias as a function of rain rate. The differences in rain rate as a function of regime are easily visualized (Figure 3.7bc). Notable differences occur between deep isolated precipitation regimes and organized regimes within convective FOVs. A clear distinction exists for convective pixels between the isolated and organized regimes for both TMI and PR, where deep isolated regimes are typically underestimated to a higher degree for all rain rates. For stratiform rainfall, positive biases are generally explained by overestimation within organized precipitation regimes, while overestimation from shallow and deep isolated regimes are constrained to lower rain rates. The convective and stratiform validation at the footprint level is able to define explicit positive and negative biases between the precipitation types, however, as described previously, the implementation of regime-based estimates becomes a necessary step to more accurately pinpoint bias sources.

3.4 Regime Related Biases

3.4.1 Precipitation regime variability over the Kwajalein region

Figure 3.1 highlights variability in regional TMI and PR differences occurring during different phases of ENSO. The validation results above describe distinct bias estimates for TMI and PR rain rate retrievals created using the overpass comparisons. The comparisons occurred during both El Niño and La Niña events; therefore, it is likely that the biases should be representative of the regional convective variability that occurs during the various ENSO events (e.g. Masunaga et al., 2006). Based on the biases results for each precipitation regime, it is presumed that the

overestimation of TMI compared to PR during an El Niño event relates to a shift toward more organized precipitation containing significant amounts of stratiform rainfall.

Table 3.5. Statistics of mean TMI and PR rain rates during the time periods from 2002-2010, El Nino events, and La Nina events. Mean rain rates are derived within a 15° × 15° region surrounding the Kwajalein Atoll.

Rain Bias	All	El Nino	La Nina
PR [mm.day]	7.01	7.69	5.43
TMI [mm.day]	6.69	8.48	5.02
TMI-PR [%]	-4.4%	+10.3%	-7.5%
Corrected	All	El Nino	La Nina
PR [mm.day]	7.66	8.56	5.91
TMI [mm.day]	7.49	8.85	5.78
TMI-PR [%]	-2.2%	+3.4%	-3.6%

To examine this, mean TMI and PR rain rates are compared for TRMM orbits within a 15°x15° degree region surrounding the Kwajalein Atoll for El Niño and La Niña events from 2002-2012. This time period contains three El Niño and La Niña events and rain rates were retrieved after the TRMM orbit was boosted to 403 km. An ENSO event is defined as when the ENSO 3.4 index reaches ± 0.5° C; this is a common threshold set to determine such events (Trenberth, 1997). For all cases, which includes all rainfall regardless of ENSO phase, over the 2002-2012 time period, the mean rain rate of 6.69 mm day^{-1} for TMI, which is lower than the mean rain rate of 7.01 mm day^{-1} from PR, yielding an underestimation of 4.4% (Table 3.5). The differences between TMI and PR rain rates become further separated when evaluating over the ENSO events.   TMI rain rates underestimate PR by 7.5% during La Niña events and overestimate PR by 10.3% during El Niño events. The TMI-PR differences during El Niño and La Niña periods are not resultant of a single event, but are found to be consistent throughout the TRMM record studied. Using the Mann-Whitney U-Test to investigate the statistical differences
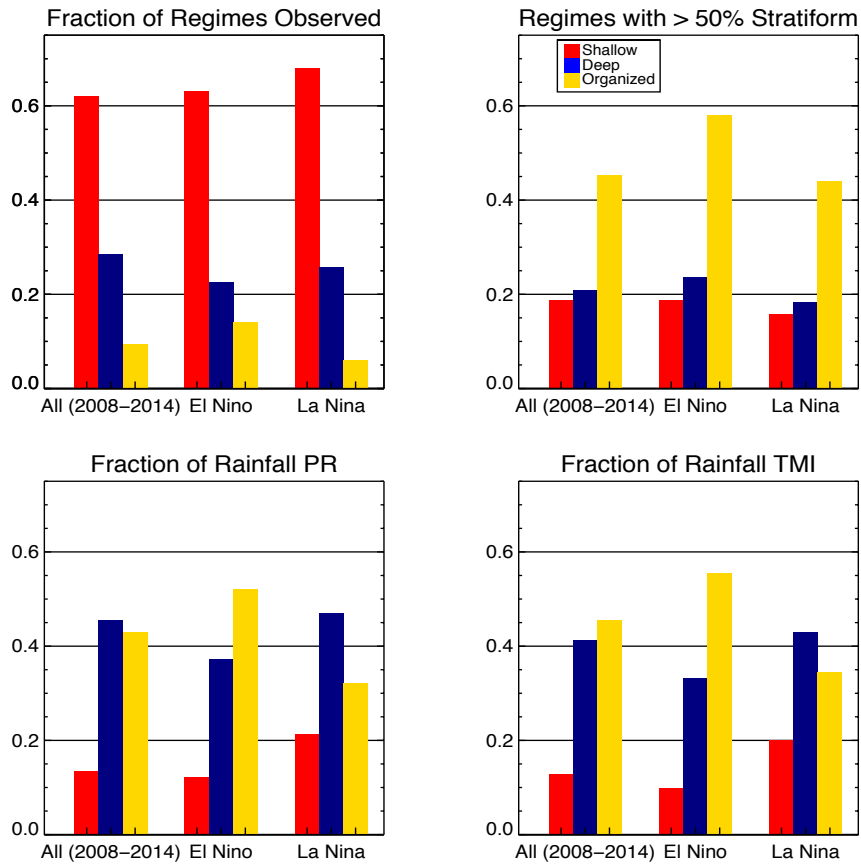
Figure 3.8. Convective regime-based statistics for PR and TMI rain rates for time periods from 2002-2010, El Nino events, and La Nina events. (a) The occurrence of each convective regime over each time period. (b) The fraction of each convective regime identified as a stratiform case (convective fraction is < 0.50). Fraction of rainfall contributed by each convective regime for (c) PR and (d) TMI rain rates.

of the rain rate distributions it was observed that mean TMI and PR monthly rain rates were significantly different from each other in both ENSO phases using a 95% significance threshold.

Variability of the precipitation regimes for each observed time period are illustrated in Figure 3.8. Shallow convective systems are most frequent, however, these systems contribute less to the overall accumulated rainfall. Compared to the mean state, La Niña events are characterized by shallow convective systems and deep isolated convective systems, whereas organized systems are more prevalent during El Niño events - occurring nearly twice as frequent compared to La Niña events. Further, during an El Niño event organized systems are more likely to be stratiform

cases as denoted by the nearly 60% of classified systems containing predominantly stratiform rainfall (Figure 3.8b). This result agrees with the biases found in Section 3.3, where an increase in organized systems should correspond with TMI overestimating against both GV and PR rain rates. This is further manifested by looking at the fraction of total rainfall for each precipitation regime (Figure 3.8cd).

For both PR and TMI, shallow convective systems contribute similar amounts to the total rainfall with a maximum contribution occurring during La Niña events. Discrepancies between the two retrievals occur with deep isolated precipitation regimes and the organized precipitation regimes. In the mean state, the highest contributions to PR rain rates derive from deep isolated systems (43.4%), while TMI rain rates have a higher contribution from organized systems (45.5%). During an El Niño or La Niña event, both retrievals agree on which precipitation regime provides the most rainfall, however, TMI favors organized rainfall to a higher degree with 58.0% of rainfall reported from organized convection compared to 53.9% from PR, where the 4% disparity in PR is made up from rainfall occurring in deep isolated precipitation regimes.

The differences in the two rainfall retrievals appear to be related to the frequency of precipitation regimes observed. The results suggest that during an El Niño event there is a systematic shift towards more organized precipitation containing large precipitating stratiform regions. Increases in stratiform rainfall have been observed within satellite estimates and models associated with an increase in SST, such as during an El Niño event (e.g. Schumacher et al. 2003, 2004; Masunaga et al., 2006, Houze et al., 2004, Posselt et al., 2012) and the increased discrepancy between TMI and PR rain rates appear to be directly related to variability in the organized regimes.
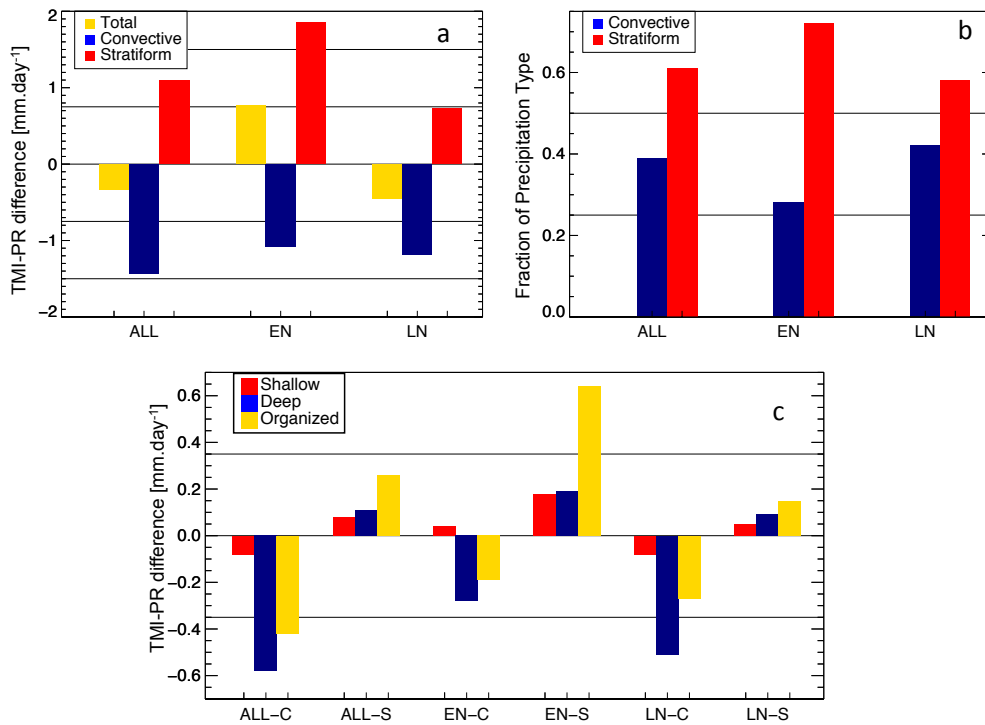
Figure 3.9 Contributions to TMI-PR rain rate differences as a function of convective/stratiform rainfall and convective regime. TMI-PR rain rate differences are for time periods from 2002-2010 (ALL), El Nino events (EN), and La Nina events (LN). Biases are first explained for (a) only convective and stratiform rainfall over the TMI footprint and (b) their occurrence. They are then explained by (c) the convective regimes, which are further split by convective fraction into convective cases (C) and stratiform cases (S) in panel (c).

To examine this further, we deconstruct the systematic differences occurring between TMI and PR to their respective precipitation regimes. Figure 3.9 displays the contribution to TMI-PR rain rate differences by each precipitation regime and convective fraction. The differences are derived using the same time period and 15°x15° region surrounding the Kwajalein GV site as above. Figure 3.9a displays the contribution from convective and stratiform only biases derived using the TMI footprint matching methodology described in Section 3.3c. It is clear that the ENSO related differences between TMI and PR could be comprehended through only convective and stratiform rain rates. The substantial increase in stratiform differences during the El Niño events are directly related to an increase in stratiform occurrence of raining pixels (Figure 3.9b). For raining pixels, stratiform occurrence increases from 61% during the mean state to 72% on

average across the El Niño events. The use of convective and stratiform pixels are able to explain the differences over the ENSO time periods, however, it is the collective information provided by the regime-based analysis provides the proper source and magnitude of the uncertainties. For the mean state and La Niña events the overall negative TMI-PR difference is derived from differences occurring in convective rainfall cases within deep isolated and organized regimes, however, the observed pattern differs during the El Niño events (Figure 3.9c). The TMI-PR differences during the El Niño events yield a positive bias for stratiform cases in organized regimes nearly double that of the mean state and accounts for 81% of the overall bias. The increase is directly related the organized precipitation regime, which also displayed the largest TMI and PR differences in stratiform rainfall at the pixel level (Table 3.4). During La Niña events, rainfall contribution shifts towards deep isolated systems, which also are characterized by more convective raining pixels compared to the mean state and El Niño.

3.4.2 Application of regime-based biases

To assess the degree these bias estimates aid in explaining differences in inter-annual variability, we apply a bias correction for TMI and PR rain rates at the 1° scale based off the differences from the KPOL-GV rain rates. Application of the biases derived using the Kwajalein GV estimates should aid our understanding of the correct distribution of rainfall between the precipitation regimes, their overall impact on TMI and PR differences, and further our understanding of the regional precipitation climatology. The advantage of this methodology is that the validation statistics are physically related to the self-similar precipitation regimes without assuming either the TMI or PR satellite retrievals are correct.

To begin, precipitation regimes are identified from 2002-2012 within the 15°x15° region described above and a bias correction is applied for each precipitation regime and their
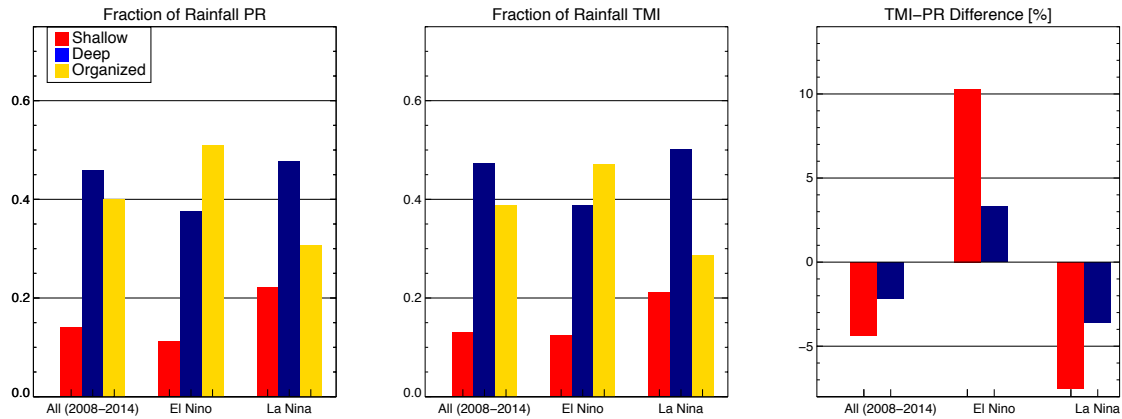
Figure 3.10. Convective regime-based statistics for PR and TMI rain rates for time periods from 2002-2010, El Nino events, and La Nina events. Fraction of rainfall contributed by each convective regime for (a) PR and (b) TMI rain rates after rain rates were corrected based upon their ratio to the Kwajalein dual-polarized rain rate estimates. (c) TMI-PR difference before correction (red) and after bias correction (blue).

convective or stratiform cases using ratios derived from the bias estimates described in Section 3.3a within Table 3.2. The resulting rain rates and TMI-PR differences are presented in Table 3.5 and the resulting fraction of rainfall for each regime contributing to the total rain rate are illustrated in Figure 3.10. The difference in rainfall fraction per regime is greatly reduced. Over the mean state, El Niño events, and La Niña events both TMI and PR retrievals now agree on the precipitation regime that contributes the most to rainfall. As a result, the gap between TMI and PR are reduced for each time period analyzed. Overall, the rain rates are increase slightly for both sensors, which is expected as both were found to underestimate the GV data. While TMI still underestimates PR for all cases and La Niña events, the difference is reduced to -2.2% overall and -3.6% for La Niña events. Further, the difference between TMI and PR during El Niño events is greatly reduced from +10.3% to +3.4%. The improvement in rainfall between TMI and PR demonstrate that the self-similar precipitation regimes provide a strong relationship with precipitation biases and provide a simple and effective technique for validating satellite retrievals and aid in precipitation uncertainty diagnosis.

3.5 Examining retrieval biases

The results outlined thus far have demonstrated that TRMM oceanic biases are dependent on both rainfall regime and the partitioning of stratiform and convective rainfall. For the PR rain rate retrieval, recent work has documented the underestimation of surface precipitation estimates for convective rainfall to errors related to the drop size distribution parameter, which tends to negatively bias the Z-R calculations of rain rate (e.g. Iguchi et al., 2009, Munchak et al. 2011; Bringi et al., 2012). Based on GPROF's physical dependence on the radar for it's a priori database, and the PR retrieval general underestimation compared to the ground radar, underestimation in convective cases for TMI would also be expected, however, in predominantly convective cases the TMI retrieval also underestimates PR by nearly 27.8% and 14.1% in deep isolated regimes and organized regimes, respectively, and for all convective cases when observed at the footprint scale. When retrieving rain rates using a Bayesian approach, biases can be introduced due to the fact that all raining profiles are included into the weighted mean. Negative biases can exist where the Bayesian retrieval is unable to completely distinguish observed brightness temperatures with those within the database, allowing the inclusion of lighter raining profiles during higher rain intensity cases. Similarly, the inclusion of all convective and stratiform FOVs in the weighting process may also lead to biases (Seo et al., 2015) if brightness temperatures within the raining FOV are not distinguishable between convective and stratiform rainfall.

We first inspect this issue by evaluating the TMI retrieval representation of convective rainfall in relation to TMI and PR differences for all precipitation regimes identified within the 15°x15° region described above spanning a three-year period from 2008-2010. The PR definition of convective and stratiform raining pixels is now considered "ground truth" for the convective

72

fraction of rainfall occurring within each 1° x 1° region; generally the PR rain type classification agrees with GV comparison in the Kwajalein region (Schumacher et al., 2000). In Figure 3.11, we derive the difference in mean rainfall for all identified precipitation regimes as a function of convective fraction within each 1° x 1° region for both the TMI and PR retrievals. Figure 3.11a presents the differences for all precipitation regimes, while Figures 3.11b-d present the differences associated with each specific precipitation regime. Overall, the differences agree with the above GV results.

At the highest PR-determined convective fractions TMI underestimates PR rain rates and overestimates PR rain rates within lower convective fractions. Notably, the GPROF retrieval struggles to accurately differentiate convective and stratiform rainfall. PR rain rates span the entire spectrum of convective fractions, whereas TMI rain rates are limited, particularly in organized convection, where convective fractions are generally constricted between 30-60%. The precipitation regimes demonstrate that the differences between the TMI and PR retrievals are not uniform, but in fact vary uniquely for each regime; demonstrating another advantage of evaluating precipitation uncertainty through the use of precipitation regimes.
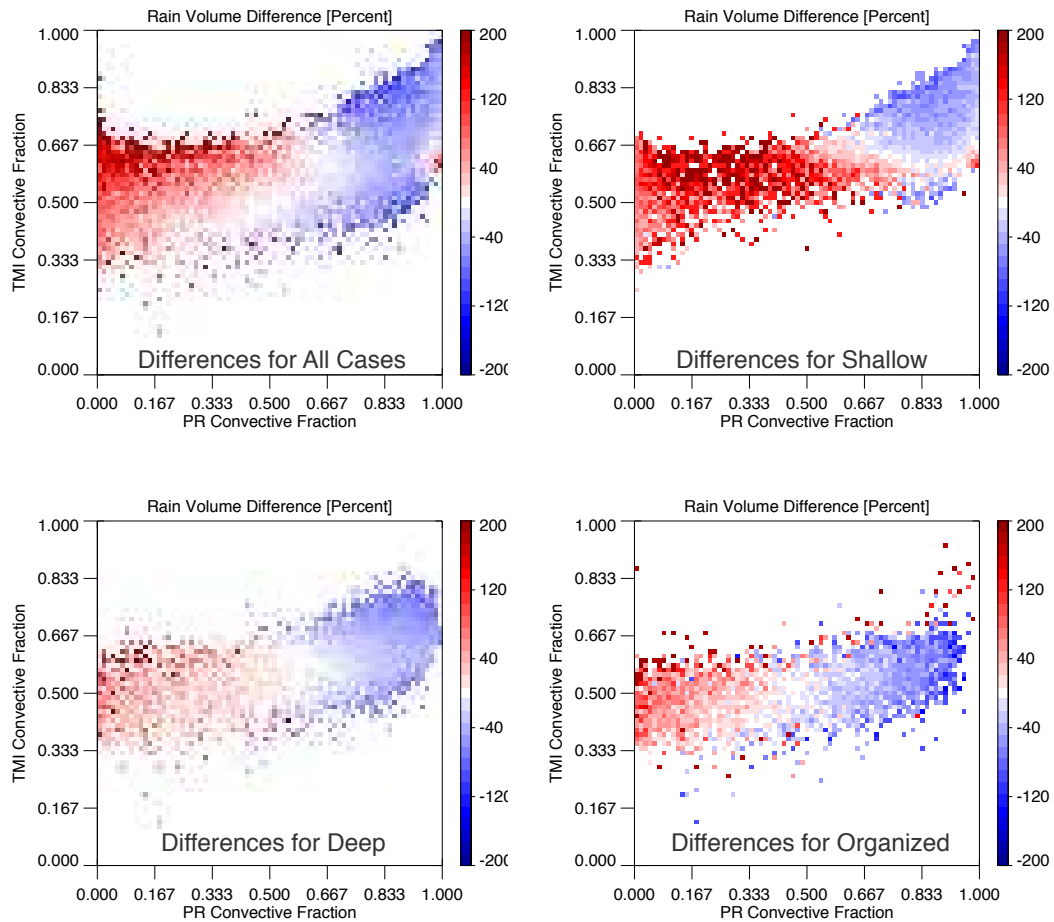
Figure 3.11. TMI-PR differences within a 15° × 15° region surrounding the Kwajalein Atoll as a function of convective fraction and convective regime. Differences are calculated over a three-year period (2008-2010) for (a) all cases, (b) rain rates within shallow convective regimes, (c) rain rates within deep isolated convective regimes, and (d) rain rates within organized convective regimes.

The TRMM biases described in Section 3.3 and Section 3.4 demonstrate that pixel level variations in convective and stratiform rainfall can begin to characterize TMI-PR differences over time. To investigate how the lack of a precipitation type classification may impact the GPROF retrieval at the pixel level, we conduct a sensitivity analysis by constraining the GPROF a priori database by the observed convective rainfall fraction. The GPROF a priori database

SST: 290K-305K, CWV: 35-55 mm

Figure 3.12. (Left) Differences between GPROF-retrieved rain rates and observed rain rates, where the a priori entries in the database are used as "observational" input to GPROF to calculate theoretical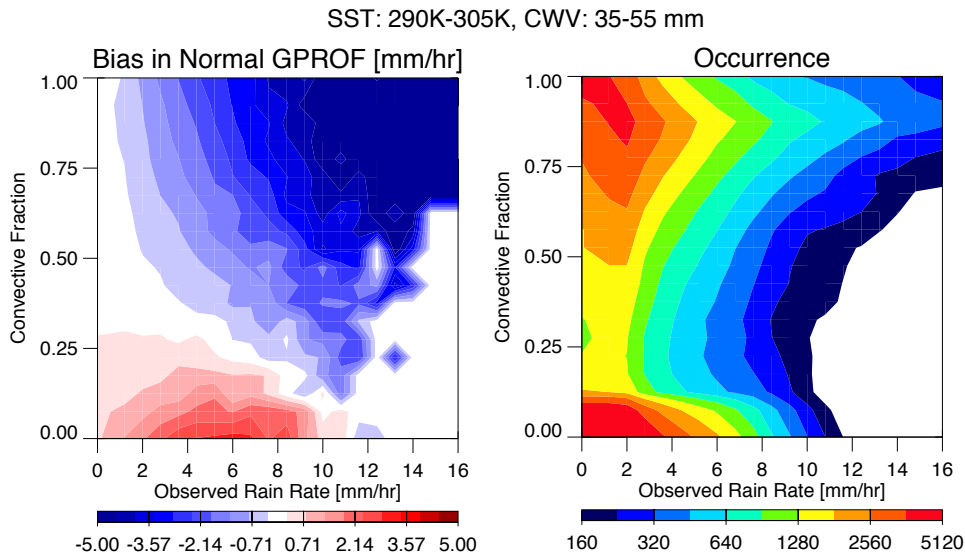 errors occurring as a function of rain rate and convective fraction. (Right) The occurrence of each rain rate comparison as a function of rain rate and convective fraction.

(Kummerow et al., 2011) contains the necessary information to test the Bayesian retrieval: brightness temperatures for each of the nine TMI frequency channels, a PR-based rain rate convolved to the TMI FOV, and its respective convective rainfall fraction from PR. The a priori data entries within the database are used as "observational" input to GPROF to calculate theoretical errors as a function of rain rate and convective fraction. The observed data points are taken within the a priori database for SST values ranging from 290 K to 305 K and column water vapor ranging from 30 mm to 55 mm. These values are commonly observed within the deep tropics, where large TMI-PR differences are found (e.g. Figure 3.1). It is important to note that the PR rain rate will now be considered truth and improvements found within the GPROF retrieval may likely still contain biases when compared to GV data. The GPROF retrieval is first tested in its natural state (control), and then the procedure is repeated constraining the convective fraction to ±15% of the observed convective fraction and ±30% of the observed convective
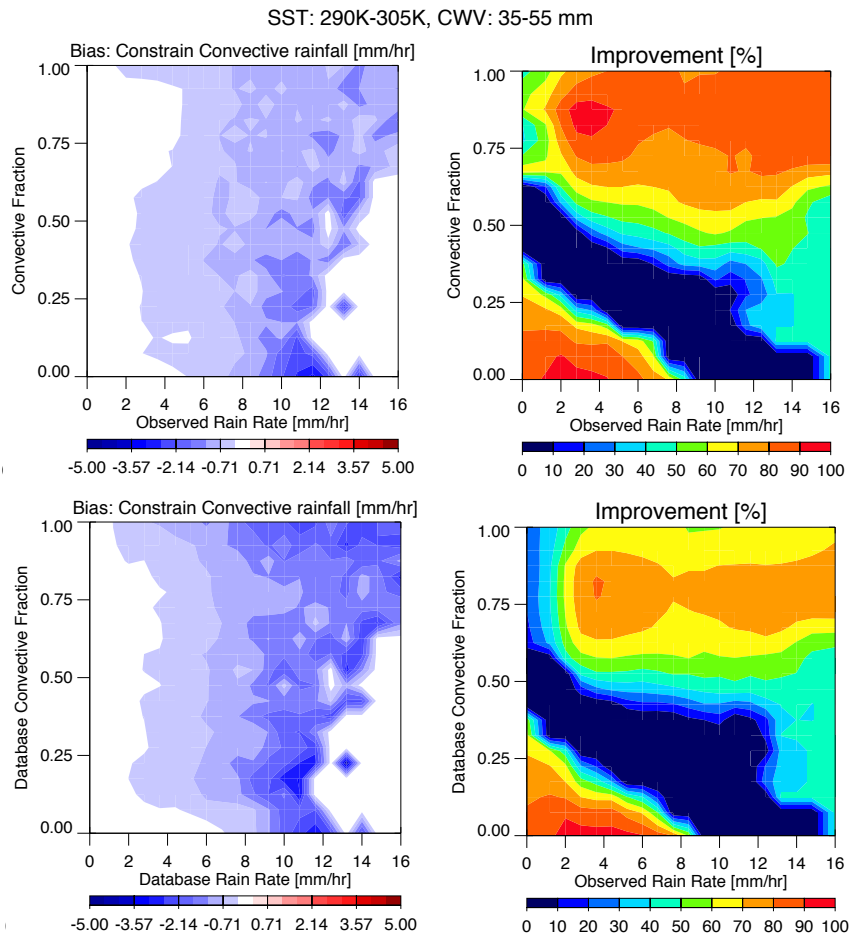
Figure 3.13. Similar to Figure 10, (Left) differences between GPROF-retrieved rain rates and observed rain rates when constraining the convective fraction in the Bayesian procedures by (top) ±15% of the observed convective fraction and (bottom) ±30% of the observed convective fraction. (Right) The improvement in bias when the convective fraction is constrained.

fraction. The convective fraction is constrained by limiting the Bayesian a priori database to only include data points with a convective fraction either ±15% or ±30% of the observed convective fraction of rainfall, therefore, it will only including raining profiles with similar convective characteristics.

Rain rate biases in GPROF, as a function of rainfall intensity and convective fraction are shown in Figure 3.12 for the control case. In a similar manner as the GV results, biases become

positive as stratiform rainfall becomes predominant and largely negative for heavier raining convective scenes. The majority of rainfall occurs where biases are either slightly negative or positive (rain rates < 2 mm hr^{-1}), however, a significant amount of comparisons occur where biases are large (rain rates > 2 mm hr^{-1}); While not as frequent, these higher intensity rain rates contribute towards the majority of total rainfall (Berg et al., 2010). Substantial improvement in GPROF related biases are found when the database is constrained by the convective fraction (Figure 3.13). When the convective fraction is constrained to ±15%, a reduction of bias > 60% is commonly found with biases reduced up to 80% in higher convective fractions. In stratiform cases, the majority of biases are reduced by 70-80%. The overall improvement when the convective fraction is constrained to ±30% is slight lower, but reduction in bias is still significant. There is still a remnant negative bias that occurs as a function of rain intensity; however, this example demonstrates that even roughly identifying the convective fraction could provide significant reductions in TMI and PR oceanic rain rate differences.

3.6 Conclusions

The TRMM satellite has provided a foundational observing system for studying precipitation characteristics across the tropics. Throughout the TRMM mission, research employed various efforts to validate the TRMM rainfall retrievals, however, we still lack an understanding of the sources of bias. This issue is particularly pertinent during El Niño and La Niña events, where regional differences between the TRMM retrievals lead to large discrepancies when averaged over the tropical oceans. This manuscript attempts to better understand biases in TRMM rain rate estimates by comparing TRMM instantaneous rain rates to ground sources with respect to distinct self-similar precipitation regimes.

To begin, TRMM TMI and PR rain rates are compared to ground validation rain rates at the Kwajalein Atoll and measurements taken during the DYNAMO field campaign. The results demonstrate that distinct biases patterns in TMI and PR rain rate estimates exist when biases are associated with the precipitation regimes and their respective convective fractions. In particular, when compared to the Kwajalein GV rain rates, TMI exhibits the largest biases within organized convection systems, which are biased by +33.4% in stratiform cases and negatively biased by -37.8% for convective cases. The bias patterns for both PR and TMI are consistent when observed at the larger scale 1°x1° scale as well as at the TMI footprint scale when split into convective and stratiform components. Analysis at the TMI footprint level reveals pixel level biases in stratiform rain are largest in TMI rain rates, which overestimate by 92.3% in organized regimes, whereas and biases in convective rain rates are driven by deep isolated regimes where TMI and PR underestimate by 66.8% and 52.2%, respectively.

Analysis of the precipitation regime variability in the West Pacific reveals close correspondence between the differences in TMI and PR rainfall and the frequency of occurrence of each precipitation regime. Application of bias correction demonstrates the ability of the precipitation regimes to explain differences found between TMI and PR over the different time periods. Most notable during El Niño events, TMI-PR differences are reduced from 10.3% down to 3.4% and significant reduction was also found during La Niña events. Further exploration into biases within Bayesian retrievals reveals that the biases may be related to differentiating convective and stratiform rainfall. The GPROF algorithm struggles to properly diagnose the convective fraction of rainfall, leading to biases dependent on the precipitation regime being observed. Constraining the selection of a priori data points within the Bayesian framework by the

convective fraction reduces biases in the GPROF retrieval, where we find that the magnitudes of GPROF biases can be reduced upwards of 70-80% in many areas.

The precipitation regimes implemented in this work provide physical sources to relate each TMI and PR bias. The self-similar nature of the regimes provides the potential application of the results across the tropical oceans and becomes a useful methodology to begin diagnosing climate scale uncertainties in precipitation products. To this end, we emphasize that understanding and reconciling the differences in active versus passive retrieved products through the use of precipitation regimes will prove helpful for continued assessment of time-varying situational-dependent biases and continue aiding development and validation of the Global Precipitation Mission (GPM, Hou et al., 2014) or other precipitation related studies.

CHAPTER 4

ENSO INFLUENCE ON TRMM TROPICAL OCEANIC PRECIPITATION

CHARACTERISTICS AND RAIN RATES

4.1 Introduction

The launch of the Tropical Rainfall Measuring Mission (TRMM, Kummerow et al, 1998) in 1997, and the follow-on Global Precipitation Mission in 2014 (Hou et al. 2014) has provided in-depth detail of the physical structures and properties of precipitating systems across the globe. The continued use of satellite-observed precipitation remains important as ground-based observations are sparsely distributed – particularly over the oceans. This importance is amplified by the fact that we currently cannot accurately represent rainfall in global models (Stephens et al., 2010). However, while satellite retrievals are continually improving, discrepancies in tropical rain rates still exist between both model-based and various satellite-based rain rate estimates. One such discrepancy occurs during El Niño events where we observe an increase in both sea surface temperatures (SSTs) and atmospheric pressure over the Pacific basin (Trenberth, 1997) leading to tropic-wide changes in precipitation intensity (Soden, 2000, Held and Soden, 2006).

Wang et al. (2008) compared ENSO variability (25S-25N) in monthly precipitation data from the TRMM radiometer (TMI) and precipitation radar (PR) to rain estimates from the radiometer-based Global Precipitation Climatology Project (GPCP). Over the tropical oceans, passive microwave driven precipitation datasets from GPCP and TRMM TMI show increases in tropical oceanic rainfall of 15.4%/°C and 16.7%/°C, respectively, related to ENSO variability. This SST relationship is less prevalent in PR rainfall estimates where little correlation exists between SST and oceanic precipitation with sensitivity of 1.7-4.4%/°C (Gu et al. 2007; Wang et al., 2008).

Similar estimates are found in Liu et al., (2012) who discovered a robust relationship between increasing SST and CMIP5 models in the tropics (30S-30N), but at a magnitude 3-5 times less than the GPCP and TMI estimates with an average increase of 3.1%/°C.

The different sensitivities may be attributed to how the retrievals interpret more frequent convection with higher rainfall intensity occurring with El Niño events (Lau et al., 2012). In CMIP5 models, the inadequate representation of rainfall processes leads to large uncertainty in the when describing ENSO amplitude, spatial patterns, atmospheric teleconnections, and the magnitude of precipitation change for different climate states (e.g. Su and Jiang, 2012; Watanabe et al., 2012), where little improvement was found from CMIP3 to CMIP5 (IPCC AR5, 2013). Overall, ENSO-induced variability occurring in oceanic rainfall in both observations and models are found to drive the discrepancies found in total rainfall variability. With the prospect of future climate scenarios pointing to a more El Niño-like state (e.g. Vecchi and Soden, 2007; Vecchi and Wittenberg, 2010), it is imperative to further constrain how precipitation changes globally with a changing climate.

In order to better understand the variability of global and regional rainfall, or infer global rainfall variability given an altered climate, a consensus must exist in rainfall observations; a process started by understanding the differences occurring between rain rates retrievals. Differences between the TRMM TMI and PR rain rate retrievals have been linked to environmental characteristics (Berg at al., 2006) and rain rate differences driven by ENSO variability could exist due to a changes in cloud structure over the Pacific (e.g. Berg et al., 2002; Masunaga et al. 2005). Previous research has implemented various classification methodologies to record climatologies of assorted precipitating systems across the tropics (e.g. Houze et al. 2007, Liu et al., 2008, Elsaesser et al., 2010; Zipster et al, 2006), however, it is still difficult to

accurately describe how regional variability in the makeup of the convective population directly influences tropics-wide averaged TRMM TMI and PR rainfall estimates.

Liu and Zipster (2014) derived mean TMI-PR differences for Version 7 TRMM products and found the largest discrepancies occurring in the Central and East Pacific, where TMI rainfall generally overestimates PR, and the largest TMI underestimates of PR rain rates residing in the Indian Ocean - differences in both regions exceed 30%. To help attain the origins of such regional discrepancies in TRMM rainfall, Henderson et al (2017a) used TRMM ground validation (GV) data from the Kwajalein Atoll to establish distinct bias patterns in TMI and PR rain rate estimates as a function of defined precipitation regimes and their convective fraction using methodologies from Elsaesser et al (2010). They found that variability in these precipitation regimes, in particular rainfall from organized precipitation (mesoscale convective systems, MCSs), was driving differences occurring between TMI and PR rain estimates during El Niño events over the Kwajalein region, whereas TMI-PR rain rate differences during La Niña events were driven by more isolated deep convection.

This work looks to expand upon the results of Henderson et al (2017a) to examine the relationship between regional variations in precipitating systems and environmental characteristics related to the TMI-PR discrepancies across the tropical oceans (25S-25N). By focusing on multiple ENSO events occurring throughout the TRMM mission, we observe the variations in regional precipitation organization, as identified by TRMM PR characteristics, to identify the physical sources leading to the TMI and PR rainfall discrepancies. These regional changes in organization will be related to regional TMI-PR rain rate differences and their impact on tropic-wide rain rate anomalies as a function of ENSO phase. Further, because tropical rainfall variability is largely driven by large-scale circulation changes in the Walker Circulation,

and MCS formation is affected by changes in large-scale environmental conditions (e.g. Houze, 2004), we relate the regional changes in precipitation regimes with their respective changes in CAPE, SST, humidity, and wind shear. The final section will focus on applying GV-derived biases in the defined precipitation regimes to investigate how we might further constrain observationally-based estimates of ENSO-induced rain rate variability occurring over the tropical oceans.

4.2 Data and methodology

This work focuses on the Version 7 TRMM TMI 2A12 and TRMM PR 2A25 products from 25S-25N over the tropical oceans for ENSO events occurring from 1998-2013, where El Niño and La Niña events are categorized using a 0.5 °C threshold in the ENSO 3.4 index. The TMI radiometer passively observes radiation using nine channels with horizontal and vertical polarization at 10.65, 19.35, 37.0, and 85.5 GHz and vertical only polarization at 21.3 GHz. Emissivity of the ocean surface is lower than that of land; therefore liquid hydrometeors (i.e. clouds and rain) are clearly detectable over oceans for the TMI radiance channels. The TRMM TMI 2A12 Version 7 rain rate product is derived using the Goddard Profiling Algorithm (GPROF) (Kummerow et al. 2015), which utilizes a Bayesian framework to instantaneously retrieve hydrometer profiles. Data from the TRMM PR Version 7 2A25 product provides radar-based surface rain rate estimates and rain type partitioning from a 13.8 GHz (Ku-band) radar. For this work we use the near surface rain rate estimate from the PR TRMM 2A25 product and stratiform-convective partitioning defined using vertical and horizontal reflectivity gradients in reflectivity (Awaka et al. 1998; Steiner et al. 1995). The PR rain rate retrieval is described in Iguchi et al. (2000; 2009), which utilizes a combination of the surface reference technique

(Meneghini et al. 2000) and the Hitschfeld and Bordan (1954) method to correct for attenuation before deriving the surface rain rates.

Analysis of precipitation characteristics are supplemented using the TRMM GV dual-polarized S-band KPOL located at the Kwajalein Atoll. The continuously scanning observing system provided by the KPOL radar is ideal for understanding the changes in precipitating systems in an oceanic setting, providing high temporal and horizontal resolution sampling of precipitating systems. The KPOL-derived TRMM 2A55 product provides stable calibrated reflectivities with a 1.5 km vertical resolution and 2 km horizontal resolution (Silberstein et al., 2008; Marks et al. 2009). KPOL rain rates (TRMM 2A53 product) and convective-stratiform partitioning (TRMM 2A54 product) are also used to aid the precipitation regime classification and to analyze variability in precipitation characteristics. For this work, KPOL data are observed over six wet season periods (September-December) from 2006-2011. The wet seasons provide the largest variability of precipitating systems and coincide with the boreal winter months, where the regional ENSO related precipitation anomalies are typically largest.

Precipitating systems over the tropical oceans are categorized following the methodology described in Elsaesser et al (2010) for all TRMM orbits from 1998-2013. Motivated by Johnson et al. (1999), the classification separates precipitation into three precipitation regimes according to their level of organization. The regimes are created by inputting the distribution of precipitating cloud echo top heights, mean convective rainfall, and the ratio of convective to stratiform rainfall contained within a 1°x1° box centered along nadir PR pixels into a k-means clustering algorithm. For the resultant k-means separated systems we adopt the definitions described by Elsaesser and Kummerow (2013) who define the three categories as shallow, deep isolated, and organized precipitation regimes, which will be used henceforth in this paper to

84

describe the level of organization of precipitating systems. As in Henderson et al. (2017a), each precipitating regime is further sorted into cases containing predominantly convective or stratiform rainfall using PR defined precipitation types; this was shown to better describe rain rate differences between TMI and PR estimates. TMI retrieved surface rainfall is matched to each 1°x1° domain along the TRMM orbit and mean rain rates from TMI and PR over each 1° x 1° region will be compared, where differences are defined as TMI minus PR rain rate estimates.

Precipitating systems from the KPOL radar are identified using the same procedure applied to the KPOL radar reflectivity and rain rates from 2006-2011, which was successfully implemented previously to study rain rate sensitivity to precipitation regimes at Kwajalein in Henderson et al. (2017b). To further study the changes in precipitating systems we implement the TRMM raining precipitation feature (TRMM RPF) database described in Liu et al. (2008). The TRMM RPF features are defined by system areal extent through contiguous pixels observed by the TRMM PR, thus providing comparison of precipitation characteristics and rain rates at the system level without the need for gridding. In this work we focus the comparisons using the TRMM RPF MCS definition described in Liu and Zipster (2013) who define MCS systems as any set of contiguous raining pixels along the PR swath containing a horizontal area > 1000 km^2.

To relate the precipitation features to their respective large-scale environments we utilize the European Centre for Medium-Range Weather Forecasts (ECMWF) Interim Re-Analysis (ERA-Interim) (Dee et al. 2011) gridded at 1° x 1° resolution and 6-hourly temporal resolution. Environmental parameters of CAPE, SST, zonal wind profiles, and relative humidity are taken from the ECMWF Interim reanalysis to compare with the precipitation regimes. The TRMM data are collocated spatially to the nearest ERA-interim grid box and temporally to the closest time preceding the TRMM observation. Environmental properties are important factors when

considering the level of organization in precipitating systems. Humidity and wind fields have been shown to be accurate when compared to the Atmospheric Infrared Sounder (AIRS) and sounding data in Tian et al (2010) as well as through comparisons with the Constellation Observing System for Meteorology, Ionosphere, and Climate (COSMIC) moisture retrievals in Kishore et al (2011), where systematic errors were found to be the lowest in ERA-interim compared to other reanalysis datasets. For these reasons, the ERA-interim reanalysis provides the best opportunity to compare environmental properties over the oceans at this time. Further, to ensure results in humidity are consistent, we also include analysis using the methodology described by Masunaga (2013) who combine collocated TRMM data with the Atmospheric Infrared Sounder (AIRS) to observe the variability in the vertical structure of environmental moisture conditions associated with TRMM precipitating systems. For this work we combine the TRMM with AIRS satellite measurements of atmospheric moisture composited over El Niño and La Niña/Neutral conditions in the Pacific (15S-15N; 160E-280E) from 2002-2009. The composite procedure records the AIRS moisture data with respect to the overpass time difference between TRMM and AIRS - providing a continuous record of mean water vapor mixing ratio in hour intervals 72 hours before and after TRMM observations of rainfall.

4.3. ENSO-Related Convective Variability in the Tropics

4.3.1 Kwajalein Atoll

This study first investigates variability in the defined precipitation regimes using the KPOL radar located on the Kwajalein Atoll. While TRMM orbital data allow broad spatial observations of precipitation, regional measurements of individual precipitating regimes can be sporadic – particularly observations containing significant amounts of rainfall (Schumacher et al. 2000). To

better understand the variability in the convective populous, the high temporal resolution GV data from the Kwajalein KPOL radar site can be used as a blueprint of what we should expect when the focus is expanded over the TRMM. Precipitation anomalies during ENSO events are typically locked seasonally to the boreal winter months (Rasmusson and Carpenter, 1982); therefore, we observe variability occurring in the physical characteristics of the precipitating regimes from 2006-2011 during the wet season months (September-December) at the Kwajalein Atoll, a period where the majority of rain accumulation occurs and fully captures two El Niño and La Niña events.

Table 4.1 Mean SST anomaly compared to the TMI-PR difference (as a percentage) occurring over each wet season at the Kwajalein Atoll form 2006-2011. Mean TMI-PR differences are calculated using all raining systems observed by TRMM in a 5°x5° region surrounding the Atoll.

	2006	2007	2008	2009	2010	2011
SST Anomaly [°C]	+0.4	-0.1	-0.6	+0.2	-0.2	-0.3
(TMI-PR)/PR [%]	9.1%	+1.8	-6.4	+10.7	-12.0	-2.9

Table 4.2 Mean precipitation system characteristics in terms of system size and occurrence for each of the precipitation regimes observed by the KPOL radar during each wet season at the Kwajalein Atoll from 2006-

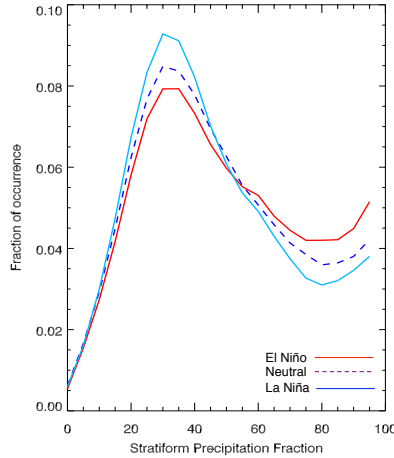|	2006	2007	2008	2009	2010	2011
Shallow						
Occurrence [%]	44.1	50.2	53.2	44.4	50.2	48.2
Rain Extent [%]	3.1	2.9	2.5	3.2	3.8	2.8
Stratiform Extent [%]	1.7	1.5	1.4	1.8	1.7	1.5
Deep						
Occurrence [%]	34.7	34.3	28.7	33.5	31.0	35.9
Rain Extent [%]	16.7	13.8	10.6	10.7	12.9	10.2
Stratiform Extent [%]	5.1	4.6	3.9	4.5	4.7	3.7
Organized						
Occurrence [%]	21.2	15.5	18.1	22.1	18.8	15.9
Rain Extent [%]	40.1	39.4	31.7	36.0	36.6	33.4
Stratiform Extent [%]	33.7	27.8	18.6	26.3	26.8	24.6

Figure 4.1 Frequency distribution of the stratiform rain fraction as observed by the KPOL radar over three wet season periods based upon SST anomalies during each wet season defined as El Niño (2006, 2009), Neutral (2007, 2010) and La Niña (2008, 2011).

To begin highlighting ENSO-based variations in the extent and frequency of the precipitation regimes, SST and TMI-PR rain rate differences for each wet season are included in Table 4.1, and precipitation properties occurring within the regimes for each wet season are presented in Table 4.2, including: precipitation regime occurrence, rain extent, and stratiform fraction. The raining extent is defined as the fractional areal coverage of radar-detected raining pixels within each 1° x 1° box. Similar to TRMM observations discussed in Henderson et al (2017a), the wet seasons associated with the two El Niño events exhibit the highest occurrence of organized precipitation and precipitation system extent, which coincides with a positive TMI-PR rain rate differences; La Niña time periods are more influenced by isolated convection, smaller system size, and negative TMI-PR differences. Further, the warmer SST periods at Kwajalein contain significantly different occurrences of stratiform precipitation extent compared to the La Niña or neutral state conditions (Figure 4.1), where there is a systematic shift toward more stratiform rainfall. It should be noted that wet seasons directly following El Niño events, where SSTs are anomalously lower, also exhibit large stratiform extent, however, the frequency of occurrence is
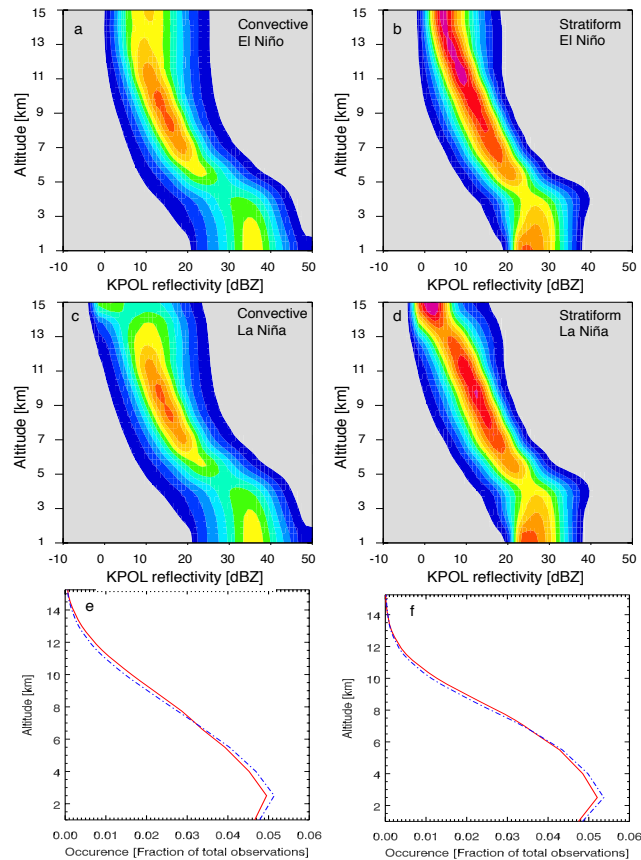
Figure 4.2 Contoured frequency by altitude diagrams (CFADs) of reflectivity profiles observed at the KPOL radar occurring for deep isolated and organized precipitaion regimes split by (left) convective rainfall and (right) stratiform rainfall. The CFADs are created over the (top) El Niño (2006, 2009) wet seasons and (middle) for La Niña/Neutral (all other wet seasons) by binning by altitude every 750 m and reflectivities are binned in 1 dB increments. (bottom) comparisons of normalized occurrence by altitude between El Niño (solid) and La Niña (dashed) conditions.

lower suggesting that the higher SST anomalies may be important to help drive more frequent convection.

Analyzing the frequency and distribution of reflectivity with height provides further detail on the variability in vertical structure and possible microphysical processes in precipitating systems. Contoured frequency by altitude (CFADs) of KPOL reflectivities for convective and stratiform rainfall originating from deep isolated and organized precipitation regimes are shown in Figure 4.2. The CFADs are divided based upon regimes occurring in warmer SST wet seasons during El

Niño events (2006 and 2009) which are compared to all other wet seasons. In general, CFADs between the precipitation types display the same vertical structure. Below the freezing level, ~5 km as indicated by the bright band signature in the stratiform precipitation, the distribution of reflectivities is generally similar between the individual precipitation types. Differences, however, exist above this level. Warmer SST periods contain a higher frequency of occurrence of precipitation particles in the upper levels in both stratiform and convective precipitation, which is confirmed by higher occurrence in the upper atmosphere within both precipitation each types (Figure 4.2de). While the CFADs exhibit the general tilting structure with height, the warmer SST periods extend more vertically in the upper levels. This indicates that larger precipitation particles, or possibly more particles, are being lofted above the freezing level in convection and then being transported to the stratiform regions during these time periods. This evidence of deeper stratiform and convective extent is consistent with the colder cloud top temperatures and echo top heights observed by (Masunaga et al, 2006) as well as in CloudSat observations (Li and Schumacher, 2010).

4.3.2 Relating TRMM TMI-PR differences to convective variability

Henderson et al (2017a) developed a conceptual model of expected biases in TMI and PR rainfall estimates for the precipitation regimes, which can be applied to discuss the origins of TMI-PR differences and how regional variability in precipitation regimes leads to the observed TRMM rain rate discrepancies. In the GV analysis described in Henderson et al (2017a), the TRMM PR rain rate estimates generally underestimated Kwajalein GV polarimetrically-tuned rain rates across all precipitation regimes, with the highest biases originating from predominantly convective rainfall. TMI rain rates exhibit similar bias patterns within predominantly convective

rainfall; however, the TMI rain rates heavily overestimated Kwajalein GV estimates in precipitation regimes containing significant amount of stratiform precipitation. Elsaesser et al (2010) described a self-similar nature observed in the precipitation regimes, therefore, we can hypothesize that the TRMM bias patterns and TMI-PR rain rate differences will exhibit consistency across other oceanic regions as well.

When solely comparing only TMI and PR rainfall estimates, Henderson et al. (2017a) observed that TMI underestimated PR rain estimates in predominantly convective rainfall and overestimated PR rain estimates in predominantly stratiform rainfall; therefore, in regions where isolated convection is most frequent TMI should be observed to underestimate the PR estimates, but both retrievals were negatively biased to GV rain rate estimates. In oceanic regions with increased occurrence in organized rainfall containing extensive precipitating stratiform regions, TMI rain rates estimates were found to be overestimated compared to PR rainfall estimates and PR rain estimates were observed to be closer to the GV truth. This information can be used to relate the discrepancies between TMI and PR rain rates occur during 1997/1998 and 2009/2010 El Niño events – the two strongest El Niño events during the TRMM record. According to the ground validation results described in Henderson et al. (2017a), these warm ENSO events should demonstrate increased frequency of organized precipitation in regions of positive SST anomalies.

During these two El Niño events the largest variability in the precipitation regime occurrence is focused toward the equatorial pacific (Figure 4.3), which is a region coincident with the positive SST and surface convergence anomalies associated with El Niño events (Kim and Yu, 2012; Ratnam et al., 2011). In the Central and East Pacific the predominant precipitation type shifts toward precipitation containing more stratiform rainfall, with largest anomalies in organized precipitation regimes. Regimes with more convective rainfall are increased in the
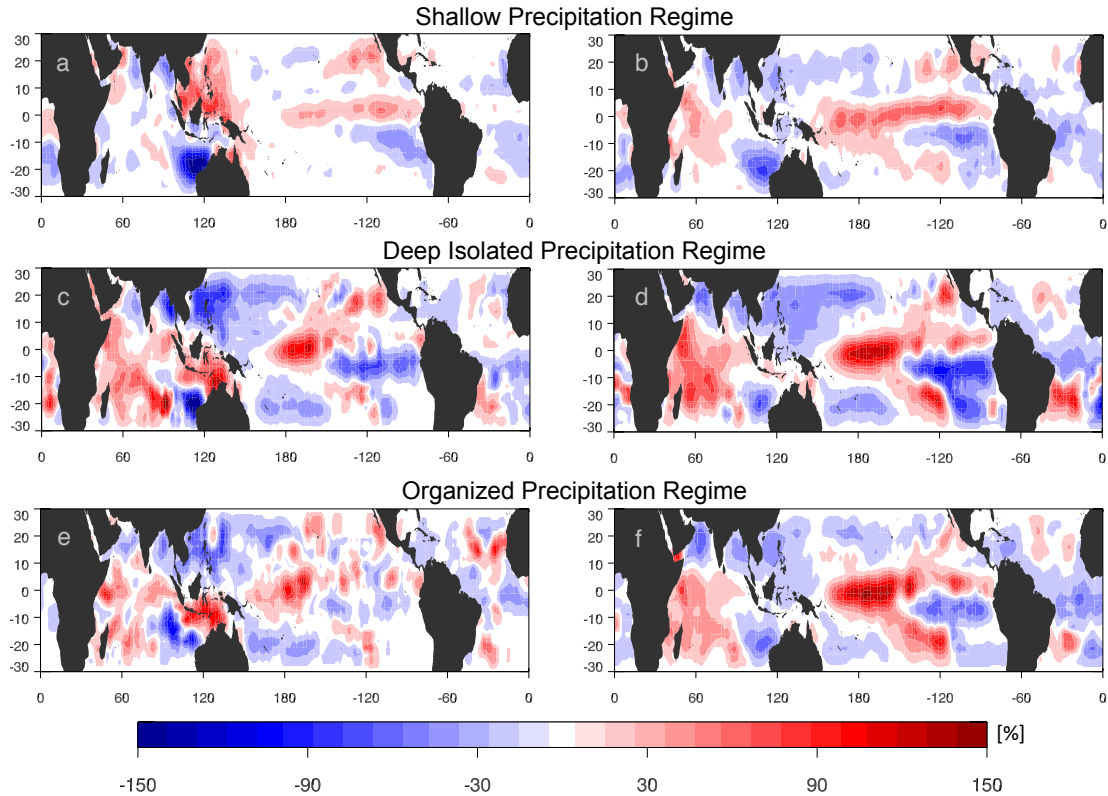
Figure 4.3 Percent change in the regional distribution of the (a,b) shallow, (c,d) deep isolated, and (e,f) organized precipitation regimes occurring during the 97/98 and 09/10 El Niño events compared to the 1998-2013 mean state. Regional maps are further split by convective fraction, where convective cases (left) are described where the convection precipitation fraction > 0.50 and (right) stratiform cases where the convective precipitation fraction is < 0.50.

Pacific basins to a lesser degree, but are also more frequent in the Indian Ocean and maritime continent area.

To evaluate the impact of the precipitation variability during ENSO phases, differences between TMI-PR are shown for El Niño and La Niña time periods, defined where the ENSO 3.4 index exceeds ±0.5 °C. Henderson et al. (2017a) demonstrated that TMI-PR rain rate differences occurring during El Niño events near the Kwajalein GV site were largely driven by a systematic shift toward more frequent organized precipitation regimes characterized by large precipitating stratiform regions, which is also observed here across the Pacific basin (Figure 4.4). Relative to the PR estimates rain rates, overestimation of rainfall by TMI is the largest and most widespread
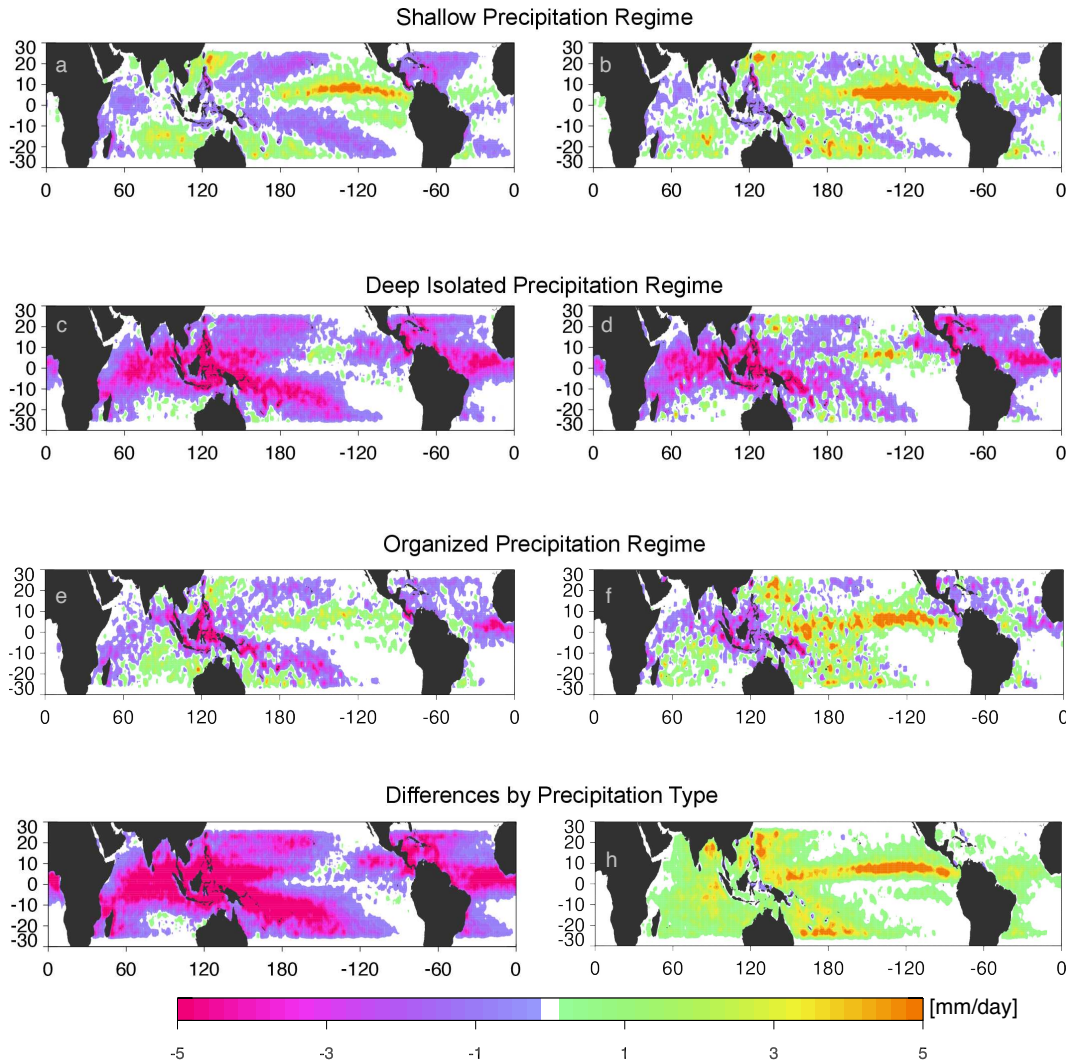
Figure 4.4 TMI-PR rainfall differences [mm/day] for the (a,b) shallow, (c,d) deep isolated, and (e,f) organized precipitation regimes. Cases are split by (left) La Niña cases, and (right) El Niño cases. (g,h) All raining regimes compared to the TRMM post boost climatological rain rates from 2002-2013 split by (left) convective cases, and (right) stratiform cases. . The difference maps were created by comparing collocated TRMM TMI and PR rain rates dataset on a 1°x 1° grid.

in the Central and East Pacific in the organized regimes. The increase in organized regimes and stratiform occurrence during El Niño conditions results in positive rainfall differences extending from the equatorial eastern pacific to the central Pacific ocean basins, which branches north and south toward the East China Sea and along the Southern Pacific Convergence Zone. This pattern is nearly mimicked by the shallow precipitation regime, where the positive TMI-PR differences exist where stratiform precipitation in predominant and negative where regimes are more

93

Table 4.3 Percentage of mean rainfall fraction as well anomalies in rainfall fraction are provided for El Niño and La Niña events occurring from 2002-2013. Percentages are defined as the total number of raining pixels detected by PR divided by the total number of pixels in a precipitation regime grid box.

	Stratiform	Convective	All
Shallow Regime			
Mean	4.5	2.1	6.6
El Nino	+4.0	+3.5	+4.0
La Nina	-2.7	+1.1	-1.4
Deep Isolated Regime			
Mean	9.9	6.2	15.1
El Nino	+3.2	+3.9	+4.8
La Nina	-2.8	-1.6	-2.7
Organized Regime			
Mean	27.2	7.8	35.0
El Nino	+7.6	-0.5	+7.1
La Nina	-0.1	-0.1	-0.4

convective focused. With the exception of the East Pacific, deep isolated precipitation contains predominately negative TMI-PR rain rate differences and exhibit less spatial variation between ENSO phases.

The TMI overestimate in rainfall compared to PR is consistent with increases in stratiform precipitation associated with the organized precipitation regimes. Further, splitting the TMI-PR differences by precipitation type helps to display the convective and stratiform dependence in the rain rate biases (Figure 4.4gh), which is consistent with Seo et al (2015) and Henderson et al. (2017a); the latter demonstrated that the magnitude of these TMI-PR differences increases as a function of precipitation regime. Similar to the Kwajalein region, when comparing El Niño to La Niña events, the changes in precipitation anomaly patterns correlate to an increase in both system size and an increase in precipitating stratiform extent (Table 4.3). Averaged across the tropics, stratiform extent, as identified by 2A25 classification flags, increases by 7.6% in organized regimes; this global signal largely caused by changes in the central and eastern Pacific basins
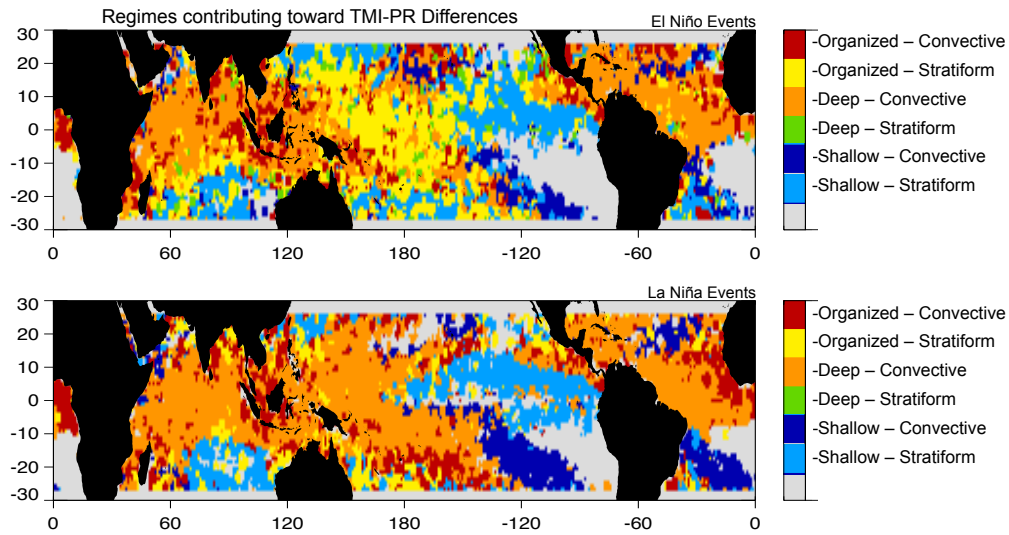
Figure 4.5 Primary precipitation regime responsible for the TMI-PR differences gridded at 1° resolution occurring during (top) El Niño and (bottom) La Niña conditions.

(not shown), where convective organized storms increase the most in frequency and stratiform extent increases by nearly 20%.

To help determine if the relationships in the distribution of regimes drive the ENSO-related variability found in the tropic-wide rain rate estimates, the regime responsible for the largest contribution towards TMI and PR rain rate differences are shown in Figure 4.5. These regimes represent the different modes of organization that likely drive differences found between TMI and PR rain rate anomalies between La Niña and El Niño events. The greatest differences between the ENSO phases are found in the West and Central Pacific basins. The large swath of TMI rain rate overestimates are driven by a switch from deep isolated regimes to organized regimes containing large precipitating stratiform anvils. The negative differences found in the Atlantic, Indonesia region, and Indian Oceans are due to predominate rainfall from deep isolated precipitating regimes containing mostly convective rainfall. For both ENSO phases, the positive differences common to the East Pacific are related to shallow precipitating systems where most
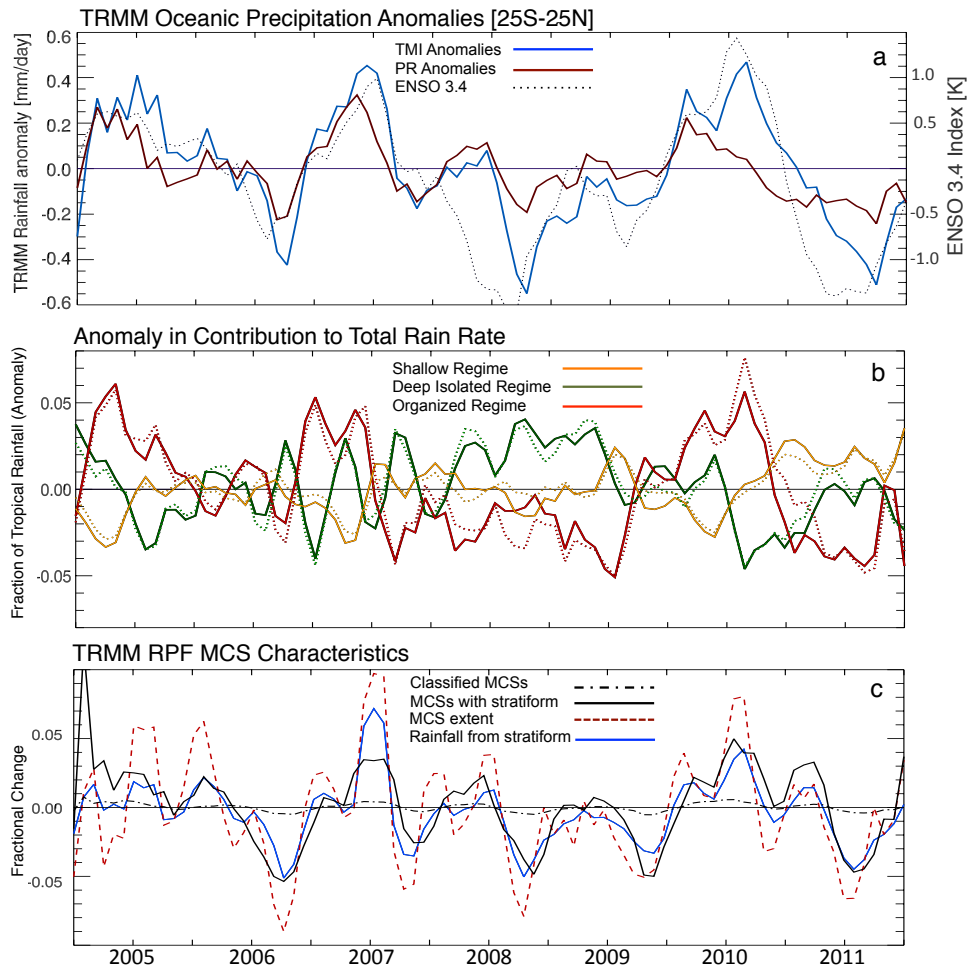
Figure 4.6 (a) Time series of tropical mean oceanic rainfall anomalies (25S–25N) from collocated TRMM TMI and TRMM PR rainfall products with the ENSO 3.4 index (dotted) included for reference. (b) Time series in the anomalies of shallow, deep isolated, and organized precipitation regimes contribution to the total rain rate for TRMM TMI (solid) and TRMM PR (dashed) rain rates. (c) Time series in the anomalies found in MCS characteristics taken from the TRMM RPF dataset. Anomalies included are the changes in MCS occurrence (dot dash), MCSs occurrence where rainfall is predominantly stratiform (solid black), MCS rainfall extent (dash), and contribution to total rainfall from all RPFs with more than four PR pixels (solid blue).

of the rainfall is defined as stratiform. This agrees with previous work, which describes the regional precipitation containing predominantly shallow, but somewhat organized systems (Liu and Zipster, 2013; Chen and Liu 2016).

The regional variability found in each precipitation regime between ENSO phases is evident when observing tropic-wide monthly rain rate anomalies. Comparisons of rain rate anomalies are now focused to the period from 2004-2011 to closely investigate the 2006/2007 and 2009/2010

El Niño events, which were both followed by La Niña events. While PR and TMI tropical rain rate anomalies differ, the contribution to the total rainfall for each precipitation regime is fairly consistent between TMI and PR retrievals (Figure 4.6b), which incur alternating periods dominated by deep isolated during La Niña conditions and organized precipitation regimes during El Niño conditions. Similar patterns are observed within MCSs defined by the TRMM RPF dataset (Figure 4.6c). Overall, variability in TRMM RPF MCSs is small, however, during the El Niño periods changes in the fractional amount of stratiform rainfall in the tropics are linked to a higher occurrence of MCSs with increased horizontal extent and stratiform rainfall. Further, periods where these MCSs are more frequent correlate with tropics-wide variability in the amount of stratiform rainfall. These changes in organized rainfall help to explain discrepancies in the TMI and PR rain rate anomalies.

Figure 4.7 displays oceanic rainfall anomalies for TMI and PR deconstructed into their individual contributions from shallow, deep isolated, and organized precipitation regimes. Similar to the TMI-PR differences found in Henderson et al. (2017a), the precipitation regimes containing predominantly stratiform rainfall describe the discrepancies found in total oceanic rainfall between the rainfall retrievals. The stratiform rainfall regions in the organized and shallow precipitation regimes account for the majority of the precipitation anomalies found in TMI rainfall estimates - a relationship less prominent in the PR rainfall anomalies. This lower amplitude in the organized and shallow regimes results in decreased PR rain rate anomalies occurring at the peak of El Niño events (Figure 4.7c). This disparity is strengthened during the 2009/2010 El Niño event where a sharp decrease in TRMM PR anomalies related to differences in in deep isolated convective precipitation regimes, regimes where TMI rain rates underestimate those retrieved by PR. The differences in deep isolated convection seem to be driven by more
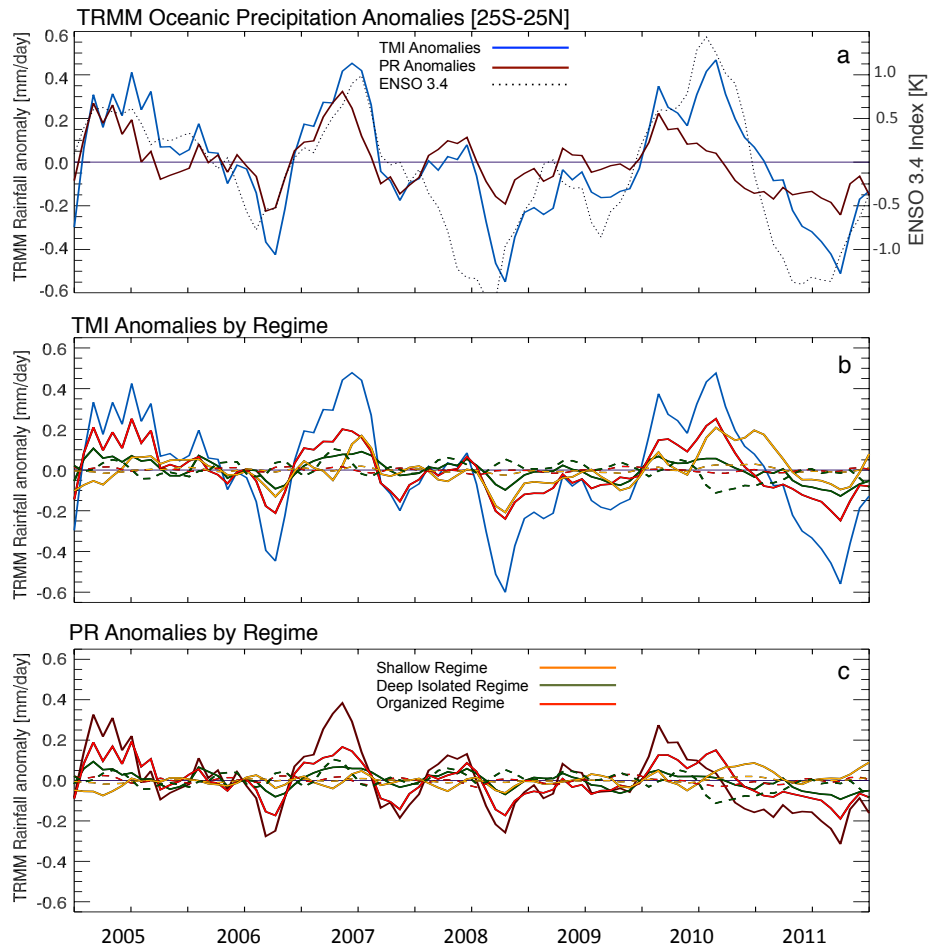
Figure 4.7 (a) Time series of tropical mean oceanic rainfall anomalies (25S–25N) from collocated TRMM TMI and TRMM PR rainfall products with the ENSO 3.4 index (dotted) included for reference. Contributions to the (b) TMI and (c) PR rainfall anomalies for each precipitation regime over the tropical oceans split into convective (dashed) and stratiform (solid) cases. Total rainfall for (b) TMI is shown in blue, and total rainfall for (c) PR is shown in dark red.

frequent deep convective rainfall over the maritime continent region during the 2009/2010 Central Pacific or Modoki El Niño event, which resulted in higher than normal convection in this region (Su and Jiang, 2012).

4.4 Environmental relationship to precipitation variability

During El Niño events, anomalous regional SST patterns shift convective activity in the western equatorial Pacific toward the Central and Eastern Pacific basins. This shift in convection
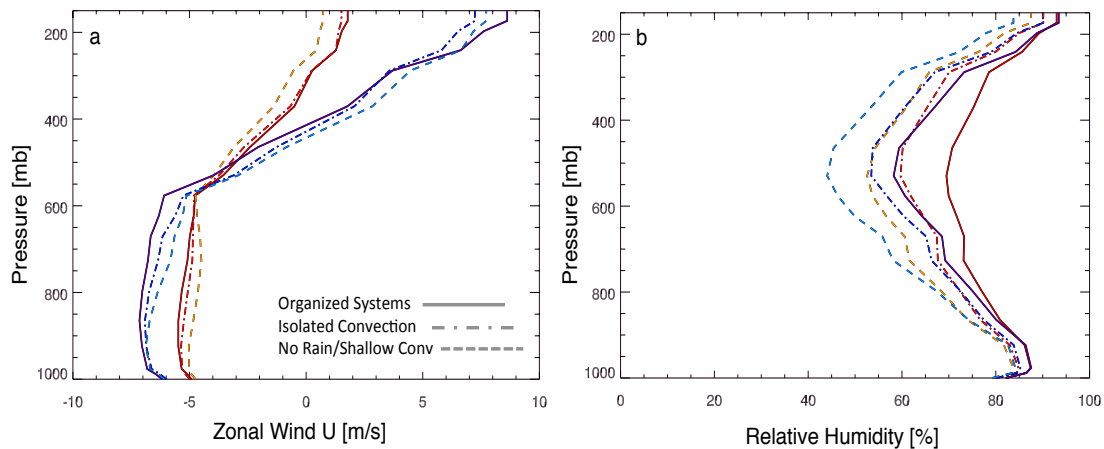
Figure 4.8 (a) Zonal wind and (b) relative humidity profiles as a function of precipitation regime and ENSO phase from the Kwajaelin Atoll radar. Included are (solid) organized regimes, (dot dashed) deep isolated regimes, and (dashed) regimes with no rainfall or shallow convection. Each regime is shown during (red) El Niño condition from the 2006 and 2009 wet season and (blue) La Niña conditions during the 2008 and 2011 wet seasons. Environmental data are based spatial and temporally matched ERA-interim reanalysis fields.

leads to an altered Walker circulation and the local synoptic environment in which convection initiates. In the results above, we demonstrate the impact of convective variability, in specific organized precipitation regimes, on TMI and PR rain rates. Formation of MCSs with broad stratiform regions is largely dependent on the thermodynamic and moisture properties of the atmosphere as well as the strength of upper-level wind shear (Yuter and Houze, 1998; Houze, 1993, 2004). In this section ERA-interim reanalysis fields are collocated to each precipitation regime for El Niño and La Niña events to better understand the large-scale environment's relationship to precipitation organization.

4.4.1 Kwajalein Atoll

As with the convective variability section above, we first compare environmental properties to the large number of samples available at the Kwajalein Atoll; warmer SST periods at Kwajalein contain significantly different occurrences of stratiform precipitation extent compared

99

to the La Niña wet seasons (Table 4.2). Figure 4.8 illustrates zonal wind profiles and relative humidity profiles for each of the precipitation regimes categorized by El Niño and La Niña events over the Kwajalein region. Each panel includes comparisons from the (solid lines) organized precipitation regimes, (dashed-dotted lines) deep isolated regimes, and (dashed lines) cases containing either no rainfall or shallow precipitation regimes. The red and blue lines distinguish the El Niño and La Niña events, respectively. Mean SST, CAPE, and wind shear values for the organized precipitation regimes are also provided in Table 4.4.

Table 4.4 Mean SST, CAPE, Mid-level Shear (800-500mb), and Upper-level Shear (500-200mb) for the Kwajalein Atoll, Central Pacific, and East Pacific regions as a function of ENSO phase.

	El Nino	La Nina
Kwajalein		
SST [K]	302.5	301.6
CAPE [J/kg]	1470.5	1273.7
Mid-level Shear [m/s]	1.5	2.2
Upper-level Shear [m/s]	4.6	12.6
Central Pacific		
SST [K]	301.9	300.7
CAPE [J/kg]	730.6	601.7
Mid-level Shear [m/s]	3.2	10.3
Upper-level Shear [m/s]	7.6	22.2
East Pacific		
SST [K]	300.8	299.6
CAPE [J/kg]	722.9	675.4
Mid-level Shear [m/s]	1.7	5.5
Upper-level Shear [m/s]	6.2	16.2

Zonal winds vary little across the individual precipitation regimes, with easterly winds throughout the lower- and mid-levels and are slightly stronger during La Niña conditions. Each regime occurs in an environment with minimal mid-level shear (850-500 mb) suggesting that stratiform precipitation formation in this region may be less reliant on shear and instead more reliant on convective rain coverage – supported by increased SST and CAPE in the organized precipitation regimes during El Niño conditions. While the lower- and mid-level wind shear

conditions vary little between the warm and cold SST events, large differences exist with upper-level wind shear (500-200 mb). The influence of the Walker Circulation is evident as upper-level wind shear strengthens in La Niña conditions by nearly a factor of two. It has been shown previously that strong upper-level wind shear can be detrimental to the formation of precipitating stratiform regions as the wind can transport ice particles farther, leading to more non-precipitating anvil regions (Schumacher et al., 2006, Li and Schumacher 2010).

For all precipitation regimes, the oceanic environment provides ample low-level moisture, resulting in marginal differences in the shape and magnitude of relative humidity profiles from the surface to 900 mb (Figure 4.8b). Significant differences, however, exist above this level between the warm and cold ENSO events; particularly noticeable near 400-500 mb where there is an increase in moisture of ~10% in El Niño conditions and organized precipitation. Overall, there is a systematic increase in relative humidity in the mid-levels based as a function of precipitating system organization where the highest humidity values occur in organized precipitation regimes during El Niño time periods. This shift in precipitation is consistent with previous work, which demonstrated moistening of the atmosphere prior to periods of significant stratiform rainfall in the West Pacific and Indian Ocean (e.g. Sobel et al. 2004; Barnes et al 2014). The increased moisture occurring in organized precipitation compared to the other regimes implies that the precipitating stratiform regions are helping to moisten the environment, however, humidity profiles at Kwajalein during El Niño events are consistently more humid overall. This could be related to the increased convective activity observed in this region, which would help sustain an environment conducive for the stratiform precipitation regions.
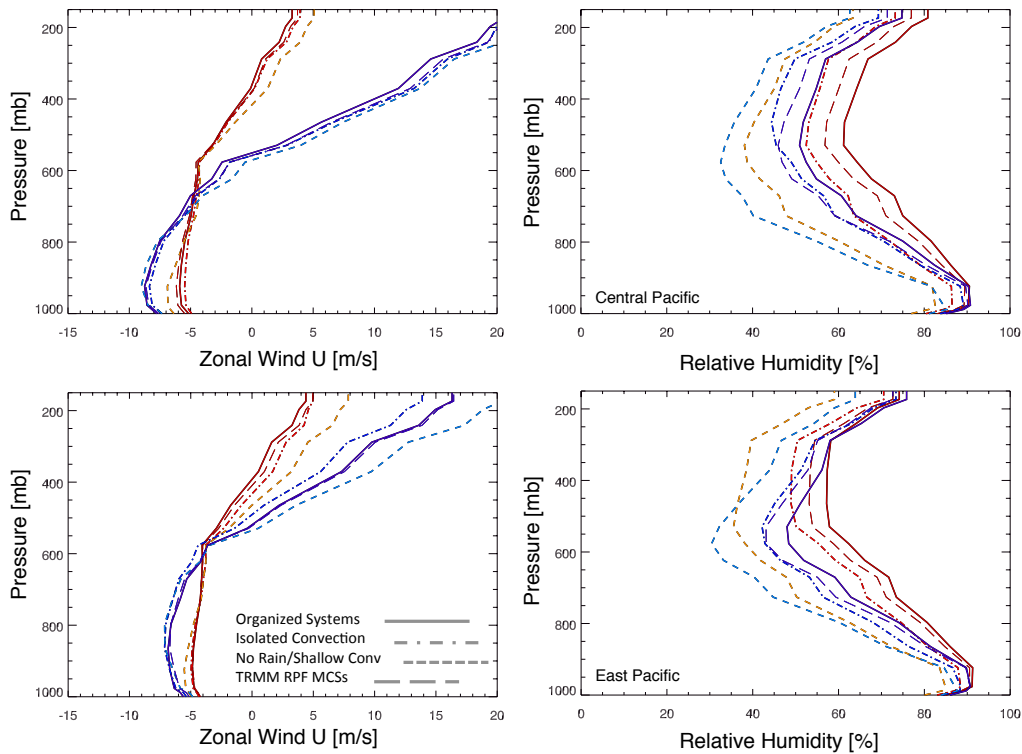
Figure 4.9 (a) Zonal wind and (b) relative humidity profiles as a function of precipitation regime and ENSO phase from the (top) Central Pacific and (bottom) East Pacific. Included are (solid) organized regimes, (dot dashed) deep isolated regimes, and (dashed) regimes with no rainfall or shallow convection. Also included are (long dashed) MCSs observed in the TRMM RPF dataset. Each regime is shown during (red) El Niño condition and (blue) La Niña conditions categorized using a 0.5 C threshold from the ENSO 3.4 index. Environmental data are based spatial and temporally matched ERA-interim reanalysis fields.

4.4.2 Central and East Pacific

To expand upon the Kwajalein analysis above, environmental conditions collocated to TRMM observations are observed within the Central Pacific (10S-10N; 180E-210E) and Eastern Pacific (10S-10N; 230E-260E) ocean basins; these are regions where differences between TMI and PR are the largest during warm ENSO events. Collocated TRMM and ERA-interim reanalysis zonal winds and relative humidity conditions are displayed in Figure 4.9 and mean SST, CAPE, and wind shear values in Table 4.4. ENSO-related differences in the vertical profile of zonal winds in the Central and East Pacific are analogous to those observed at the Kwajalein

Atoll, however, the shape of the wind profiles differs from 1000-600 mb. During El Niño years, winds remain easterly ($\sim$5 ms^{-1}) throughout the lower and middle troposphere. During La Niña years the easterly winds reach a maximum around 900 mb and then weaken with height resulting in a large increase in zonal winds from 500-200 mb aloft. The Central and Eastern Pacific basins are characterized by this sharp increase in winds (strengthening westerlies) near the 600 mb level, where the upper-level wind shear increases from 7.6 ms^{-1} during El Niño conditions to 22.2 ms^{-1} during La Niña conditions in the Central Pacific. Not only is this change uniform across the precipitation regimes and for conditions matched to the TRMM RPF MCSs, but in general the upper-level shear increases as the precipitating regimes become more isolated and shallow.

Similar to the Kwajalein region, there exists little variability in the regional distribution of relative humidity within the lower troposphere and the largest discrepancies in moisture occur above 800mb; humidity values during La Niña conditions diverge towards drier conditions. This divergence in moisture is consistent throughout the precipitation regimes, which exhibit systematic increases in moisture as a function of system organization. Relative humidity differences in MCSs from the TRMM RPF dataset are generally consistent in shape vertically, however the humidity difference is larger between ENSO phases. Overall, the Kwajalein region exhibits the largest differences in humidity in mid-levels near 500 mb, however, the Central and East Pacific basins contain larger moisture disparities between ENSO events in the lower troposphere. The largest variability in moisture occurs within the Eastern Pacific basin. In the East Pacific, the moisture minimum is lower in altitude during La Niña events where relative humidity reaches a minimum around 600 mb before increasing again in the upper troposphere. In contrast, during El Niño years each regime reaches a minimum near 500 mb and then remains
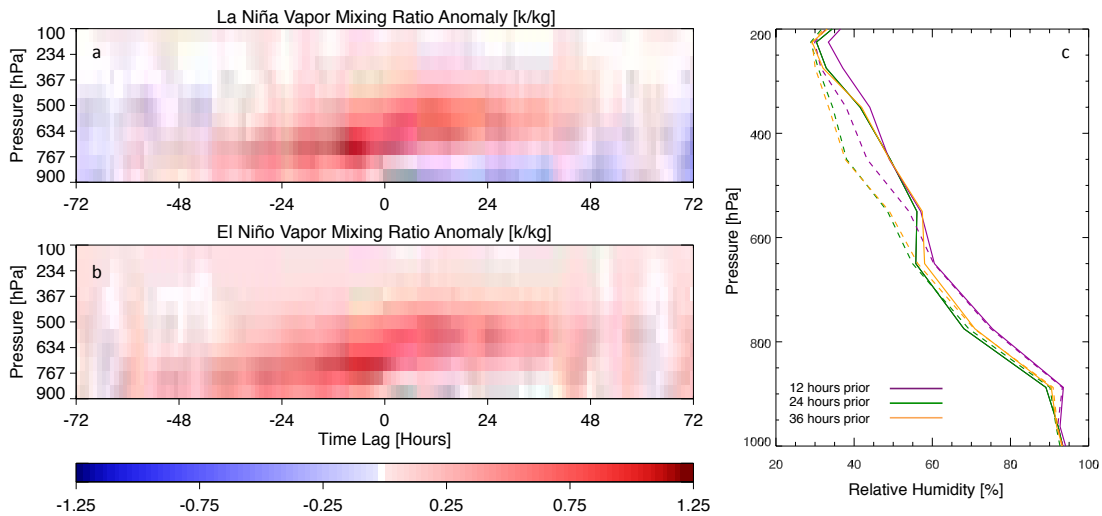
Figure 4.10. Using methods of Masunaga (2013), the time–pressure cross section of large-scale mean vapor mixing ratio [g/kg] during (a) El Niño events and (b) La Niña events in composite space for highly organized systems occurring from 2002-2009. The anomalies are created by subtracting the background state defined as the mean of the first and last 12 hours for all cases. (c) Comparison of mean relative humidity profiles from (solid) El Niño and (dashed) La Niña 12-36 before the occurrence of the organized precipitation.

nearly constant with height. These drier mid-tropospheric conditions in the East Pacific have been shown to be associated with shallow organized precipitation (Chen and Liu, 2016).

Collocated composite analysis with TRMM and AIRS retrieved water vapor and relative humidity (Masunaga, 2013) supplements our understanding of the humidity differences (Figure 4.10). TRMM and AIRS data from 2002-2009 are composited in space and time over the Pacific Ocean (15S-15N; 160E-280E) and separated monthly into La Niña/Neutral and El Niño conditions based on the ENSO 3.4 index for highly organized systems identified in Masunaga (2013). The temporal analysis confirms the increased moisture levels in the mid- and upper-levels during El Niño conditions. Figure 4.10b indicates that this increased humidity might relate to increased transport of moisture to the upper levels of the troposphere. Both ENSO phases demonstrate lower level moistening in the atmosphere before the precipitation occurrence at time zero. The El Niño composites illustrate that this moistening reaches deeper into the free troposphere, suggesting deeper convection occurring more frequently during the warm ENSO

events. This upper level moistening is echoed in relative humidity profiles (Figure 4.10c) well before the initiation of the organized precipitation event where higher moisture levels are found above 600 mb.

Based on the results above, the increased occurrence of stratiform precipitation observed during the El Niño events can be related to changes in large-scale environment. In the Pacific basins, an increase in stratiform precipitation is accompanied by increased environmental humidity in the mid- and upper-troposphere during warm events along with a weakening in upper-level wind shear. The warmer SSTs and CAPE during El Niño events lead to increased occurrence in deep convective precipitation and due to the lower mid-level shear. This increased convective activity may be important for transporting moisture in the upper-levels to help sustain stratiform precipitation regions. On the opposite end, the drier upper atmosphere and increased mid- and upper-level shear in La Niña conditions could act to enhance dry air entrainment and transport hydrometeors further from the convective sources, which might inhibit stratiform precipitation growth. This would result in a decreased occurrence in organized precipitation and thus making deep isolated convection the dominant source of precipitation and TMI-PR differences.

4.5 Precipitation relationship to ENSO-induced SST variability

Using GV from KPOL radar located on the Kwajalein Atoll, Henderson et al. (2017a) determined that precipitation regimes exhibited distinct bias patterns, which explained the majority of TMI-PR differences in a region surrounding the Kwajalein Atoll. In this section we apply the bias corrections described in Henderson et al. (2017a) to the precipitation regimes to aid in a better understanding of the mechanisms responsible for the observed rain rate differences

and the inter-annual variability of oceanic precipitation. The advantage of the Elsaesser et al. (2010) classification lies in the fact that the convective systems identified are found to be self-similar in nature across the tropical oceans, and as shown thus far the validation statistics seem to be extendable to other oceanic regions observed by the TRMM satellite. For reference, the GV-based biases from Henderson et al (2017a) are displayed in Table 4.5.

Table 4.5. Bias statistics, as derived in Henderson et al (2017a), between the TRMM PR and TMI rain rates compared to the dual-polarized rain rates estimates at the Kwajalein GV site as a function of convective regime. Values are first compared for convective cases (convection fraction > 0.50) and then for stratiform cases (convection fraction < 0.50).

Convective	All	Shallow	Deep Isolated	Organized
PR Bias [%]	-22.4	-12.8	-23.4	-26.1
TMI Bias [%]	-32.2	+5.5	-37.8	-30.3
Stratiform	All	Shallow	Deep Isolated	Organized
PR Bias [%]	-6.1	-11.4	-8.4	-2.6
TMI Bias [%]	+27.9	+25.5	+8.1	+33.4

The regime-based correction was applied to the TMI and PR rain estimates for the TRMM post-boost period from 2002-2013. Comparing the results shown in Figure 4.11 with the original TMI-PR difference maps in Figure 4.4, regional biases are still visible, however, several notable areas are improved. First, the large positive biased regions in the Central and Eastern Pacific are greatly decreased, where stratiform precipitation from TMI rainfall was decreased related to TMI retrievals significantly overestimating stratiform precipitation compared to the KPOL radar. Further, differences occurring in the deep isolated precipitation regimes in the Indian Ocean are reduced and the rain rate differences appear more or less randomly dispersed. Larger residual differences remain in deep isolated regimes occurring in the Maritime continent region and precipitating systems advected off the western coast of Africa into the Atlantic basin, however in
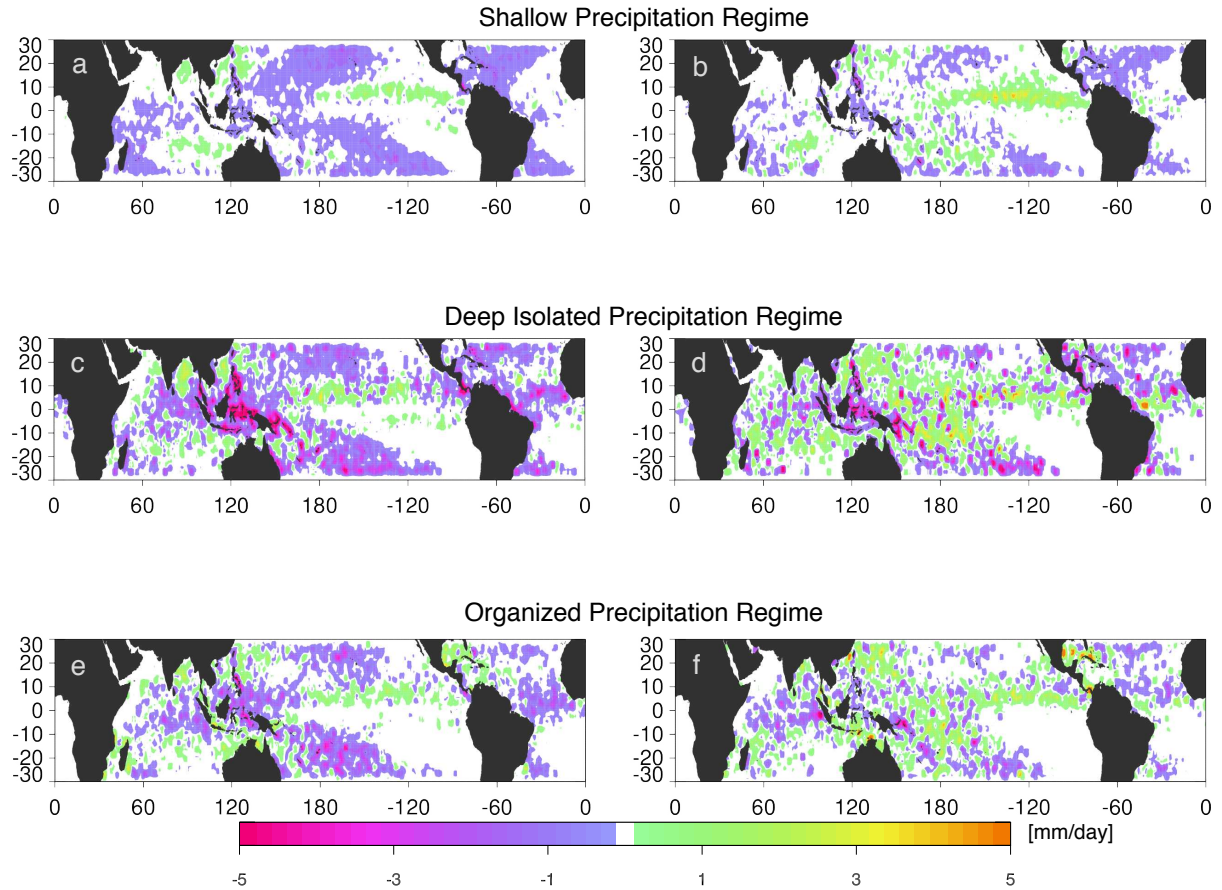
Figure 4.11. TMI-PR rainfall differences [mm/day] after the application of a bias correction described in Henderson et al. (2017a) for the (a,b) shallow, (c,d) deep isolated, and (e,f) organized precipitation regimes compared to the TRMM post boost climatological rain rates from 2002-2013 split by (left) convective cases and (right) stratiform cases.

general the regime-based corrections result in an overall reduction in TMI-PR differences in most regions.

The regional improvements in TMI-PR differences also result in changes in the tropical mean precipitation anomalies (Figure 4.12). Over the tropical oceans, the applied correction increases rain rates where PR generally always underestimated across the regimes and brings the PR variability more in line with the radiometer-based estimates of TMI and GPCP. PR variability still drops off sharply during the 2009/2010 El Niño event, which seems to be caused by differences in deep isolated regimes occurring in the Maritime Continent and African coast
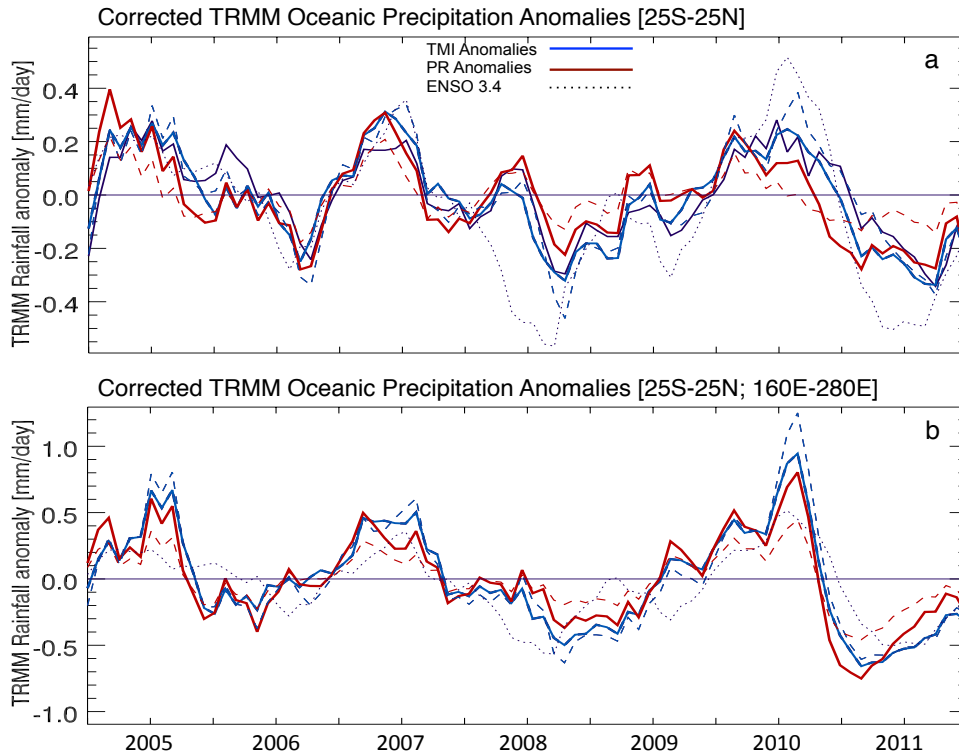
Figure 4.12. (a) Time series of tropical mean oceanic rainfall anomalies (25S–25N) from collocated TRMM TMI and TRMM PR rainfall products after the application of a bias correction described in Henderson et al. (2017a). Rain anomalies (dashed) before correction are included for comparison. (b) same as Panel A except within a region covering only the West, Central, the East Pacific basin (150E-280E). The ENSO 3.4 index (dotted) is included for reference in both panels.

regions. The maritime continent region areas are largely impacted by land-based orography, which can be difficult for radiometer-based estimates (e.g. Shige et al., 2013) and precipitating systems off the African coast are largely land-based rainfall transported over the oceans. For these regions it is likely that the ocean-based biases obtained from Kwajalein might not be fully representative. When constraining the observed region to the Pacific basin (150E-280E), the TMI and PR rain rate anomalies converge toward each other and are nearly in full agreement (Figure 4.12b).

To understand how these corrections can help constrain the precipitation relationship to tropical SST variability, the mean monthly rainfall measurements from TRMM TMI and PR are
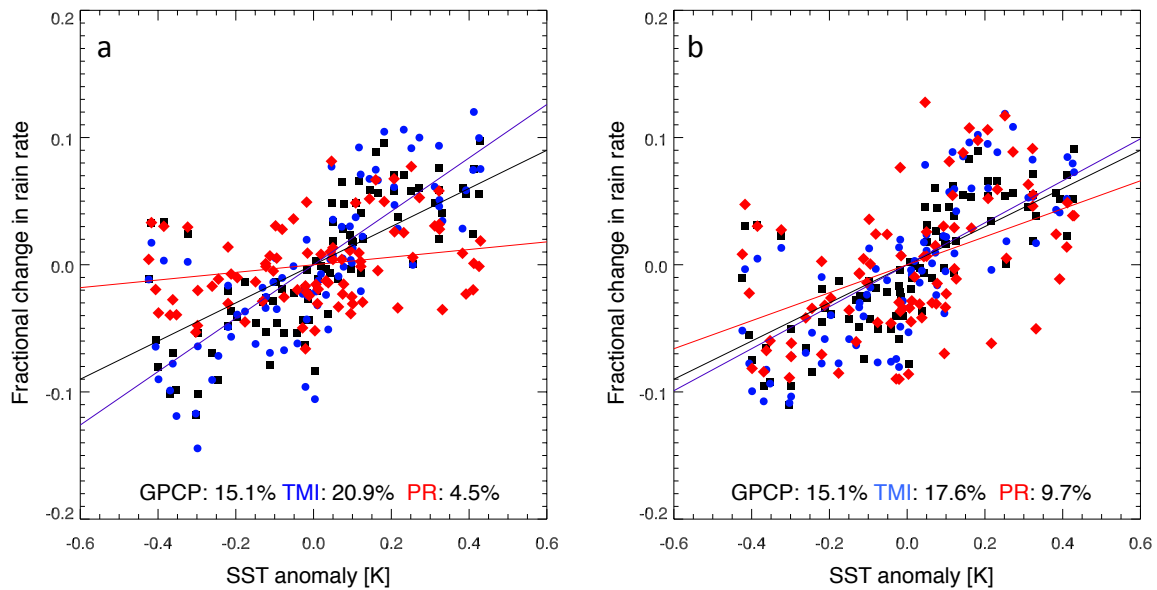
Figure 4.13. Scatter plot of the fractional change in (a) TRMM and GPCP precipitation anomalies compared to SST anomalies (°C) and (b) TRMM corrected precipitation anomalies and GPCP precipitation anomalies compared to SST anomalies over the tropical oceans (25S-25N). Each panel includes the retrieval percentage of rain rate increase per °C.

compared to the mean tropical SST (25°S–25°N) in Figure 4.13. Similar to previous work (e.g. Wang et al. 2008), before the correction, the TMI rain rates are positively correlated with mean ocean SST and the PR rain rates show little correlation with SST with a nearly flat relationship. The GPCP relationship is also positively correlated, but the sensitivity with SST is less in magnitude compared to the slope of TRMM TMI rain rates. The TMI and GPCP sensitivities are higher than reported previously, however the radiometer precipitation and SST relationships are in line with more current values derived from TRMM version 7 products (Robert Adler, personal communication). When the TRMM bias correction is applied both of the TMI and PR sensitivities converge toward the GPCP results Figure 4.13b. Over the tropical oceans, the TMI (GPCP) rainfall data exhibit similar responses to SST with changes 17.5%/°C (15.1%/°C). The increased rain rates in the PR rainfall increases the sensitivity from 4.4%/°C to 9.7%/C - converging toward the microwave radiometer-based rain rate relationships.

109

4.6 Summary and Conclusions

This work utilizes distinct self-similar precipitation regimes observed across the tropical oceans to characterize the ENSO impact of the regional precipitating cloud population on inter-annual rain rate anomalies estimated by TRMM TMI and PR retrievals. The analysis uses a combination of ground validation data and TRMM orbital data to observe changes in precipitation organization, precipitating system characteristics, and their respective large-scale environments. Precipitation variability is observed by categorizing TRMM rainfall using defined self-similar precipitation regimes following the methods of Elsaesser et al. (2010). We have shown that the spatial coverage of each precipitation regime varies significantly between the El Niño and La Niña ENSO phases, which can have significant impacts on the TMI and PR retrievals – particularly notable within the Pacific basin where SST anomalies are most prevalent.

Over the Kwajalein region, organized precipitation regimes were found to be more frequent during El Niño conditions with larger and deeper precipitating stratiform extent. Similarly, in the equatorial Pacific organized precipitation regimes become the dominant source of precipitation during El Niño events with greater amounts of the rainfall classified as stratiform rain; these features are observed in the East Pacific, however a large number of these systems are shallower in nature. The increased areas of stratiform precipitation are consistently positively biased toward TMI rainfall estimates and seem to drive the majority the discrepancies found in total oceanic rainfall anomalies occurring between TMI and PR rain rate estimates. TMI consistently underestimates PR rain rates in the regions of the West Pacific and Indian Ocean basins where the deep isolated convection is most prevalent and varies less between the ENSO phases. While the contribution of deep isolated precipitation is reduced overall during El Niño periods, during

the 2009-2010 Modoki El Niño event deep isolated precipitation is increased over the Maritime Continent region, leading to larger than normal discrepancies observed during this time period.

The increased stratiform rainfall occurs in regions where convective frequency is increased and where there are systematic increases in mid- and upper-level relative humidity. Mid-tropospheric relative humidity dramatically increases as a function of convective organization, however, moisture during El Niño events is consistently higher for all precipitation regimes compared to La Niña events. AIRS analysis suggests that this increased moisture is consistent throughout the mid-troposphere well before the occurrence of organized convective events, where water vapor is transported deeper into the troposphere compared to La Niña events. Barnes and Houze (2014) demonstrated that TRMM observed precipitation during the MJO in the Indian and West Pacific basins exhibited a large decreased in occurrence of broad stratiform regions associated with decreases in mid-tropospheric humidity and strong mid- or upper-level shear. The occurrence of more isolated convection during La Niña events is associated similar drier conditions and increased mid- and upper-level wind shear related to shifts in the Walker Circulation. The increased shear and decreased humidity is likely a less favorable environment for precipitating stratiform regions, where hydrometeors can be transported farther from the convective sources where drier air can be entrained further inhibiting the growth of stratiform precipitation.

Understanding the precipitation regime regional variability helps constrain observational relationships between the tropical oceanic rainfall and sea surface temperature. Application of GV-based bias correction described by Henderson et al (2017a) demonstrates a decrease in TMI-PR differences both regionally and tropic-averaged rain rate anomalies. The correction results in a decrease in TMI rainfall where stratiform rain is prevalent resulting, but also increases in

convective rainfall leading to an overall closer agreement with variability observed by GPCP. The increase in rainfall across all regimes for PR results in better agreement within PR rain rate variability and radiometer-based estimates when considering the response in precipitation to inter-annual variability in tropical SSTs. This precipitation response in Version 7 TRMM TMI (PR) shifts from 20% (4%) to 17% (10%), which are also closer to the GPCP value of 15%.

It should be noted that while the TMI-PR differences found in this work could vary with future iterations of the precipitation retrievals. The advantage of the self-similar regimes is the ability to diagnosing climate scale uncertainties in precipitation products by providing a physical source to identify and subsequently correct for errors resulting from these systematic changes. The regime classification is largely based upon the vertical distribution of reflectivity and convective-stratiform ratios in rainfall; therefore the regional variability in regimes would likely not be affected. The regime-based analysis not only provides an improved understanding of inter-annual variability in TRMM rainfall, but also provides a blueprint in precipitation variability in relation to its environment to aid in future model and satellite validation studies.

CHAPTER 5

CONCLUSIONS

The overarching objective of this dissertation is to gain understanding of the physical processes driving discrepancies between TRMM TMI and PR rain rates, particularly between ENSO phases, to increase our confidence in the relation between tropical precipitation and surface temperatures occurring at inter-annual time scales. The dissertation implements a recently developed precipitation classification methodology described in Elsaesser et al (2010) to evaluate ground validation and satellite based rainfall to address TRMM TMI and PR rain rate biases and their impacts on global rain rates across the tropical oceans.

In Chapter 2, the precipitation regimes are used to examine the performance of GV rainfall retrievals at the Kwajalein Atoll during two wet season periods; months when significantly more rainfall accumulation from deep convection and organized precipitating systems is observed. The statistically based Z-R relationships derived from the TRMM GV program are found to generally underestimate rainfall compared to the rain gauge network (up to 35% in organized precipitating regimes), whereas polarimetrically-tuned rainfall estimates compared well with rain gauge estimates. The underestimation in the GV retrievals are due to sampling issues in the WPMM process, where the Z-R relationship is unable to capture the differences in drop microphysics between deep isolated and deep organized precipitation regimes. This was demonstrated further when regime-based WPMM and regime based individual convective and stratiform relationships were implemented and resulted in reduced rain rate biases when compared to polarimetrically-tuned estimates.

The polarimetrically-tuned rainfall estimates derived from the KPOL radar provided the best match with ground gauges for each of the precipitation regimes and thus motivate the use of these rain rate estimates when evaluating satellite-based rainfall products. In Chapter 3, we utilize polarimetric rain rates to assess biases in TRMM TMI and PR retrievals as a function of system organization and convective fraction. The regime-based bias study identified the physical precipitation characteristics associated with TRMM rain rate biases. Not only was it discovered that retrieval biases varied as a function of system organization, but that TMI and PR retrievals exhibited different biases characteristics within convective and stratiform rainfall. Similar to previous studies, the PR rain rate estimates were found to underestimate rain rates for all regimes, whereas TMI rain rates are heavily underestimated for predominantly convective rainfall and overestimated for predominantly stratiform rainfall, which is most noticeable within organized precipitation regimes; the same pattern holds when comparing the differences in TMI-PR rain rates.

With the bias patterns defined for each regime, the role of precipitation regime variability and its relation to TMI-PR differences was investigated. Over the Kwajalein region, it is argued that the differences in regional rain rates between the TRMM rainfall estimates is driven by a shift from more isolated convection during La Niña events (periods where TMI generally underestimates PR rainfall) toward an increased occurrence in organized precipitation with larger stratiform rainfall contributions during El Niño events (periods where TMI generally overestimates PR rainfall). During the El Niño time periods the largest contributor in TMI-PR differences originates from organized precipitation regimes containing predominantly of stratiform rainfall – explaining 81% of the TMI-PR differences. Using the derived TMI and PR biases from Kwajalein, application of a bias correction yields increased agreement between the

TMI and PR rain rates – reducing differences during El Niño periods from 10% to 3%. It is hypothesized that tropics-wide discrepancies in TMI-PR rain rates due to ENSO variability are related to a systematic shifts in the frequency of organized precipitation regimes occurring between the warm and cold phases of ENSO.

In Chapter 4, TRMM-defined precipitation regimes are compared between El Niño and La Niña conditions to evaluate which regions are impacted the most by precipitation regime variability and the environmental conditions driving changes in system organization. The TRMM bias estimates derived in Chapter 3 are used as an aid to determine how regional changes in precipitating systems impact tropic-wide averaged rain rates – leading to the source in the space and time distributions of TMI-PR discrepancies and how are they related on an inter-annual scale. It is found that the largest variability in regimes occurs in the Pacific basin where SST anomalies are the greatest and there is a shift in precipitation contribution towards organized precipitation regimes containing widespread precipitating stratiform regions. This leads to a large swath of rainfall overestimated by TMI compared to PR across the Pacific basin during El Niño conditions. Regions where TMI generally underestimates PR are characterized by deep isolated convective precipitation and the persistent positive TMI-PR differences in the East Pacific are due to shallower more organized precipitating systems containing stratiform regions. It is suggested that the shift toward more organized precipitation during El Niño events is aided by increased moisture in the mid-troposphere and increased convective frequency. This is contrasted in La Niña conditions where a drier troposphere is observed with strong mid- and upper-level wind shear, which provides more unfavorable conditions for stratiform precipitation development.

The TMI and PR rain rate differences observed across the tropical oceans exhibited similar patterns to those observed in the GV analysis provided in Chapter 3. By applying bias corrections described in Chapter 3, increased agreement in TMI and PR rain rate anomalies are observed, particularly in the Pacific Basin, and helps constrain the relation between tropical precipitation and surface temperature on inter-annual time scales. By increasing rain rates where PR generally underestimated across all regimes, PR rain rate anomalies display increased magnitude in inter-annual rain rate anomalies more in line with the radiometer-based estimates of TMI and GPCP. Further, the peaks of TMI anomalies are decreased slightly related to the retrievals overestimation in organized precipitation. Overall, rain rate relations to ENSO-induced SST variability across the tropical oceans of 15.1%/°C, 9.7%/°C, and 17.6%/°C are found for GPCP, PR, and TMI rain rates, respectively.

The self-similar regimes implemented in this work have demonstrated remarkable applicability for investigating precipitation characteristics and uncertainties across the tropical oceans. Along with ideas interspersed throughout this dissertation, regime-based analysis can provide further applications within precipitation retrieval and climate research. The regime-based analysis was able to prescribe the precipitation sources leading to TMI-PR differences, however, as shown in Chapter 4, there are regions in which land-based influences could impact the retrieved rain rates. Many precipitation retrievals and studies depend on convective and stratiform partitioning, however, recent work has shown that convective and stratiform DSDs could be variable across the globe (Thompson et al. 2015; Brenda Dolan, personal comm). This was also demonstrated in Chapter 2, where errors in the rain rate retrievals could be attributed to assumptions in DSD differences found between the different precipitation regimes.

The application of regime-based analysis could be used to strengthen our understanding in retrieval processes requiring microphysical assumptions. Such analysis has been proven useful in understanding microphysical-related biases in passive microwave rainfall retrievals (e.g. Petkovic and Kummerow, 2016); however, this would also allow further investigation into convective and stratiform power law relationships implemented in TRMM/GPM single wavelength radar retrievals as well as the dual-frequency retrieval for the GPM DPR, which utilizes the Ku and Ka radar bands to derive both number concentration and median drop diameter to correct for attenuation and derive rain rates (Seto et al. 2013). A regime-based analysis provides a tool to evaluate the retrieval assumptions, such as in microphysics or attenuation correction which been shown to lead to rainfall underestimation (e.g. Munchack et al., 2012, Bringi et al., 2012), and provide validation procedures beyond convective and stratiform partitioning.

The analysis can also be extended to model-observational comparisons through the use of a tool such as Quickbeam (Haynes et al., 2009) to simulate radar reflectivities. Such application of the regime information could also provide potential improvements in the evaluation and development of TRMM and GPM latent heating retrievals by segregating precipitating heating profile variability associated with the individual regimes, which could be useful to help resolve observation and model disagreements in heating, such as those observed in the East Pacific (e.g. Back and Bretherton, 2009; Yokoyama et al., 2014).

The precipitation regimes provide an excellent medium for analyzing precipitation trends and impacts on large-scale atmospheric interactions. Recent work has begun to document longer-term changes in precipitation structures across the tropics within modeling and observational studies, where precipitation is becoming more focused along the ITCZ with possible shifts in
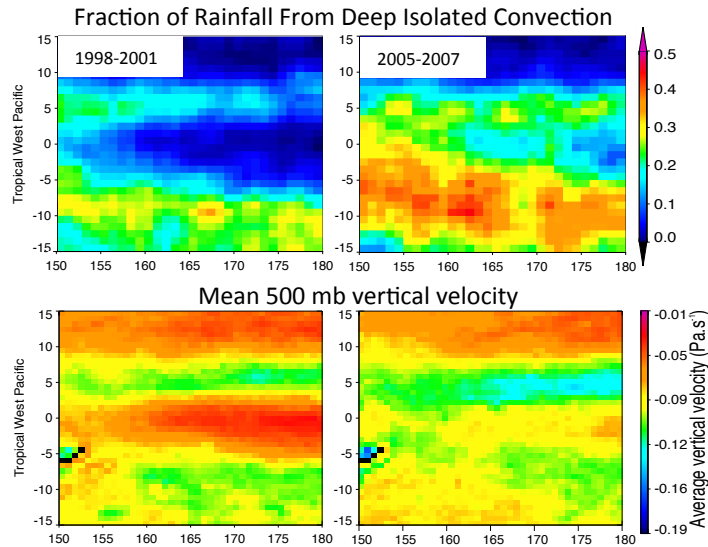
Figure 5.1 (top) Increased frequency of observed deep isolated convection in the West Pacific from 1998-2007 (smoothed). (bottom) Collocated mean 500 mb vertical velocities from MERRA (Courtesy of Paula Brown).

precipitation type (e.g. Tan et al. 2015, Wodzicki and Rapp, 2016, Lau et al., 2015). Such differences in precipitation regimes have been observed in the Western Pacific basin. During the TRMM mission, a systematic shift in the precipitation regimes is observed where precipitation increases can be related to increased occurrence of deep isolated and organized regimes over time, resulting in an overall increase in regional vertical velocities (Figure 5.1). Further, the regime-based analysis can be combined with other classification techniques such as the TRMM RPF dataset (Liu et al, 2008; as shown in Chapter 4) as well as the convective echo-based classification described by Houze et al. (2007). Implementing a combined analysis of collocated features would provide a physical classification of system organization, description of the systems large-scale features, and variability of convective and stratiform elements occurring within each precipitating system, which could offer an effective tool for monitoring precipitation and its characteristics over time. Such analysis of regional properties could aid in validation research by serving as observational benchmarks in climatological analysis of precipitation characteristics and their variability over time.

REFERENCES

Adler, R. F., J.-J. Wang, G. Gu, and G. J. Huffman, 2009: A ten-year tropical rainfall climatology based on a composite of TRMM products. *J. Meteor. Soc. Japan*, 87A, 281–293

Adler, R. F., G. Gu, and G. J. Huffman, 2012: Estimating climatological bias errors for the Global Precipitation Climatology Project (GPCP). *J. Appl. Meteor. Climatol.*, 51, 84–99.

Alexander, M.A., and Co-authors 2002: The atmospheric bridge: The influence of ENSO teleconnections on air–sea interaction over the global oceans. J. Climate, 15, 2205–2231.

Amitai, E., 2000: Systematic variation of observed radar reflectivity–rainfall rate relations in the Tropics. *J. Appl. Meteor.*, **39,** 2198–2208.

Awaka, J., T. Iguchi, and K. Okamoto, 1998: Early results on rain type classification by the Tropical Rainfall Measuring Mission (TRMM) Precipitation Radar. Proc. Eighth URSI Commission Open Symp., Aveiro, Portugal, URSI, 22–25.

Barros, A. P. and coauthors, 2014: NASA GPM-Ground Validation: Integrated Precipitation and Hydrology Experiment 2014 Science Plan, Duke University, Durham, NC, 64 pp., doi:10.7924/G8CC0XMR.

Barnes, H. C., Zuluaga, M. D. and Houze, Jr.R. A., 2015: Latent heating characteristics of the MJO computed from TRMM Observations. J. Geophys. Res. Atmos., 120: 1322–1334. doi:10.1002/2014JD022530.

Berg, W., C. Kummerow, and C. Morales, 2002: Differences between east and west Pacific rainfall systems. *J. Climate*, **15,** 3659–3672.

Berg, W., T. L'Ecuyer, and C. Kummerow, 2006: Rainfall climate regimes: The relationship of regional TRMM rainfall biases to the environment. *J. Appl. Meteor. Climatol.*, **45,** 434–454.

Berg, W., T. L'Ecuyer, and J. M. Haynes, 2010: The distribution of rainfall over oceans from spaceborne radars. *J. Appl. Meteor. Climatol.*, 49, 535–543.

Bidwell, S.W., J.F. Durning, D.F. Everett, M.R. Schwaller, E.A. Smith, and D.B. Wolff, "Preparations for Global Precipitation Measurement (GPM) Ground Validation", Geoscience and Remote Sensing Symposium, 2004. IGARSS 2004. Proceedings. Volume 2, pp. 921-924, 2004.

Bringi, V. N., T. Tang, and V. Chandrasekar, 2004: Evaluation of a new polarimetrically based *Z–R* relation. *J. Atmos. Oceanic Technol.*, **21**:612–623.

Bringi, V. N., G.-J. Huang, S. J. Munchak, C. D. Kummerow, D. A. Marks, and D. B. Wolff, 2012: Comparison of drop size distribution parameter (D0) and rain rate from S-band dual-polarized ground radar, TRMM precipitation radar (PR), and combined PR–TMI: Two events from Kwajalein Atoll. *J. Atmos. Oceanic Technol.*, **29**, 1603–1616, doi:10.1175/JTECH-D-11-00153.1.

Campos, E. and I. Zawadzki. 2000. Instrument uncertainties in *Z–R* relations. J. Appl. Meteor 39:1088–1102.

Chandrasekar, V., V. N. Bringi, N. Balakrishnan, D. S. Zrnic, 1990: Error structure of multiparameter radar and surface measurements of rainfall. Part III: specific differential phase. *J. Atmos. and Oceanic Technol.*,7, 621-629. doi: http://dx.doi.org/10.1175/1520-0426(1990)007<0621:ESOMRA>2.0.CO;2

Chandrasekar, V., Eugenio Gorgucci, Gianfranco Scarchilli, 1993: Optimization of multiparameter radar estimates of rainfall *J. Applied Meteor.*,32, 1288-1293. doi: http://dx.doi.org/10.1175/1520-0450(1993)032<1288:OOMREO>2.0.CO;2

Chandrasekar, V., A. Hou, E. Smith, V. N. Bringi, S. A. Rutledge, E. Gorgucci, W. A. Petersen, and G. S. Jackson, 2008: Potential role of dual- polarization radar in the validation of satellite precipitation measurements: Rationale and opportunities. *Bull. Amer. Meteor. Soc.*, **89,** 1127–1145.

Chen, B., and C. Liu, 2016: Warm organized rain system over the tropical Pacific. J. Climate, **29**, 3403–3422, doi:10.1175/JCLI-D-15-0177.1

Dee, D. P., and Coauthors, 2011: The ERA-Interim reanalysis: Configuration and performance of the data assimilation system. *Quart. J. Roy. Meteor. Soc.*, **137**, 553–597, doi:10.1002/ qj.828.

Duncan D. I., C. D. Kummerow, and G. S. Elsaesser, 2013: A Lagrangian Analysis of Deep Convective Systems and Their Local Environmental Effects. *Journal of Climate*, **27**, 2072–2086, doi: 10.1175/JCLI-D-13-00285.1.

Elsaesser, G. S., C. D. Kummerow, T. S. L'Ecuyer, Y. N. Takayabu, and S. Shige, 2010: Observed self-similarity of precipitation regimes over the tropical oceans. *J. Climate*, **23**, 2686–2698.

Elsaesser, G.S., and C.D. Kummerow, 2013: A multisensor observational depiction of the transition from light to heavy rainfall on subdaily time scales. *J. Atmos. Sci.*, **70**, no. 7, 2309-2324, doi:10.1175/JAS-D-12-0210.1.

Fiorino, S. T. 2002. Investigation of microphysical assumptions in TRMM radiometer's rain profile algorithm using KWAJEX satellite, aircraft, and surface datasets. Ph.D. dissertaion, The Florida State University, 128 pp.

Gorgucci, E., G. Scarchilli, V. Chandrasekar, and V. N. Bringi, 2000: Measurement of mean raindrop shape from polarimetric radar observations. *J. Atmos. Sci.*, **57,** 3406–3413.

Gorgucci, E., G. Scarchilli, V. Chandrasekar, and V. N. Bringi, 2001: Rainfall estimation from polarimetric radar measurements: Composite algorithms independent of raindrop shape-size relation. *J. Atmos. Oceanic Technol.*, **18,** 1773–1786.

Gu, G., R. F. Adler, G. Huffman, and S. Curtis,2007: Tropical rainfall variability on interannual-to-interdecadal and longer time scales derived from the GPCP monthly product, *J. Clim.*, **20**,4033–4046, doi:10.1175/JCLI4227.1.

Habib, E., and W. F. Krajewski, 2002: Uncertainty analysis of the TRMM ground- validation radar-rainfall products: Application to the TEFLUN-B field campaign. *J. Appl. Meteor.*, **41,** 558–572.

Hannah, W.M., B.E. Mapes, and G.S. Elsaesser, 2016: A Lagrangian view of moisture dynamics during DYNAMO. *J. Atmos. Sci.*, 73, no. 5, 1967-1985, doi:10.1175/JAS-D-15-0243.1.

Held, I. M. and B. J. Soden, 2006: Robust responses of the hydrological cycle to global warming. *Journal of Climate*, *19*(21), 5686-5699.

Henderson, D. S., C. D. Kummerow, W. Berg and D. A. Marks, 2017a: Regime based evaluation of TRMM oceanic biases, *J. Atmos. Oceanic Technol.*, accepted

Henderson, D. S., C. D. Kummerow, and D. A. Marks, 2017b: Sensitivity of rain rate estimates related to convective organization: observations from the Kwajalein, RMI, radar, *J. Appl. Meteor. Climatol.*, in press

Hou, A. Y., and Coauthors, 2014: The Global Precipitation Measurement (GPM) Mission. *Bull. Amer. Meteor. Soc.*, **95**, 701–722, doi:10.1175/BAMS-D-13-00164.1.

Houze, R. A., S. Brodzik, C. Schumacher, S. E. Yuter, and C. R. Williams, 2004: Uncertainties in Oceanic Radar Rain Maps at Kwajalein and Implications for Satellite Validation. *J. Appl. Meteor.*, **43**, 1114–1132.

Houze, R. A. 1993. Cloud Dynamics. Academic Press: San Diego.

Houze, R. A., Jr., D. C. Wilton, and B. F. Smull, 2007:, Monsoon convection in the Himalayan region as seen by the TRMM precipitation radar, Q. J. R. Meteorol. Soc., 133, 1389–1411.

Iguchi, T., T. Kozu, R. Meneghini, J. Awaka, and K. Okamoto. 2000:. Rain-profiling algorithm for the TRMM precipitation radar. J. Appl. Meteor 39:2038–2052.

Iguchi, T., T. Kozu, J. Kwiatkowski, R. Meneghini, J. Awaka, and K. Okamoto, 2009: Uncertainties in the rain profiling algorithm for the TRMM precipitation radar. *J. Meteor. Soc. Japan,*87, 1–30, doi:10.2151/jmsj.87A.1.

Iguchi, T., S. Seto, R. Meneghini, N. Yoshida, J. Awaka, and T. Kubota, 2010: GPM/DPR level-2 algorithm theoretical basis document. NASA-GSFC, 72 pp.

Jiang, J.H., and coauthors, 2012: Evaluation of cloud and water vapor simulations in CMIP5 climate models using NASA "A-Train" satellite observations. *J. Geophys. Res.*, **117**, no. D14, D14105, doi:10.1029/2011JD017237.

John, V. O., R. P. Allan, and B. J. Soden, 2009: How robust are observed and simulated precipitation responses to tropical ocean warming? Geophys. Res. Lett., 36, L14702, doi:10.1029/2009GL038276.

Johnson, R. H., T. M. Rickenbach, S. A. Rutledge, P. E. Ciesielski, and W. H. Schubert, 1999: Trimodal characteristics of tropical convection. J. Climate, 12, 2397–2418.

Kim, J. M. Ou, J. Park, K. R. Morris, M. R. Schwaller, and D. B. Wolff, 2014: Global Precipitation Measurement (GPM) Ground Validation (GV) Prototype in the Korean Peninsula. *J. Atmos. Oceanic Technol.*, **31**, 1902–1921.

Kishore, P., Ratnam, M. V., Namboothiri, S., Velicogna, I., Basha, G., Jiang, J., Igarashi, K., Rao, S., and Sivakumar, V.: Global (50S– 50N) distribution of water vapor observed by COSMIC GPS RO: Comparison with GPS radiosonde, NCEP, ERA-Interim, and JRA-25 reanalysis data sets, J. Atmos. Solar-Terr. Phys., pp. 1849–1860, doi:10.1016/j.jastp.2011.04.017, 2011

Kummerow, C. D., W. S. Olson, and L. Giglio, 1996: A simplified scheme for obtaining precipitation and vertical hydrometeor profiles from passive microwave sensors. *IEEE Trans. Geosci. Remote Sens.,*34, 1213–1232, doi:10.1109/36.536538.

Kummerow, C., W. Barnes, T. Kozu, J. Shiue, and J. Simpson, 1998: The Tropical Rainfall Measuring Mission (TRMM) sensor package. *J. Atmos. Oceanic Technol.,***15,** 809–816.

Kummerow, C., and Coauthors, 2000: The status of the Tropical Rainfall Measuring Mission (TRMM) after two years in orbit. *J. Appl. Meteor.,***39,**1965–1982.

Kummerow, C. D., D. L. Randel, M. Kulie, N.-Y. Wang, R. Ferraro, S. J. Munchak, and V. Petkovic,2015: The evolution of the Goddard profiling algorithm to a fully parametric scheme. *J. Atmos. Oceanic Technol.*, 32, 2265–2280, doi:10.1175/JTECH-D-15-0039.1.

Kummerow, C. D., S. Ringerud, J. Crook, D. Randel, and W. Berg, 2011: An observationally generated a priori database for microwave rainfall retrievals. *J. Atmos. Oceanic Technol.*, 28, 113–130, doi:10.1175/2010JTECHA1468.1.

Lau, K-M., R. P. Allan, and G. J. Huffman (2012), Climatology and changes in tropical oceanic rainfall characteristics inferred from Tropical Rainfall Measuring Mission (TRMM data J. Geophys. Res., 116, D17111, doi:10.1029/2011JD015827.

Li, W., and C. Schumacher, 2010: Thick anvils as viewed by the TRMM precipitation radar, *J. Climate*, **24**, 1719–1735.

Liu, C., R. P. Allan, and G. J. Huffman, 2013: Co-variation of temperature and precipitation in CMIP5 models and satellite observations, Geophys. Res. Lett., 39, L13803, doi:10.1029/2012GL052093.

Liu, C., E.J.Zipser, D.J.Cecil, S.W.Nesbitt, and S. Sherwood, 2008: A cloud and precipitation feature database from 9 years of TRMM observations. *J. Appl. Meteor. Climate*, **47**, 2712-2728.DOI:10.1175/2008JAMC1890.1

Liu C., and E. Zipser, 2013: Regional variation of morphology of the organized convection in the tropics and subtropics, Part I: regional variation, *J. Geophys. Res.*, **118**, 453–466, doi:10.1029/2012JD018409.

Liu, C., E.J. Zipser, D.J. Cecil, S.W. Nesbitt, and S. Sherwood, 2008: A cloud and precipitation feature database from 9 years of TRMM observations. *J. Appl. Meteor. Climate,* ***47***, *DOI:10.1175/2008JAMC1890.1*

Liu, C., and E. Zipser, 2014: Differences between the surface precipitation estimates from the TRMM precipitation radar and passive microwave radiometer version 7 products. *J. Hydrometeor.*, **15**, 2157–2175, doi:10.1175/JHM-D-14-0051.1

Liu, J., C.D. Kummerow, and G.S. Elsaesser, 2016: Identifying and analyzing uncertainty structures in the TRMM Microwave Imager precipitation product. *Int. J. Remote Sens.*, accepted.

Marks, D. A., D. B. Wolff, D. S. Silberstein, A. Tokay, J. L. Pippitt, and J. Wang, 2009: Availability of high-quality TRMM ground validation data from Kwajalein, RMI: A practical application of the relative calibration adjustment technique. *J. Atmos. Oceanic Technol.*, **26,** 413–429.

Marks, D. A., D. B. Wolff, L. D. Carey, and A. Tokay, 2011: Quality control and calibration of the dual-polarization radar at Kwajalein, RMI. *J. Atmos. Oceanic Technol.*, **28**, 181–196.

Masunaga, H., T. S. L'Ecuyer, and C. D. Kummerow, 2005: Variability in the Characteristics of Precipitation Systems in the Tropical Pacific. Part I. Spatial Structure. *J. Climate*, 18, 823-840

Masunaga, H., and C. D. Kummerow, 2005: Combined radar and radiometer analysis of precipitation profiles for a parametric retrieval algorithm. *J. Atmos. Oceanic Technol.*, 22, 909–929.

Masunaga, H., 2012: Short-term versus climatological relationship between precipitation and tropospheric humidity *J. Climate*, **25**, 7983-7990

Masunaga, H, 2013: A satellite study of tropical moist convection and environmental variability: a moisture and thermal budget analysis. *J. Atmos. Sci.*, 70, 2443–2466. doi: http://dx.doi.org/10.1175/JAS-D-12-0273.1

Meneghini, R., T. Iguchi, T. Kozu, L. Liao, K. Okamoto, J.A. Jones, and J. Kwiatkowski, 2000: Use of the surface reference technique for path attenuation estimates from the TRMM Precipitation Radar. *J. Appl. Meteor.*, 39, 2053–2070, doi:10.1175/1520-0450(2001)040<2053:UOTSRT>2.0.CO;2.

Moncrieff, M. W., D. E. Waliser, M. J. Miller, M. E. Shapiro, G. Asrar, and J. Caughey, 2012: Multiscale convective organization and the YOTC Virtual Global Field Campaign. *Bull. Amer. Meteor. Soc.*, **93**, 1171–1187.

Munchak, S. J., C. D. Kummerow, and G. Elsaesser, 2012: Relationships between the raindrop size distribution and properties of the environment and clouds inferred from TRMM. *J. Climate*, 25,2963–2977

Nesbitt, S.W., E. J. Zipser, and D.J. Cecil, 2000: A census of precipitation features in the tropics using TRMM: Radar, ice scattering, and lightning observations. *J. Climate*,**13** (23), 4087-4106

Petersen, W. A. and coauthors, 2013: Bias and Random Error Estimates Using Pre-GPM Satellite Products and Ground Validation Rain Rate Estimates, *Global Precipitation Measurement (GPM) Science Implementation Plan, Tech. Rep. Appendix J*, Goddard Space Flight Program. 17 pp.

Petersen, W. A., and W. Krajewski, 2013: Status update on the GPM Ground Validation Iowa Flood Studies (IFloodS) field experiment.*Geophysical Research Abstracts*, Vol. 15, Abstract 13345.

Petkovic, V., and C. D. Kummerow, 2016: Understanding the sources of satellite passive microwave rainfall retrieval systematic errors over land, *J. Appl. Meteor. Climatol.*, accepted.

Posselt, D.J., S.C. van den Heever, G.L. Stephens, and M.R. Igel, 2012: Changes in the interaction between tropical convection, radiation and the large scale circulation in a warming environment. *J. Clim.*, 25, 557-571.

Rao, T.N., Rao, D.N., Mohan, K. and Raghavan, S., 2001: Classification of tropical precipitating systems and associated *Z-R* relationships. *Journal of Geophysical Research 106: doi: 10.1029/2000JD900836. issn: 0148-0227.*

Rasmussen, K. L., S. L. Choi, M. D. Zuluaga, and R. A. Houze Jr., 2013: TRMM precipitation bias in extreme storms in South America. *Geophys. Res. Lett.*,**40,** 3457–3461, doi:10.1002/grl.50651.

Rasmussen, K. L., S. L. Choi, M. D. Zuluaga, and R. A. Houze Jr., 2013: TRMM precipitation bias in extreme storms in South America, Geophys. Res. Lett., 40, 3457–3461

Rasmusson, E. M., and T. H. Carpenter, 1982: Variations in tropical sea surface temperature and surface wind fields associated with the Southern Oscillation/El Niño. *Mon. Wea. Rev.*, **110**, 354–384, doi:10.1175/1520-0493(1982)110<0354:VITSST>2.0.CO

Ratnam, J. V., and Co-authors (2012), Anomalous climatic conditions associated with the El Niño Modoki during boreal winter of 2009, Clim. Dyn., 39(1–2), 227–238.

Rosenfeld, D., D. B. Wolff, and E. Amitai, 1994: The window probability matching method for rainfall measurements with radar. *J. Appl. Meteor.*,**33**, 682–693.

Rossow, W. B., G. Tselioudis, A. Polak, and C. Jakob, 2005: Tropical climate described as a distribution of weather states indicated by distinct mesoscale cloud property mixtures. Geophys. Res. Lett., 32, L21812, doi:10.1029/2005GL024584

Schumacher, C. and R. A. Houze Jr.. 2000. Comparison of radar data from the TRMM satellite and Kwajalein oceanic validation site. J. Appl. Meteor. 39:2151–2164.

Schumacher, C. and R.A. Houze, Jr., 2003: Stratiform rain in the tropics as seen by the TRMM Precipitation Radar. *J. Climate*, **16**, 1739-1756.

Schumacher, C.and R. A. Houze, Jr., 2000: Comparison of Radar Data from the TRMM Satellite and Kwajalein Oceanic Validation Site. *J. Appl. Meteor.*, **39**, 2151-2164.

Schumacher, C., R. A. Houze Jr., and I. Kraucunas, 2004: The tropical dynamical response to latent heating estimates derived from the TRMM precipitation radar. *J. Atmos. Sci.*, **61,** 1341–1358.

Schumacher C, Houze RA Jr. 2006. Stratiform precipitation production over sub-Saharan Africa and the tropical East Atlantic as observed by TRMM. Q. J. R. Meteorol. Soc. 132: 2235–2255.

Seo, E.-K., B.-J. Sohn, and G. Liu, 2007: How TRMM Precipitation Radar and Microwave Imager retrieved rain rates differ. *Geophys. Res. Lett.*,**34,** L24803, doi:10.1029/2007GL032331.

Seo, E.-K., S. Hristova-Veleva, G. Liu, M.-L. Ou, and G.-H. Ryu, 2015: Long-term comparison of collocated instantaneous rain retrievals from the TRMM Microwave Imager and Precipitation Radar over the ocean. *J. Appl. Meteor. Climatol.*, 54, 867–879, doi:10.1175/JAMC-D-14-0235.1.

Shige, S., T. Watanabe, H. Sasaki, T. Kubota, S. Kida, and K. Okamoto, 2008: Validation of western and eastern Pacific rainfall estimates from the TRMM PR using a radiative transfer model. J. Geophys. Res., 113, D15 116.

Shige, S., H. Sasaki, K. Okamoto, and T. Iguchi, 2006: Validation of rainfall estimates from the TRMM precipitation radar and microwave imager using a radiative transfer model: 1. Comparison of the version-5 and -6 products. *Geophys. Res. Lett.*, 33, L13803, doi:10.1029/2006GL026350

Silberstein, D. S., D. B. Wolff, D. A. Marks, D. Atlas, and J. L. Pippitt, 2008: Ground clutter as a monitor of radar stability at Kwajalein, RMI. *J. Atmos. Oceanic Technol.*, **25,** 2037–2045.

Sobel, A. H., S. E. Yuter, C. S. Bretherton, and G. N. Kiladis, 2004: Large-scale meteorology and deep convection during TRMM KWAJEX. *Mon. Wea. Rev.*, **122,** 422–444.

Soden, B. J., 2000: The sensitivity of the tropical hydrological cycle to ENSO. *J. Climate*, **13**, 538–549, doi:10.1175/1520-0442(2000)013<0538:TSOTTH>2.0.CO;2.

Steiner, M., R. A. Houze Jr., and S. E. Yuter, 1995: Climatological characterization of three-dimensional storm structure from operational radar and rain gauge data. *J. Appl. Meteor.*, **34**, 1978–2007, doi:10.1175/1520-0450(1995)034<1978:CCOTDS>2.0.CO;2

Steiner, M., J. A. Smith, and R. Uijlenhoet, 2004a: A microphysical interpretation of radar reflectivity–rain rate relationships. *J. Atmos. Sci.*, **61,**1114–1131.

Steiner, M., and J. A. Smith, 2004b: Scale dependence of radar rainfall rates—An assessment based on raindrop spectra. *J. Hydrometeor.*, **5,**1171–1180.

Stephens, G. L., and Coauthors, 2010: Dreary state of precipitation in global models. *J. Geophys. Res.*, **115**, D24211, doi:10.1029/2010JD014532.

Su, H., J. H. Jiang, Jiang, 2013: Tropical Clouds and Circulation Changes during the 2006/07 and 2009/10 El Niños. *J. Climate*, **26**, 399–413. doi: JCLI-D-12-00152.1

Thompson, J. E., S. A. Rutledge, B. Dolan, and M. Thurai, 2015: Drop size distributions and radar observations of convective and stratiform rain over the equatorial Indian and west Pacific Oceans. *J. Atmos. Sci.*, **72**, 4091–4125, doi:10.1175/JAS-D-14-0206.1.

Tian, B., D. E. Waliser, E. J. Fetzer, and Y. L. Yung (2010), Vertical moist thermodynamic structure of the Madden-Julian Oscillation in Atmospheric Infrared Sounder Retrievals: An update and a comparison to ECMWF Interim Re-Analysis, *Mon. Weather Rev.*, **138**(12), 4576–4582

Trenberth, K. E., 1997: The definition of El Niño. *Bull. Amer. Meteor. Soc.*, 78, 2771–2778.

Trenberth KE, Dai A, Rasmussen RM, Parsons DB (2003) The changing character of precipitation. Bull Am Meteorol Soc 84:1205–1217

Trenberth, K. E., 2011: Changes in precipitation with climate change. *Climate Res.*, **47**, 123–138

Vecchi, G. A. and B.J. Soden, 2007:. Global warming and the weakening of the tropical circulation. *Journal of Climate*, *20*(17), 4316-4340.

Vecchi, G., and A. Wittenberg, 2010: El Niño and our future climate: Where do we stand? *Wiley Interdiscip. Rev.: Climate Change*, **1**, 260–270.

Wang, J.-J., R. F. Adler, and G. Gu, 2008: Tropical rainfall–surface temperature relations using TRMM precipitation data. *J. Geophys. Res.*, 113, D18115, doi:10.1029/2007JD009540.

Wang, J., B. L. Fisher, and D. B. Wolff, 2008: Estimating rain rates from tipping-bucket rain gauge measurements. *J. Atmos. Oceanic Technol.*, **25,**43–56.

Wang, J., and D. B. Wolff, 2010: Evaluation of TRMM ground-validation radar-rain errors using rain gauge measurements. *J. Appl. Meteor. Climatol.*, **49**, 310–324.

Wang, J. J., R. F. Adler, G. J. Huffman, and D. Bolvin, 2013: An updated TRMM composite climatology of tropical rainfall and its validation. *J. Climate*, **27**, 273–284, doi:10.1175/JCLI-D-13-00331.1

Watanabe, M., and Coauthors, 2012: Uncertainty in the ENSO amplitude change from the past to the future. *Geophys. Res. Lett.*, 39, L20703

Wolff, D. B., D. A. Marks, E. Amitai, D. S. Silberstein, B. L. Fisher, A. Tokay, J. Wang, and J. L. Pippitt, 2005: Ground validation for the Tropical Rainfall Measuring Mission (TRMM). *J. Atmos. Oceanic Technol.*, **22,** 365–380.

Wolff, D. B., and B. L. Fisher, 2008: Comparisons of instantaneous TRMM ground validation and satellite rain-rate estimates at different spatial scales. *J. Appl. Meteor. Climatol.*, **47**, 2215–2237.

Wolff, D. B., and B. L. Fisher, 2009: Assessing the relative performance of microwave-based satellite rain-rate retrievals using TRMM ground validation data. *J. Appl. Meteor. Climatol.*, **48**, 1069–1099

Wolff, D.B., David A. Marks, and Walter A. Petersen, 2015: General Application of the Relative Calibration Adjustment (RCA) Technique for Monitoring and Correcting Radar Reflectivity Calibration. *J. Atmos. Oceanic Technol.*, **32**, 496–506.

Xu, Weixin, Steven A. Rutledge, 2014: Convective Characteristics of the Madden–Julian Oscillation over the Central Indian Ocean Observed by Shipborne Radar during DYNAMO. *J. Atmos. Sci.*, 71, 2859–2877. doi: http://dx.doi.org/10.1175/JAS-D-13-0372.1

Yoneyama, K., C. Zhang, and C. N. Long, 2013: Tracking pulses of the Madden–Julian oscillation. *Bull. Amer. Meteor. Soc.*

Yokoyama, C., E. J. Zipser, and C. Liu, 2014: TRMM-observed shallow versus deep convection in the eastern Pacific related to large-scale circulations in reanalysis datasets. *J. Climate*, **27**, 5575–5592

Yuter SE, Houze RA Jr. 1998. The natural variability of precipitating clouds over the western Pacific warm pool. Q. J. R. Meteorol. Soc. 124: 53–99.

Zipser, E., C. Liu, D. Cecil, S. W. Nesbitt, and S. Yorty, 2006: where are the most intense thunderstorms on Earth?, *Bull. Am. Meteorol.Res.*, **87**, 1057-1071.